Mechanism of Cation Exchange Process for Epitaxy of Superconducting $HgBa_2CaCu_2O_6$ Films and Passive Microwave Devices

Hua Zhao

B.S., Harbin Institute of Technology, Harbin, China, 1983
M.S., Harbin Institute of Technology, Harbin, China, 1988

Submitted to the Department of Physics and Astronomy and the Faculty of the Graduate School of the University of Kansas in partial fulfillment of the requirement for the degree of Doctor of Philosophy

Dissertation Committee:

_____
Chair: Dr. Judy Z. Wu

_____
Dr. Hui Zhao

_____
Dr. Siyuan Han

_____
Dr. Douglas W. McKay

_____
Dr. Brian B. Laird

Date Submitted:_____

The Dissertation Committee for Hua Zhao certifies
That this is the approved version of following dissertation:

Mechanism of Cation Exchange Process for Epitaxy of Superconducting $HgBa_2CaCu_2O_6$ Films and Passive Microwave Devices

_____

Chair: Dr. Judy Z. Wu

Date approved: _____

Abstract

The record high superconducting transition temperature (T_c) in Hg-based High temperature superconducting (HTS) cuprates make them very promising for both fundamental physics and practical applications. The high volatile nature of Hg presents a major challenge in epitaxy of high quality Hg-based HTS films. In a novel cation exchange process developed by our group recently, epitaxial $HgBa_2CaCu_2O_{6+\delta}$ (Hg-1212) films can be obtained by diffusing volatile Tl cations out of, and simultaneously diffusing Hg cations into, the lattice of epitaxial $Tl_2Ba_2CaCu_2O_8$ (Tl-2212) or $TlBa_2CaCu_2O_7$ (Tl-1212) precursor films. Aiming at the remained issues in understanding the mechanism of the cation exchange (CE) process, this thesis work has studied the reversibility of CE. We have found that the CE process is completely reversible between Hg-1212 and Tl-2212, confirming further the thermal perturbation diffusion model. One of the experimental works unveiled that the conversion from Hg-1212 to Tl-2212 involves two steps: conversion from Hg-1212 to Tl-1212 via CE followed by Tl intercalation to form double Tl–O plans in each unit cell.

Two improvements have been made in raising the quality of the Hg-1212 films. First, by successfully introducing micro-channels in Tl-1212 precursor with reversible CE, purer HTS Hg-1212 thin films have been obtained. Secondly, by

pinning lattice with nonvolatile Re atoms, the surface morphology of Hg-1212 films have been improved.

In addition to making the high quality Hg-1212 films, we have fabricated a two-pole *X*-band Hg-1212 microstrip filter and then investigated its nonlinearity by measuring the third-order intermodulation (IM3) signals since the major limitation for real application still comes from the nonlinearity. By a comparison between different structural materials of Hg-1212, Tl-2212 and $YBa_2Cu_3O_7$ (YBCO), the third-order intercept (IP3) of the Hg-1212 filter is consistently higher than that in the YBCO and Tl-2212. The surprising similarity in the curves of dc critical current density J_c and the rf J_{IP3} derived from the IP3 against reduced temperature suggests that the magnetic vortex depinning in HTS materials dominates the microwave nonlinearity at elevated temperatures. These encouraging results have marked Hg-1212 out as a promising alternative material for passive microwave devices at above 77 K operating temperature.

This dissertation is dedicated to my husband

Acknowledgments

I have been fortunate in my career and my life to be surrounded by and to work with great people. In this short page, I would like to thank my friends and colleagues who helped me with the research works presented in this thesis.

First and foremost I must thank my advisor, Prof. Judy Z. Wu, for her unfaltering support and excellent mentorship during my challenging graduate school years, academically, metaphorically, and linguistically. I have the greatest admiration for her command of condensed matter physics on both an experimental and theoretical level and hope to one day have at least a comparable amount of knowledge myself.

I would like to thank Prof. Siyuan Han for his great support in granting me a full access of the microwave related facility in his laboratory, in addition to his careful reviewing my research proposal in his extremely tight schedule.

I would also like to thank all other members of my thesis committee, Dr. Brian Laird, Dr. Douglas McKay and Dr. Hui Zhao for reviewing my thesis. Special thanks go to Prof. Douglas McKay, who has paved me a smooth path towards establishing theoretical model regarding my research work, benefiting from the courses taught by Him, Quantum Mechanics, Mathematical Physics, and General Relativity.

The experimental involving microwave characterization of high temperature superconducting films could not be smoothly performed without the help of Dr. Wei Qiu, who was working in Dr Han's lab as PhD student that time.

Most heartfelt thanks go to Jonathan R. Dizon, Rose Lyn S. Emergo, Rongtao Lu, and Xiang Wang, for many valuable discussions at the lab, countless timely helps in their tight schedules, and enjoyable extracurricular activities at homes.

Of course all of labmates and friends have been a great source of joy and inspiration, throughout my time at KU. Thanks to everyone in the KU Thin Film Group for being there during good and bad times, and for helping me out in my research efforts in almost every way.

Last but not least, I would like to thank my parents Renliang Zhao and Yuxian Guo for their love and continuous support during all the years I have spent in another country, and my beloved husband Jingwen for his patience and affection, which he demonstrated in so many most difficult periods of this thesis, especially for his prayers before God. Finally, I would like to thank my dad, mom and sister for their kind and loving support throughout the years I spent in graduate school. My parents always enjoy boasting of my accomplishments, big and small.

List of Figures

Fig. 4.2 Diffusion channel of "1212" structure (a) the diffusion of the Tl and Hg cations may have to follow a layer-by-layer pattern. (b) the voids actually serve as diffusion channels through the film thickness and therefore enable dominance of ab-plane cation diffusion.

Fig. 4.3 XRD θ-2θ spectra of the sample films (a) a regular Tl-1212A film annealed in an Al_2O_3 crucible in Tl vapor at 840ºC for 1 hour; (b) the Tl-1212B film with micro-channels ; (c) the Hg-1212A film made from the Tl-1212A film; (d) the Hg-1212B film from Tl-1212B film; All films except Tl-1212A made in a sealed quartz tube in Hg vapor at 700º C for 12 hours to get target Hg-1212 films or in Tl vapor at 730º C for 2 hrs to achieve target Tl-1212B films.

Fig. 4.4 Scanning electron microscopy images of: (a) the regular Tl-1212A; (b) The Tl-1212B film; (c) The Hg-1212A film made from Tl-1212A; (d) The Hg-1212B film from Tl-1212B. (e) The Hg-1212AA film from Hg-1212A film

Fig. 4.5 Magnetic susceptibility as a function of temperature measured in zero-field-cool mode for the superconducting films. The applied field is 10 gauss and perpendicular to the film.

Fig. 4.6 The J_cs of all Hg-1212 films at different temperatures (a) at 5K, (b) at 77K and (c) 100K and the inlets are the normalized J_c.

Fig. 4.7 Temperature dependence of resistivity (ρ) of Hg-1212A and Hg-1212B films.

Fig. 4.8 XRD θ–2θ spectra of the sample films: (a) the starting Tl-2212 film; (b) after its first cation exchange in Hg vapor at 700 °C for 12 h; (c) after a half-time of the second cation exchange in Tl vapour at 760 °C for 1.0 h; (d) after completion of the second cation exchange in Tl vapor at 760 °C for 2.0 h; (e) after the third cation exchange in Hg vapor at 700 °C for 12 h; and (f) after the fourth cation exchange in Tl vapor at 760 °C for 2 h. All films were made in sealed quartz tubes except the starting Tl-2212 film.

Fig. 4.9 Schematic description of the two steps of the conversion from Hg-1212 to Tl-2212.

Fig. 4.10 SEM images of a representative sample after several cation exchanges: (a) after the first cation exchange in Hg vapor from a Tl-2212 precursor film; (b) after the second cation exchange in Tl vapor; (c) after the third cation exchange in Hg vapor; and (d) after the fourth cation exchange in Tl vapor.

Fig. 4.11 (a) Magnetic susceptibility as a function of temperature measured in zero-field-cooling mode for a sample experiencing several cation exchanges. (b)

Contents

Chapter 1

Introduction

1.1 Brief Review of Superconductivity and High Temperature Superconductors

Superconductivity is one of the revolutionary discoveries within the past century. Since its discovery, the research works have experienced several tides. The latest tide is the highest one, which is still here and relates to high temperature superconductors (HTS_s), and has last over two decades. It is no exaggeration to say that deeper impact on the science, technology and even our daily life expects to come sometimes soon.

1.1.1 The Basic Phenomena

In 1911, the first observation of the superconductivity in mercury made many people extremely excited because they observed, for the very first time, resistless conductor at temperature T below a certain value T_c then [see Fig. 1.1 (a)] and believed that the old dream about the perpetual mobile had come true. Many thought at that time the superconductor was a perfect conductor. In 1933, after the verification of Meissner's effect, scientists and engineers were full of curiosity about this brand new thermodynamics state. Employing all theoretical

and experimental scientific means in electrodynamics, thermodynamics, quantum mechanics plus wild imagination power, they could hardly have in-depth understanding of this elusive new phenomenon for decades in many ways. Illustrated in Fig.1.1 (b) is Meissner's effect. When a magnetic field (not very strong) is applied on superconductor at $T>T_c$, the magnetic flux penetrates through the body of the superconductor. However, if the superconductor is cooled to $T < T_c$ (so called superconducting state), the magnetic flux lines are expelled out, namely, the magnetic field is zero inside the superconductor. In another words, the superconductor works like a magnetic field screening entity, working the similar way as a conductor screens an electric field.

Superconductivity, as a brand new physical phenomenon, has indeed puzzled many scientists to establish a satisfied theoretical model. After over two decades waiting of the discovery of Meissner's effect, Nobel Prize winning BCS (Bardeen, Cooper, and Schrieffer) theory has finally been published in 1957. The key idea is: an (isotropic) attractive interaction leads to bind electron pair states ("Cooper pairs"). A Cooper pair, as an entire entity that does not lose energy to the lattice, can continue running through a ring superconductor for millions of years after started, unless the temperature of the conductor is raised up over T_c[1.1] Simply, it can be described as: in the superconducting state, the supercurrent is carried by Cooper pairs, which are electron pairs bounded by a certain physical interaction, such as a phonon-electron interaction, or a magnetic interaction.

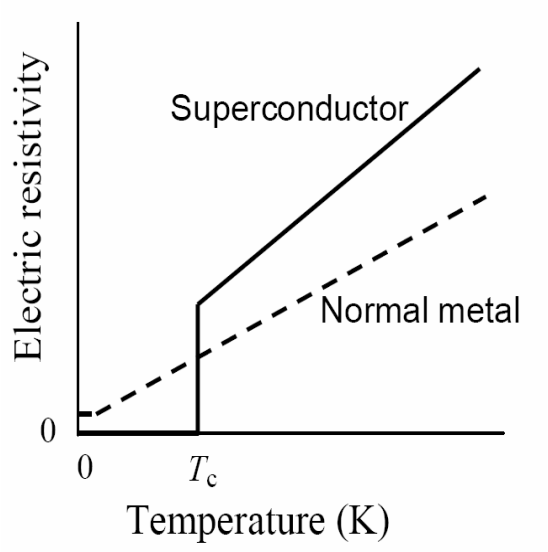

(a)

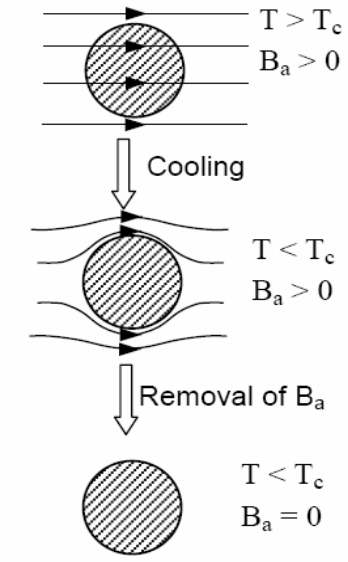

(b)

Fig 1.1 (a) A typical dependence of the resistivity on the temperature of a superconductor [1.1]; (b) The reversibility of the diamagnetism in an ideal superconductor [1.2].

Cooper pairs' binding energy can be expressed as $2\Delta \approx \gamma\, k_B T_c$, where γ is a fixed universal value according to BCS theory and varies between 1.9 to 7.0 for different materials or different phases of the same material in HTSs [1.1].

Within decades after discovery of superconductivity, it had only been observed below or around liquid helium temperature, too far away from room temperature. Searching superconductors with higher temperature is of course a great interest from the standpoint of applications.

In 1986, Bednorz and Müller discovered oxide high-temperature superconductor (HTS), which can reach 35 K [1.3] in La-M (Ba, Sr, Ca)-Cu-O ceramics at that time. After this turning point, through two-decade tremendous efforts, scientists are still working on the models and techniques. In past 20 years, cuprate HTS series have been greatly improved towards high materials quality and can be in fact nowadays be prepared in a remarkably reproducible way. However, the HTS materials quality level still need a lot more efforts to reach the standards of classical superconductors for the reasons stemming from multiple-element attributes. Because of their liquid nitrogen operating temperature, the pursuit towards real-world applications have driven intensive worldwide research activities in last two decades, which can be seen by over 100 000 related publications within this narrow field. From the perspective of applications, the potentiality of real world research and development in microwave electronics and transmission cables using YBCO has been envisioned right after the discovery of HTSs. Currently, though cooling down from its overheat status of HTS field in the last decade, many dedicated theoretical scientists as well as material scientists are still cultivating in this field to seek breakthroughs both theoretically and experimentally. In one hand, a theoretical model which can equate to the BCS

theory for the classical superconducting materials awaits to be established, in another hand, the new techniques needed to be proposed to raise the samples quality of the known HTSs, both bulks and films, also more desirable to raise operating temperature further.

1.1.2 Theory of Superconductivity

After discovery of the superconductivity and then the verification of Meissner's effect, many theoretical models have been established, including the phenomenological Landau-Ginzburg equations and the successful microscopic BCS theory.

I. The Microscopic BCS Theory

The fundamental physical picture of the BCS theory is based on the pairs of electrons (Cooper Pairs) as entities traveling through lattices without energy dissipation. In the BCS theory, it was shown that an arbitrarily small attraction between electrons in a metal can cause a paired state of electrons to have a lower energy than the Fermi energy, which implies that the pair is bounded. The attraction between electrons is indirect via electron-phonon interaction, which applies well to low temperature superconductors (LTSs). The indirect interaction proceeds when one electron interacts with the lattice and deforms it; a second electron sees the deformed lattice and adjusts itself to take

advantage of the deformation to lower its energy. This leads to phonon-mediated electron-electron interaction that dominates the electron pairing.

Several important theoretical predictions have been derived directly from BCS theory. These have been confirmed in numerous experiments as follows:

- Since the electrons are bound into Cooper pairs, a finite amount of energy is needed to break them apart into two independent electrons.
- The ratio between the value of the energy gap (binding energy of Cooper Pairs) at zero temperature and the T_c value (expressed in energy units) takes the universal value of 3.528, independent of materials.

$$E_g(0)=2\Delta(0)=3.528\ kT_c,$$

- The discontinuity of the electronic specific heat at T_c has been obtained. The specific heat $C_{es}(T)$ below T_c depends exponentially on the inverse temperature:

$$C_{es}(T)= a \exp.(-\Delta / k_B T).$$

- This is in contrast to the normal state value $C_{en}=\gamma T$. The normalized magnitude of the discontinuity is

$$(C_{es}-C_{en})_{Tc}/C_{en} = 1.43$$

- In its simplest form, BCS theory gives the superconducting transition temperature in terms of the electron-phonon coupling potential and the Debye cutoff energy:

$$k_B T_c = 1.14\hbar\omega_c e^{-1/N(0)U_0}$$

Where N (0) is the density of normal state electrons at the Fermi energy. The $\hbar\omega_c$ is related to the Debye cutoff energy. In addition, BCS theory had predicted a theoretical limit of 30 K of T_c (due to thermal vibrations).

II. The Ginzburg- Landau theory

In 1950, Ginzburg and Landau introduced a complex pseudo-wavefunction ψ to describe the superconducting electrons. According to quantum mechanics, the local density of superconducting electrons can be expressed as

$$n_s = |\psi|^2$$

$$F = F_n + \alpha|\psi|^2 + \frac{\beta}{2}|\psi|^4 + \frac{1}{2m}|(-i\hbar\nabla - 2eA)\psi|^2 + \frac{|H|^2}{2\mu_0}$$

where α and β are introduced phenomenological parameters, F_n is the free energy in the normal phase, **A** the electromagnetic vector potential, and **H** the magnetic field. Ginzburg-Landau equations were derived by simply minimizing the free energy with respect to fluctuations in the order parameter and the vector potential.

$$\alpha\Psi + \beta|\Psi|^2\Psi + \frac{1}{2m}(-i\hbar\nabla - 2eA)^2\psi = 0$$

$$J = \frac{2e}{m}[\Psi^*(-i\hbar\nabla - 2eA)\psi]$$

where **J** is the electrical current density. The first equation determines the order parameter ψ based on the applied magnetic field. The second equation provides the superconducting current. The Ginzburg-Landau equations have brought many interesting results. Perhaps the well known is the prediction of the existence of two characteristic lengths in a superconductor. The first is called as coherence length, denoted by ξ, given by

$$\xi = \sqrt{\frac{\hbar^2}{2m|\alpha|}}.$$

This characteristic length describes the size of thermodynamic fluctuations in the superconducting phase. The second characteristic length is the London penetration depth, denoted by λ and given by

$$\lambda = \sqrt{\frac{m}{4\mu_0 e^2 \psi_0^2}}$$

where ψ_0 is the equilibrium value of the order parameter in zero electromagnetic field. The ratio $\kappa = \lambda/\xi$ is called as the Ginzburg-Landau parameter, which is used to differentiate Type I and Type II superconductors. Type I superconductors are those with $\kappa < 1/\sqrt{2}$, and Type II superconductors are those with $\kappa > 1/\sqrt{2}$.

1.1.3 Type I and Type II Superconductors and Flux Pinning

Type I and Type II superconductors have dramatically different behaviors in applied magnetic field H. Type I superconductor includes most metals, such as titanium, aluminum, tin, mercury, and lead. The superconductivity in these materials is destroyed when H exceeds the thermodynamic critical field H_c, below which the Meissner state prevails. The value of H_c is related to the free-energy difference between the normal and the superconducting state.

In type II superconductors, two critcal fields: lower critical field H_{c1} and upper critical field H_{c2} exist. Below H_{c1}, the superconductor is in the Messiner state and magnetic flux penetration starts when H exceeds H_{c1} while superconducting state remains. With increasing H, more magnetic flux penetrate into the superconductor and the superconducting state is destroyed when H reaches H_{c2}. While the class of type-I superconductors is composed entirely of metallic chemical elements, type-II superconductors may be metal alloys or even some pure metals, such as Niobium (Nb) and Vanadium (V), and also different oxide compounds. All metals and metal alloys have their T_c below 30 K and are referred to as low temperature superconductors (LTS), while the oxide superconductors have their T_c above 30 K and are referred to as high temperature superconductors (HTS).

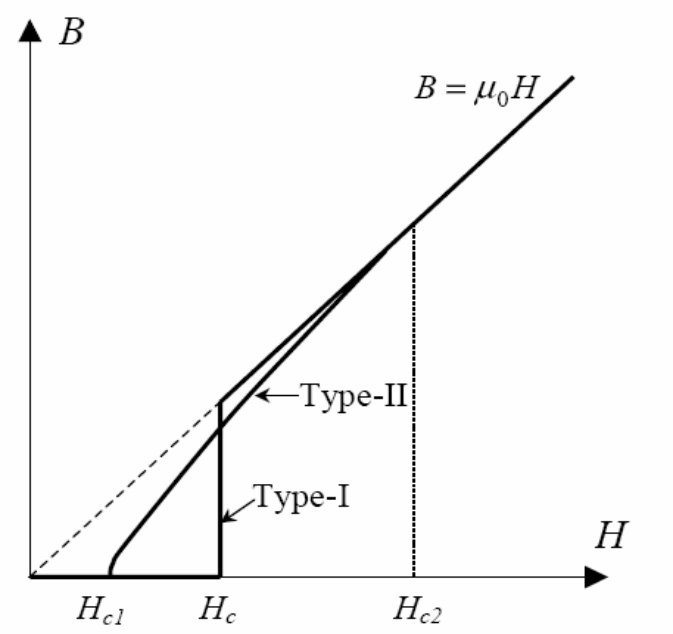

Fig 1.2 Comparison of flux penetration behavior of type-I and type-II superconductors with the same thermo-dynamic critical field H_c [1.1]

The flux penetration (B-H) curves in type-I and type-II superconductors are depicted in the Fig. 1.2. A great advantage of type-II superconductors is that a substantial critical current is present in the presence of H, which is critical to real applications. Researches on flux pinning, flux creep, and flux flow in type II superconductors in the so-called mixed state ($H_{c1}<H<H_{c2}$) have been the long term topics for many groups. In the mixed state, the existence of normal regions in the superconducting material is allowed [Fig. 1.3(a) and (b)]. When electric current with density *J* is carried by a type-II superconductor, it passes the flux lines and creates a Lorenz force $F_L = J \times \Phi_0$ upon each vortex. The quantized magnetic flux or fluxons will remain in place as long as the pinning force F_0 on them is larger than the Lorenz force F_L.

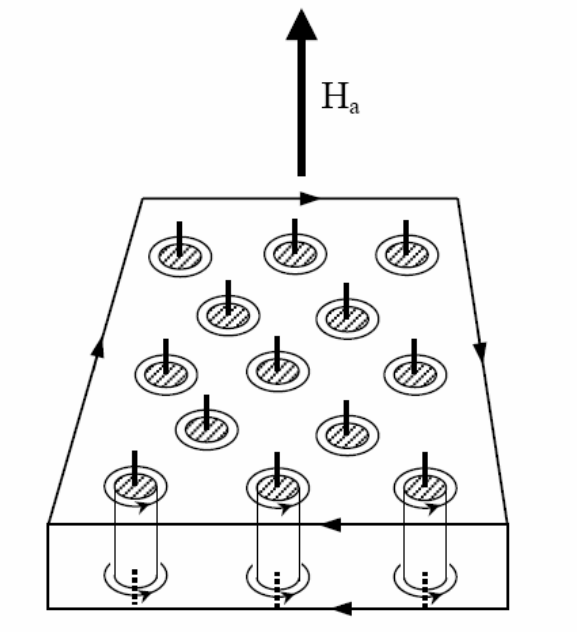

(a)

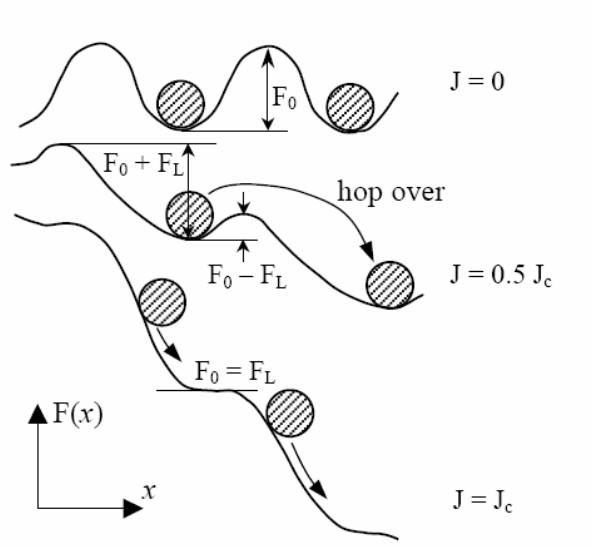

(b)

Fig 1.3 (a) The mixed state, showing normal cores and encircling supercurrent vortices; (b) Mechanism of flux-flow. The presence of current in a magnetic field generates a Lorentz force, which tilts the staircase, allowing flux lines to hop out of their pinning wells more easily [1.2].

At critical current density J_c, the Lorentz force will become greater than the pinning strength, and fluxons will start to move [also see the drawing in Fig. 1.3 (b)]. This movement is referred to as *flux-flow*. J_c is an important parameter, above which the material becomes resistive. In HTS, certain fluxon motion may be activated by thermal fluctuation of the fluxons; this motion is slower and random so it is called *flux-creep*.

1.2 Layered Structure of HTS

1.2.1 The Features of Layered Structure in HTS

HTSs are type II superconductors. This, together with their high Tc values, make them promising candidates for superconducting devices including passive microwave devices, power transmission cables and other electric devices and systems. A main striking feature of cuprate superconductors is in their layered structure, as shown in Fig. 1.4. Almost all HTSs discovered so far can be represented by a generic formula $A_mE_2R_{n-1}Cu_nO_{2n+m+n}$, where A, E, and R are various cations, often with E = Ba, Sr, or Ca, and R = Ca or a rare-earth element (see Fig. 1.4). They can be represented simply by Am2(n-1)n. For example, Hg-1212, Tl-2212, and Hg-1223, we are going to use this notation frequently in the rest of my thesis.

In order to show clearly the stacking sequence of this layered structure, $A_mE_2R_{n-1}Cu_nO_{2n+m+n}$ can also be written as $(EO)(AO)_m(EO)]\{(CuO_2)\ [R(CuO_2)]_{n-1}\}$, illustrating the order of m (AO)-layers inserted between 2 (EO)-layers on top

of *n* (CuO2)-layers interleaved by (n-1) R-layers. As a result, *n* describes the number of (CuO2)-layers per unit formula. The (AO)-layer may be replaced by a complex oxide slab, or the R-layer by a complex (RO)-slab. Although they are fairly complex at first glance, these layers can be grouped into two blocks: the charge reservoir block (CRB) of $(EO)(AO)_m(EO)]$ and the active block (AC) of $\{(CuO_2)[R(CuO_2)]_{n-1}\}$. The CuO_2 layers, which exist in all the HTS, are believed to be the location of the mobile charge carriers in the cuprate family of HTS compounds.

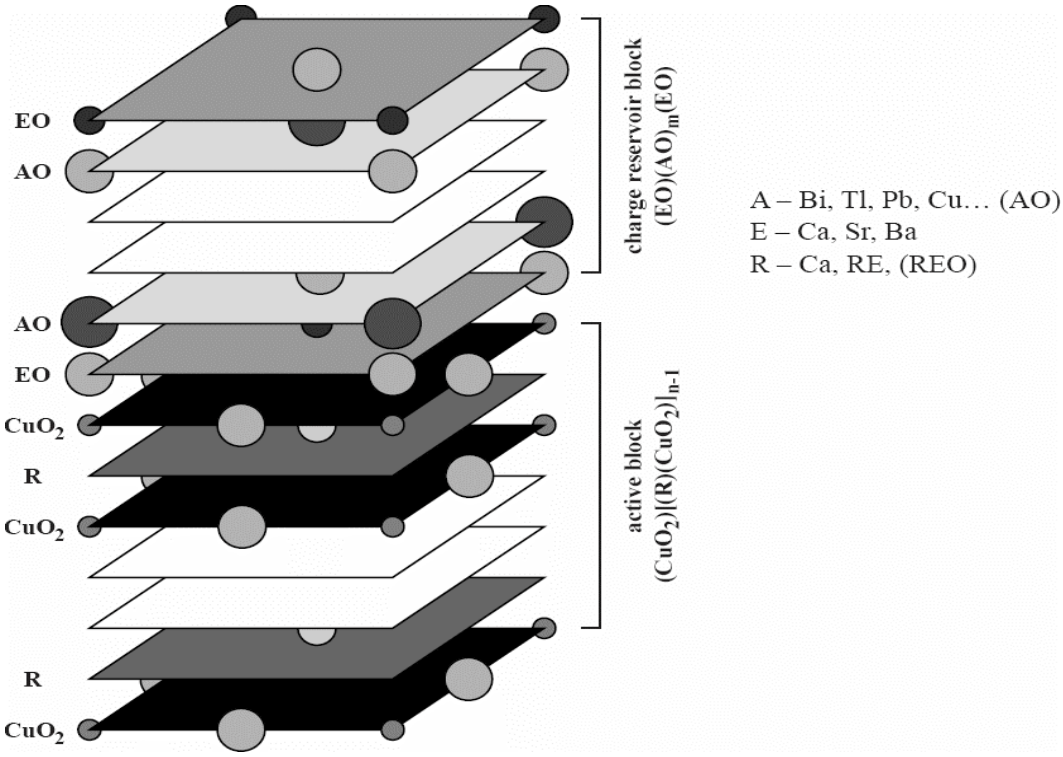

Fig 1.4 Typical layered structure of the cuprate HTS, two dimensional superconductor [1.4].

HTS materials are extreme type-II superconductors with penetration length $\lambda > 100$ nm and coherent length ξ up to 1 nm. This extreme short ξ

(comparable to the crystallographic length, a, b) make the HTSs special in many ways. The superconductive coupling between these CuO_2 layers [within a given $(CuO_2/Ca/)_{n-1}CuO_2$ stack ("interlayer coupling")] is much weaker than the intralayer coupling within the CuO_2 layers, but still much stronger than the coupling between the $(CuO_2/Ca/)_{n-1}CuO_2$ stacks which can be described as Josephson coupling [Fig. 1.5(a)] [1.5].

This quasi-two-dimensional nature of superconductivity in HTS materials leads to remarkable anisotropy of the superconducting properties. The J_c along the CuO_2 planes is much higher than that in the perpendicular direction, (a property which is not at all appreciated with respect to technical applications but can be compensated by additional engineering efforts). In some superconductors, material imperfections with the dimension of the coherence length can serve as "parking area" for vertex cores. As shown in the Fig. 1.5(b), without these pinning centers, each layer has its own pancake vortex, much flexible and independent. This is called quasi-disintegration of magnetic vortices. To bring HTS materials into broader applications, there are many techniques have been developed to increase the flux pinning effect and hence J_c. For example, one can use high energy ion beams to generate columnar defects, which provide correlated pinning when vortices are aligned with them and much enhanced J_c has been obtained.

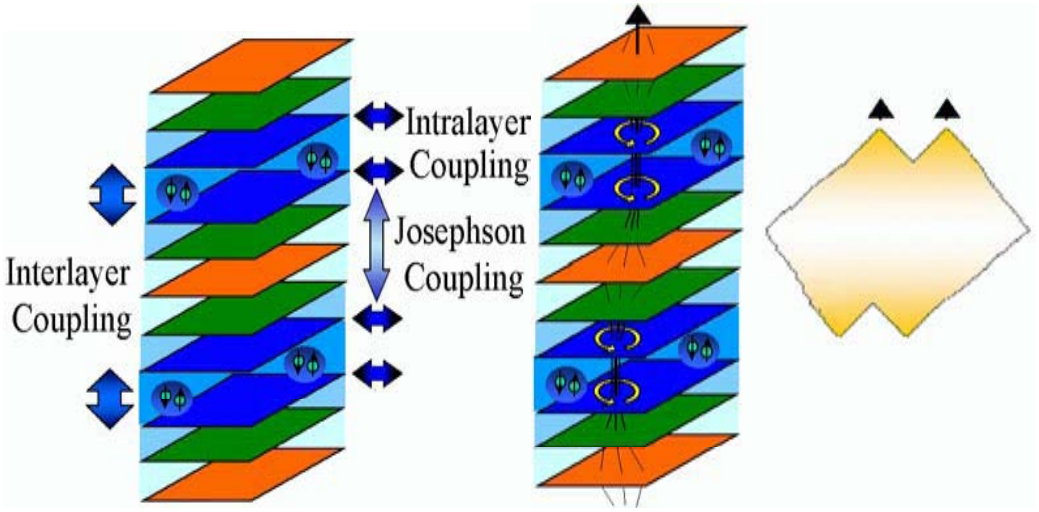

(a) (b)

Fig 1.5 Schematic diagram showing (a) Short coherence length and weak interlayer coupling; (b) Pancake vortices due to weak SC interlayer coupling [1.5]

1.2.2 Hg-Based HTSs and Their Special Features

Fig. 1.6 depicts the structure of the Hg-based HTSs, which have the highest Tc above 130 K among superconductors so far discovered.

The blocks $(BaO)(HgO_{\delta})(BaO)$ have the rock-salt structure, with a thickness of about 5.5 Å. The alternating blocks (CuO_2) $[(Ca)(CuO_2)]_{(n-1)}$ have a perovskite-like structure, with an approximate thickness of [4.0 + 3.16(n-1)] Å. The crystal structures for n = 1, 2, and 3 are schematically illustrated in the figure above.

The crystal structures of Hg-based HTSs consist of two generic building blocks: the vital, superconducting copper-oxide layers or planes, and the insulating block layers, which can act as electronically active charge-reservoirs for hole or electron donation to the copper-oxygen layers.

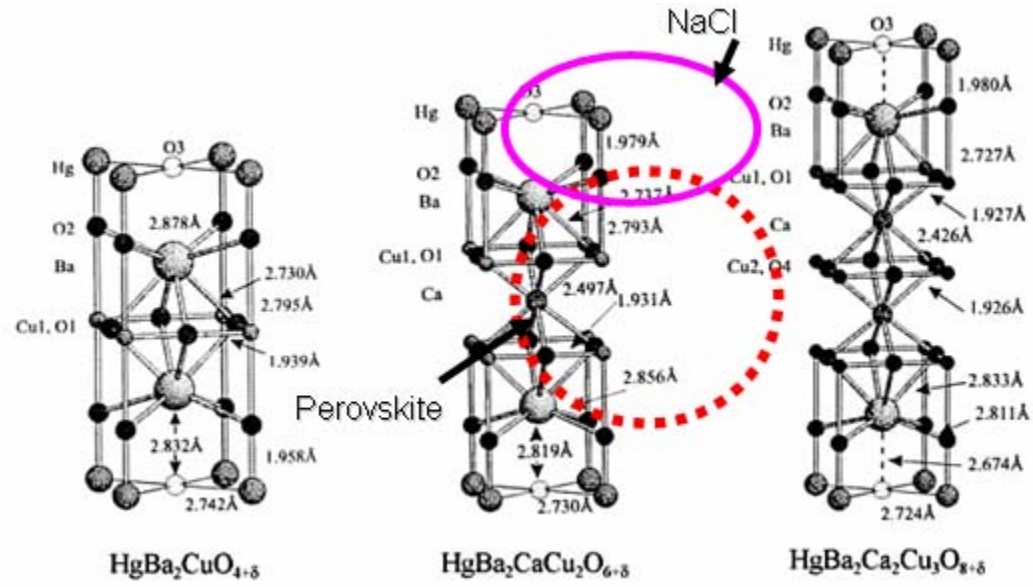

Fig 1.6 Crystal structures of mercurocuprate HTS:$HgBa_2Ca_{n-1}Cu_nO_{2n+2+\delta}$ [1.6]

At the Hg atom site, many other kinds of atoms can fit in also to form superconductors with suitable oxygen off stoichiometric ratio. Some researchers (among them are Antipov's research group) argued that Hg atoms are the best fit because of the weak bond between Hg and O3. This weak bond actually, has less impact on the bond between Hg and O2, thus the Cu-O1 plane near the perfect plane, so the superconducting properties are the best [1.7]. This picture is in agreement with the pressure dependence of the T_c number. Hg-atoms are the best candidates for the highest T_c without external pressure. Actually, the angle for the Cu-O1 plane is not most ideal one. When an external pressure is applied, this angle can be adjusted towards the ideal value and higher T_c~166±1 K was

observed on fluorinated Hg-1223 at 23 GPa. At higher pressures, T_c begins to decrease because the distortion pushes the Hg O1 plane over the best configuration [1.7].

In fact, the real case is more complex in these multiple elements (quaternary) compounds. However, this simple physical picture can provide us a rough guidance when we want to optimize the properties by doping. We will come back to this point later in my research work.

Interestingly, the T_c dependence on the periodic elemental table is shown from the peer publications [1.8]. From the table there is an increase moving in the periodic table from Pb to Hg. However, continuing to Au, the reported T_c is already substantially lower. The trend is believed to be related to the chemical A-O bond [1.8]. Actually, the ionic radii are complicated, the valence are also playing active roles. However, we can conclude, the different elements occupy the same site result in very different superconducting properties.

Another trend can also be seen from this table, that is: when the number of CuO_2 layer increases, namely, the number n increases in the general HTS formula, the T_c increases monotonously at beginning, it peaked for a certain number. However, many HTS scientists believe, the peak come from the limitation of the difficulties of post oxygenation, as well as from the difficulties of the sample preparation, because it is believed that the more CuO_2 layers are formed from so called “stack faults”. This means that after formation of Hg-1212, another stack of CuO_2 need to squeeze into the lattice, by intercalation. Therefore, one can

imagine the difficulties in the preparation of the high quality materials, in the forms of films or bulk.

1.2.3. The Unique Properties of Hg-Based HTSs

Among a few HTSs that have T_c above 100 K, Hg-based cuprate family (usually formulated as $HgBa_2Ca_{(n-1)}Cu_nO_{(2n+2+\delta)}$, n =1, 2, 3), has attracted a great attention since first reported concerning this family in 1991 [1.9-1.18]. Two members, $HgBa_2CaCu_2O_{(6+\delta)}$ (Hg-1212, n=2) and $HgBa_2Ca_2Cu_3O_{(8+\delta)}$ (Hg-1223 n=3) have stood out with excellent superconducting properties. Their remarkable T_c values at ambient pressure, 124 K and 135 K, respectively, as well as critical current density (J_c) up to 1MA/cm^2 at 100K and self-field, have indeed made them very attractive in high current-density applications and devices operating at above 100 K.

Considering high T_c and J_c values, growth of high quality epitaxial Hg-based HTS thin films is highly desirable for numerous applications. However, high quality Hg-based HTS films are extremely difficult to be achieved due to their intrinsic compositions of multiple elements plus their highly volatile nature of Hg-based compounds. In addition, as a further complication, the large numbers of adjacent phases in the phase diagram constituted by the contributing elements hamper the preparation of phase pure samples, because the formation enthalpy of the compound in one form differs only slightly from that in another. A

sophisticated process control during sample preparation is essential in order to reduce the yield of samples.

1.3 Application of HTS at Microwave Frequencies

Over the last decade and a half, research on the microwave applications of HTSs has been active and fruitful. The increasing interest was brought about by the perceived potential on the marketability of superconducting electronics especially in the wireless communications industry [1.19,1.20]. A large variety of passive microwave devices have already been fabricated and characterized using different HTSs including $YBa_2Cu_3O_7$ (YBCO) and $Tl_2Ba_2CaCu_2O_8$ (Tl-2212) [1.21-24]. The much improved performance of these HTS microwave devices over their normal metal counterparts has been attributed to the nearly an order of magnitude lower microwave surface resistance R_s of HTS films, which can only be realized when the HTS devices are kept at liquid nitrogen temperature of 77 K much below their T_c. Since a higher operation temperature implies lower capital cost and system maintenance, HTS materials are advantageous for practical applications such as microwave bandpass filters. Again, Hg-1212 is among few HTSs with a T_c exceeding 120 K. Although comparable R_s [1.25] and power handling capability [1.26] to that of YBCO and Tl-2212 at 77 K have been observed on Hg-1212 films at much higher temperatures, little progress has been made so far in application of Hg-1212 in microwave devices due to the difficulties in epitaxy of large-area Hg-1212 films with sufficient uniformity. The

development of a cation exchange process [1.16] has resolved some major technical issues in Hg-1212 film epitaxy and Hg-1212 films of dimension of 12×12 mm^2 have been achieved recently [1.27]. Using this technique, we have successfully fabricated two-pole *X*-band microstrip filters with Hg-1212 films and characterized their microwave performance. The two-pole filter was selected because of its simplicity in the design and ease in fabrication and packaging.

Studying the nonlinearity of microwave properties in HTS thin film devices is of great importance for both applications and fundamental science. From the viewpoint of applications, power handling capability of HTS films has been substantially limited the applications HTS microwave devices since nonlinearity deteriorates performance of the linear devices (filters, delay lines, antennas) and hinders the optimization of properties of nonlinear devices (modulators, switches, power limiters). At the standpoint of fundamental science, delving into nonlinear properties allows the study of the dynamics of various types of vortices in a unique way. It is believed that the power handling of HTS films in the current state is most likely limited by extrinsic sources, such as growth defects and impurities within the films. To identify the extrinsic origins of nonlinearity, it is appropriate to correlate microwave, DC and morphological characterizations

Microwave nonlinear properties of HTS films are usually studied by measuring (i) the power dependence of the surface impedance, (ii) harmonic

generation and (iii) intermodulation distortion (IMD). Intermodulation distortion has been chosen to investigate the nonlinearity in this research work.

My research work on microwave mostly concentrates on the nonlinear properties in Hg-1212 films, with comparison with $Tl_2Ba_2CaCu_2O_x$(Tl-2212) and $YBa_2Cu_3O_{7-\delta}$ (YBCO) films. Taking the advantage of the great progress made in the fabrication of Hg-based HTS fims, some pioneer works have been performed to fill the blank along this line.

Chapter 2

Development of Cation Exchange Process for Epitaxy of High Quality Hg-1212 Films

2.1 Difficulties in Preparation of Hg-based HTSs

The conventional *ex situ* thermal-reaction process, which has been extensively employed in preparation of Hg-HTS films, consists of two consecutive steps (Fig. 2.1). In the first step, an amorphous Ba-Ca-Cu-O precursor film is fabricated by any of several film deposition techniques such as pulse laser deposition (PLD), magnetron sputtering, electron-beam, chemical vapor deposition, etc [2.1]. Then the amorphous Ba-Ca-Cu-O precursor is reacted in an evacuated quartz tube at high temperature around 800ºC, in controlled high Hg-vapor pressure (5 to 10 atms) to form Hg-HTSs. The method of precursor deposition (first step) is less important than the post-annealing (second step). There are only three criteria that precursor films must meet to be used for successful growth of good HTS films. First of all, it is important that the precursor films be chemically stable in air to maintain both good adhesion to the substrates and to remain chemically pure. Second, it is also helpful to have the elements homogeneously mixed to limit the atomic diffusion necessary to form crystalline structures. Finally, the precise cation composition of the precursor film on the

desired stoichiometry or off-stoichiometry is very important[2.1]. Having prepared precursor films meeting three criteria mentioned above, now one can move to next crucial step, the annealing process, in which is really the science of growing HTS films. From the above brief overview about the HTS cuprates, it is no surprise to see overwhelming difficulties in the fabrications of the Hg-HTS samples with conventional thermal-reaction process.

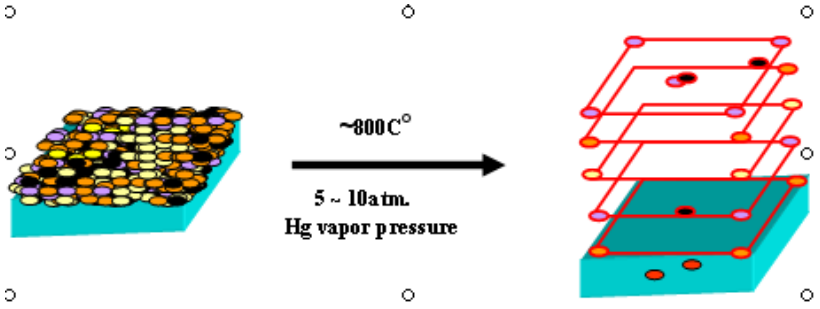

Fig 2.1 Schematic description of the conventional thermal-reaction process in which a material is formed via reaction of simple-compound precursor

The difficulties in epitaxial growth of Hg-HTS thin films are at least threefold. Firstly, it is nearly impossible to accurately control the processing parameters, such as Hg-vapor pressure, due to the highly volatile nature of the Hg-based compounds. Actually, the Hg-based compounds have much lower decomposition temperature, around 470ºC. When using these compounds as vapor source, technically speaking, it is extremely hard to control a constant pressure. From the brief analysis last paragraph base on the thermodynamic phase stability research performed within last decade on the HTS's, this results in typically multiple superconducting impurities in Hg-HTS samples, which substantially

degrades the sample quality [2.1]. Secondly, Hg vapor reacts with most metals as well as oxides, which prohibits epitaxial growth of Hg-HTS thin films on most technologically compatible substrates. Even on a few chemically stable substrates such as $SrTiO_3$, serious film/substrate interface chemical diffusion was observed. Consequently, most Hg-HTS films have to be made with large thickness (~1μm) and most of them are c-axis oriented uniaxial films with rough surfaces. Finally, the precursors are extremely sensitive to the air to form nonsuperconducting phases such as $Ca(OH)_2$ and $CaCO_3$ phases which are hardly to decompose at processing temperature ~800ºC. To overcome three main difficulties, some time-consuming processes need to be applied, such as two-zone furnace processing and glove-box processing. Tremendous efforts have indeed been recompensed by some successes [2.2] although still far away from standards of the real world applications.

2.2. Novel Cation Exchange Process and its Advantages

2.2.1. Cation Exchange Processing

In order to circumvent these difficulties in epitaxy of Hg-1212 films, our group has developed a simple diffusive cation exchange technique (Wu,Yan and Xie,1999) [2.3]. This process employs an epitaxial precursor matrix, instead of an amorphous precursor film, and achieves epitaxial Hg-HTS films via replacement of certain cations in the precursor matrix. The schematic diagram shown in Fig. 2.2 illustrates the cation exchange process. In the cation-exchange process, the

precursor matrices are chosen to have a similar structure and composition to that of the target material. There is at least one weakly bonded cation (cation "A") to be replaced later by another cation (cation "B") to form the target material. When the cation A is perturbed using various methods such as thermal heating or light/particle-beam irradiation, it will vibrate around the equilibrium site where the Gibbs free energy is minimized. The spatial deflection of the cation A is proportional to the energy of perturbation. When the threshold perturbation energy (U_{th}) is reached, at which the deflection of cation A is comparable to the lattice constant, the cation A may escape from the site where it originally occupies, leave the vacant site temporarily in the precursor matrix. In the cation exchange process, however, the temperature, hence the perturbation energy is purposely maintained to be close to a point so that the cation A is slowly escaping. If the population of cation B in the mixed vapor of cation B+A is dominant, the vacant site left behind by cation A will be occupied soon by cation B. One can see that similar replacement can takes place for every single site after enough time given to the processing and finally the target material is formed (refer to the cartoon in Fig. 2.2 below).

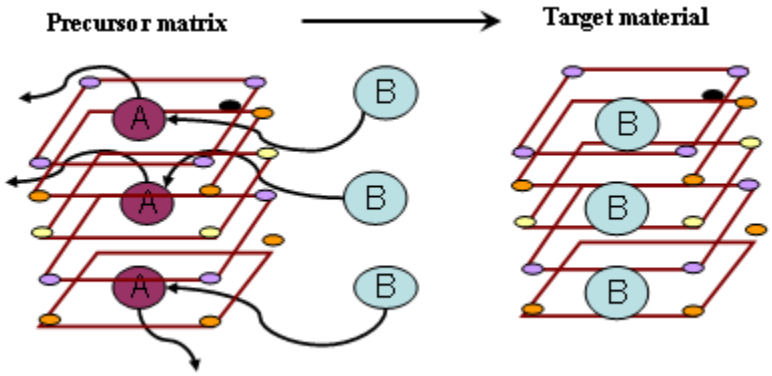

Fig 2.2 Schematic description of the cation-exchange process in which the same material is formed by replacement of a weakly bonded cation A in a precursor matrix by a volatile cation B.

Using cation exchange process, the epitaxial Hg-1212 films have been obtained successfully from both epitaxial $Tl_2Ba_2CaCu_2O_8$ (Tl-2212) and $TlBa_2CaCu_2O_8$ (Tl-1212) "precursor" films by replacing Tl cations on the lattice with Hg ones [2.3-2.5] since (1) Tl-HTS's are much less volatile, insensitive to air, and easy to be obtained; (2) Tl-HTS's have nearly the similar structures to that of Hg-HTS's . Fig.2.3 shows the conversion from Tl-1212 or Tl-2212 to Hg-1212 films during cation exchange.

In this newly developed cation exchange processing, the sample fabrication consisted of two steps: (1) preparation of epitaxial Tl-2212 precursor films was followed by (2) conversion to epitaxial Hg-1212 films via Tl-Hg cation exchange. In the first step, the precursor Tl-2212 thin films were deposited on single crystal (100) $LaAlO_3$ substrate at room temperature using dc magnetron sputtering from a pair of Tl-2212 superconducting targets. A gas mixture of argon and oxygen at a ratio of 4:1 was used for sputtering process. The as-deposited Tl-

2212 films were amorphous and nonsuperconducting. Superconductivity and epitaxy were obtained after these films were annealed in a closed Al_2O_3 crucible together with a pressed Tl-2212 pellet (Tl vapor source) and annealed at 820°C for 1 h. It is worth pointing out here that unlike Hg vapor Tl is much less reactive with substrates. In the second step, the Tl-2212 superconducting films obtained from the previous step were sealed in an evacuated quartz tube together with two pellets. One pellet was an unreacted Hg $Ba_2Ca_2Cu_3O_x$ pellet as Hg vapor source and the other, a $Ba_2Ca_2Cu_3O_x$ pellet as Hg vapor absorber to balance the pressure of the Hg vapor. The weight ratio between the former and the latter was 3:1. The entire assembly was kept in a furnace at 700°C which is close to the threshold perturbation energy ($U_{th}=k_BT_{th,}$ 700°C) of Tl-2212 film for 12 h. The Hg-1212 films were then annealed in flowing oxygen at 300°C for 3 h to optimize their oxygen composition. In this second step, the Hg vapor, which consist of high speed flying molecules, cannot bombard the substrates directly, have much less chances to diffuse into the substrates. In addition, because the crucial second step in the cation exchange processing is most diffusive [2.6, 2.7], the requirement for the controlling of Hg vapor pressure is much relaxed, the formation of poly phase sample will be reduced dramatically. The extensive experiments done in our group have supported this mechanism analysis here.

When Tl-2212 film is chosen as the precursor film, the two Tl-O layers will collapse into one Hg-O layer to form Hg-1212 film during cation exchange.

The collapse will result in a disorder along a-b plane and the formation of the voids, which we will mainly discuss later on.

2.2.2. Mechanism study of cation-exchange process

I. Threshold of the cation exchange

Because the cation–exchange process is a powerful way to prepare high quality epitaxial Hg-HTSs films, the study of the mechanism is significantly important to harness the processing to reproducibly generate thin films and devices made of thin films. Some primary work done in our group paved a path into this unexplored area. Firstly, it was confirmed that the cation exchange is perturbation process that can performed in a large window of the processing temperature. In fact, the Tl-Hg cation exchange was observed at the temperature as low as 620ºC (sublimation temperature of HgO source is around 570ºC), which is substantially lower than that required for the conventional process (typically ~ 800ºC or higher for Hg-1212 phase). The rate of the cation exchange was proved to increase monotonically with the operating temperature. For the same annealing time, the completion of the cation exchange depended on the processing temperature [2.9].

In the straightforward experiments, a possibility of cation exchange is verified to qualitatively follow a relationship $\sim\exp(-U_{th}/k_BT)$, where $U_{th}=kT_{th}$ is crystal lattice decomposing energy and k_B is Boltzmann's constant. To find out U_{th}'s for Tl-1212, Tl-2212, and Hg-1212 films, Tl-2212, Tl-1212, and Hg-1212

films were heated at 0.8 atm O_2 up to different temperatures and stayed for 1 h and cooled down back to room temperature [see Fig. 2.4].

After each thermal cycle, the XRD θ-2θ spectra, T_cs and J_cs of the samples were measured. At low temperature, the values were almost constant, however, when the temperature reached over a certain temperature, the normalized J_cs experienced a sharp drop ($T_{th,onset}$) and became zero at slightly higher temperatures ($T_{th,zero}$). The sharp drop in J_cs was found to be accompanied by dimishing of (001) peaks in the XRD spectra of the film, signaling collapse of the crystal lattice. Taking the midpoint between the $T_{th,onset}$ and $T_{th,zero}$ as T_{th}, the T_{th}s for Tl-1212, Tl-2212, and Hg-1212 were 620ºC, 680ºC, and 780ºC (Fig.2.4). The T_{th} defines the upper limit of the perturbation energy one might provide to a precursor matrix without destroying it. The experiments thus performed has confirmed this speculation, beyond this limit, the degraded quality of the films indicated dramatic lattice collapsing [2.9].

One can see that T_{th} for Hg-1212 is slightly higher than that of Tl-1212 and Tl-2212. From the picture given above, it is expected that the cation exchange from Hg-1212 to Tl-1212 is harder, thus need higher operating temperature. This speculation was agreed with the experiments performed for verifying reversibility in our group.

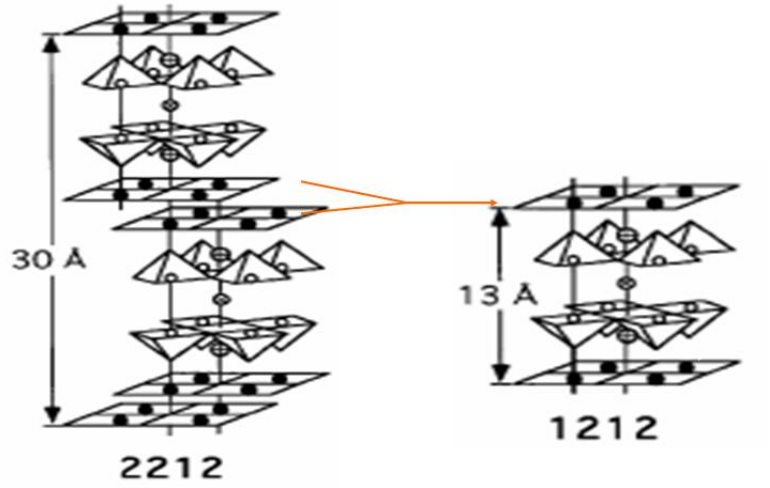

Fig 2.3 Using different precursor structure Tl-2212 film, the lattice shrinks in c-axis by ~13.3% (c=2.93nm to 1.27nm). [2.3]

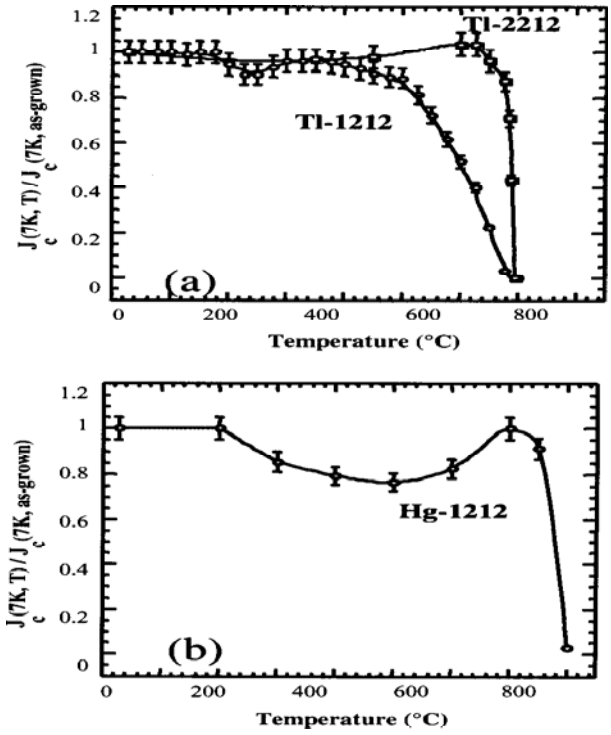

Fig 2.4 Dependence of superconducting properties on the operating temperature [2.9]

II. Diffusion mechanism in cation exchange

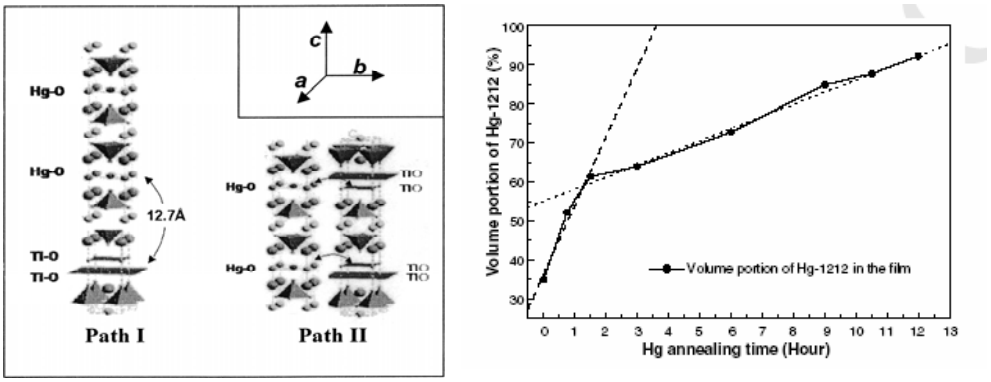

(a) (b)

Fig. 2.5. (a) Schematic of the diffusion mechanism in cation exchange, Path I: layer-by-layer along c-axis Path II : By channeling through vertical defects and then along a-b plane the rate along a-b plane is faster than that along c axis [2.6]; (b) The Hg-1212 volume portion converted from Tl-2212 precursor film in the Hg – Tl cation exchange process is plotted as a function of the processing time. The dashed and dotted lines are linear fitting of the period from t=0 to 1.5 h and the period from t=1.5 to 12 h, respectively [2.7].

For the HTS materials, it is well known for their layered structures. In these layered structure, it is reasonable to believe that there are two diffusion direction, Path I: cation diffusion occurs layer by layer along the c-a axis, and Path II: by channeling through vertical defects in the films such as voids and growth defects, and then moving laterally along the a-b planes into grains [see Fig. 2.5(a) below][2.6]. Which diffusion process is dominant? The experimental results suggest that the pathway of Hg cations in thin films (thickness < 0.5 μm) is to channel through defects across the thickness of the films then diffuse into grains along a-b planes and vice versa for Tl cations. A two stage model has been proposed to explain the conversion from Tl-2212 to Hg-1212. At the first stage,

Tl-2212 collapse structurally into 1212 that contains both Hg and Tl when Hg diffuses into grains, while at the second stage Tl cations diffuse out while Hg cations diffuse in, resulting in the formation of pure Hg-1212 phase. A time constant τ_1 about 45-60 min was found for the first stage and the time constant τ_2 beyond 2 τ_1 for the second stage [refer to Fig. 2.5 (b)] [2.7].

2.3 Comparison between Cation Exchange and Conventional Methodology

In order to draw a clearer picture about the efficacy of the cation exchange, let us choose the best values available and compare them with ones from cation exchange processing. The table below lists some typical parameters which are critical for real world applications. It is worthwhile to point out that for extremely thin films, range from 50 nm to 80 nm, conventional methodology can hardly fabricate any films, neither for films deposited on the metal substrates.

If merely judging from the plain numbers in the table above, one may put a question mark on advantage of the cation exchange methodology. However, if one knows that all the films from conventional processing come from time-consuming dry-box operating with very low reproducibility, he (she) will happily select highly reproducible cation exchange processing, which can be operated in the air without anxiety about the degradation stemming from the carbon dioxide and moisture.

Table I Comparison of critical superconducting properties of films fabricated from conventional processing and cation exchange one.

Film/substrates	method	Phase purity/ Thickness	Tc(K)	Jc(5K)/(77K)/(100K) (MA/cm^2), H=0
Hg-1212/$LaAlO_3$	Conventional	Pure/200-300nm	116-124K	20/3/1.5
	Cation exchange	Pure/200-300nm	120-125K	20-40/2-5/0.5-2
Hg-1223/$LaAlO_3$	Conventional	Predomin/200-300nm	120-128K	13/1.4/1.5
	Cation exchange	Pure/300-500nm	125-130K	10-20/1-1.5/0.1-0.5
Hg-1212/$LaAlO_3$	Cation exchange	Pure/50-80nm	110-118K	5-10/0.7-1.1/0.1-0.4
Hg-1212/Ni	Cation exchange	Predomin/300-800nm	123-125K	5-10/1-2/0.5-0.7

2.4. Some Solid Works Done in Our Group Using Cation Exchange

- **Surface morphology improvement**

Although the collapse of the lattice has been evidenced in the conversion between Tl-2212 and Hg-1212, the surface morphology of the resulted Hg-1212 films have shown surprisingly good quality, namely, they are much smoother than its counterparts fabricated from the conventional processing, provided the amorphous precursor films from the same sputtering processing were chosen for better comparison. Judging from the fairly good surface morphology and X-ray diffraction data, it seemed that the collapsing of the lattice is contained the scale close atomic dimension or so. It is worth pointing out this better surface can only be achieved when the operating temperature is lower than a certain threshold. The remarkable surface improvement of the Hg-HTS film made in the cation exchange process resulted in much better value of J_c, which has exceeded $1x10^6$ $A.cm^{-2}$ at T=100 K.

- **Low microwave surface resistance**

It is no surprise that the better surface morphology can result in low microwave surface resistance. In Hg-HTS films fabricated from cation exchange methodology, the value similar to that of other HTS at 77 K, was observed at temperature above 100 K. (10 GHz, ~0.2 mΩ at 77 K, and 0.3 m Ω at 120 K for Hg-1212 film). This result suggests that Hg-1212 films are very promising for microwave applications above 100 K [2.10, 2.11].

- **A large processing window**

Cation exchange shows a different growth mechanism from conventional thermal reaction process which requires stringent phase equilibrium.

a. Films processed at dramatically different Hg vapor pressure P_{Hg} of $1.0P_0$, $0.75P_0$, and $0.5P_0$ have nearly identical T_cs and J_cs.

b. The processing temperature range falls in range from 700ºC to 780ºC.

This flexible pressure and temperature requirements have indeed open a door to modification of the Hg-HTS films to meet real world applications (see Fig. 2.6) [2.3].

- **Hg-HTS coated conductors**

Hg-1212 films have been coated on biaxially textured Ni substrates buffered with CeO_2/YSZ/CeO_2 trilayers with T_c=124 K, J_c=2.23×10^6 A/cm^2 at 77 K and J_c= $0.73\text{x}10^6$ A/cm^2 at 100 K [2.12].

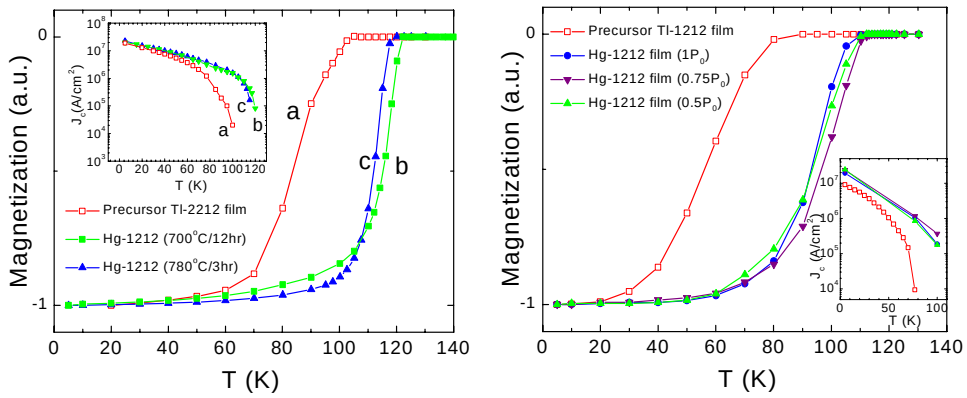

Fig. 2.6 Large windows of processing temperature and vapor pressure have been shown.

➢ **Critical current density**

Critical current density is doubled by fluorine-assisted oxygen overdoping. It has been seen that the fluorine-assisted method help the diffusion of the oxygen into the film as well as the uniformity. The crystallographic constant versus doping (annealing time) is also shown in the experiments [2.13].

➢ **Sample dimension**

Using cation exchange process, Hg-1212 films of 12x12mm^2 with uniform superconducting properties had been prepared [2.13].

➢ **Micro-strips fabrication**

Micro-strips made of Tl-1212 films applying standard photolithography and converted to Hg-1212 devices in cation exchange process successfully.

From the works just reviewed, we can see that the cation exchange processing has indeed shed bright light to road towards further improvement of the film fabrications. Using this cation-exchange technique, one can circumvent the multifold road blocks confronted in the conventional processing. Further efforts in microwave applications will demonstrate the power of the cation exchange methodology.

2.5 Critical Issues Remained in Cation Exchange Processing

2.5.1 Voids on the Surface of Hg-HTS Films

Although the cation-exchange process provides a simple and highly reproducible method for epitaxy of Hg-1212 films, these films are by no means optimized, a number of large-size voids on the film surfaces still worry us. From the SEM picture (Fig. 2.7) we can see a remarkable difference from the films after conversion into the Hg-based films from Tl-2212 films. The range of the voids dimension is from submicrometer to several micrometers. As we reviewed in the last section, there are several possible reasons for the formation of the voids. The first reason is that the voids may be formed as the vertical channels for Tl-Hg exchange. Since no similar voids were observed on Hg-1212 films converted from Tl-1212, the

voids formed in Hg-1212 film might be the exits through them the extra Tl cations were evacuated out. The second cause might be the thermal fluctuation, which shakes off a large number of Tl atoms from their equilibrium sites in the lattice simultaneously, and hence results in collapse of the lattice at macroscopic scale to form voids. The last possible reason is the lattice collapse due to the conversion from double-layer Tl-O to single-layer Hg-O, resulting in a disorder (dislocation) along a-b plane and causing the formation of the voids.

These voids can be scattering centers to electromagnetic waves that are propagating along the superconducting films and cause significant loss. This might explain the lower microwave power handling capability of Hg-1212 films in the normalized temperature scale as compared to its yttrium barium copper oxide and Tl-2212 counterparts. Moreover, these voids provide entrance channels for moisture and other contaminants, making Hg-1212 films vulnerable even in standard characterization and device fabrication processes. This problem may be partially solved by lowering cation exchange processing temperature so as to reduce the probability that many Tl cations are thermally excited out of the lattice simultaneously from the same local area. Indeed, the void population was reduced [15] when the processing temperature was decreased from ~800 °C to ~700 °C but the dimension of the voids remained more or less the same. This is not surprising since simply lowering the processing temperature does not imply

a fine control over the Tl diffusion pattern at a microscopic scale. In addition, the cation exchange becomes much less efficient at temperatures close to the binding energy of Tl cations, 700 °C to the Tl-2212 lattice. So, we need to find a new avenue to reduce the size of voids.

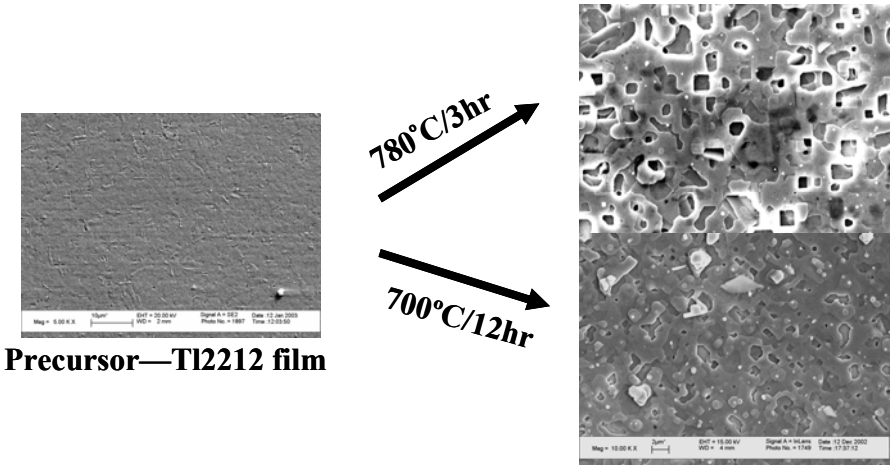

Fig 2.7. Micrometer size of voids seen on the surfaces of thin films prepared with cation exchange, lower operating temperature cannot solve this issue radically.

2.5.2 The Reversibility and Applicability of Cation Exchange Methodology

After a brief review about the cation exchange processing, its procedure, its mechanism, and its efficacy of making Hg-HTS films, as well as the comparison between the conventional processing and cation exchange one, it is natural to seek the expanding applications of the newly developed powerful means to harness processing of other materials that have one volatile element. If the same scheme of the cation exchange is also applicable to other volatile materials that are difficult to obtain in conventional process? What are the necessary and sufficient conditions for the cation exchange to occur?

2.5.3 Nonlinearity in Microwave Devices

In our previous study, we have observed low microwave surface resistance (R_s) and high power handling capability in Hg-1212 films and microstrip line up to 110 K. Developing the Hg-1212 microwave devices and investigating mechanism of nonlinearity in microwave devices, which limits the real application, are the important issues so far.

2.6 Works done in my thesis

In chapter 3, we introduce a new method to eliminate such large-scale voids stemming from lattice collapse. “Lattice pins” were introduced on the original Tl-2212 lattice by partially replacing volatile Tl cations with nonvolatile Re ones. Since the Re cations remain on the lattice during the Tl-Hg cation exchange, they pin the lattice around them. $HgBa_2CaCu_2O_6$ films obtained from these Re-doped Tl-2212 precursor films have much improved microstructures with the pore dimension reduced by an order of magnitude.

A detailed works regarding reversibility of the cation exchange processing have been fully described in Chapter 4. Firstly, we have demonstrated the conversion from Hg-1212 to Tl-2212 structure can be achieved at relatively higher Tl vapor pressure and the conversion consists of two steps: from Hg-1212 to Tl-1212 via Tl–Hg cation exchange on the ‘1212’ lattice followed by Tl-1212 to Tl-2212 via Tl cation intercalation. Secondly, by introducing micro-channels

and consequently completion of cation exchange processing as well as superconducting characteristics with more runs of processing carried out. The obvious increase of critical current density J_c in the Hg-1212 film out of third cation exchange conversion demonstrated the major role played by two-pathways diffusion processes, i.e. the dominant cations diffuse into the films through the channel pathways originated from vertical defects across the thickness of films and then followed by diffusion within a-b planes.

Since nonlinear effects in HTS passive microwave devices are considered to be the major cause that limits the power handling capability of the devices, in Chapter 5, third-order intermodulation is studied in two-pole X-band high-temperature superconducting Hg-1212 microstrip filters at $\geq$ 77 K. The third-order intercept (*IP3*) of the Hg-1212 filters is consistently higher than that of the $YBa_2Cu_3O_7$ filter of the same geometry in this temperature range. At 110 K, the *IP3* of 38 dBm remains for the Hg-1212 filters, the best so far achieved at T > 100 K. The dc critical current density J_c and the rf one J_{IP3} derived from the *IP3* have a similar reduced temperature dependence, suggesting that the magnetic vortex depinning in HTS materials dominates the microwave nonlinearity at elevated temperatures.

Chapter 3

Pinning Lattice: Effect of Rhenium Doping on the Microstructural Evolution to Hg-1212 Films Pinning Lattice

3.1 The Working Principle of the Rhenium Doping

In the previous chapter, we have discussed the voids formed on the surface of Hg-HTS films, which are undesirable for applications. Then a question arises naturally: how to limit the sizes of the voids if not possible to completely prevent the formation of the voids during the cation exchange processing?

Chemical doping/substitution may provide a direct solution to the void-forming problem by modifying diffusion patterns of Tl cations out of the lattice at a microscopic scale. In the cation exchange process, the thermal energy provided to the crystal lattice causes deflection of atoms. The weakly bonded volatile elements, such as Tl, may acquire enough energy to break their bonds from the lattice while other elements remain. This lattice deformation may occur at a macroscopic scale if a large number of volatile elements leave the lattice simultaneously. If the volatile elements, such as Tl in Tl-2212, are replaced partially with nonvolatile elements, the nonvolatile cations remain on the lattice during the cation exchange so as to pin the lattice and to minimize macroscopic lattice deformation. Many elements, such as Re [3.1-3.3], Bi [3.4] and Pb [3.5]

may be chosen to replace Hg in the Hg-1212 lattice. Among others, Re is of special interest because of its benefits to Hg-1212. There are at least three reasons that Re atoms can help to raise the quality of the outcome films.

1. Re cations have been probed to be of high valence (6.01-6.84+) in the sites where the Tl or Hg-cations originally occupied, so these introduced Re cations can prevent excess formation of the oxygen vacancies, which are believed to be responsible to the metastablity of Hg-based cuprate samples.
2. The radius of the Re cation is much smaller than that of Hg and Tl cations, consequently, Re-O bond lengths are detected much shorter than the corresponding Hg-O distances. The lattice distortion originates from these ions contraction might lead columnar defects at least for a few layers of the CuO blocks and then could serve as flux pinning centers because of relatively short coherence length in the layer-structural cuprate HTS superconductors.
3. Addressing the void formation issue we brought at the beginning of this paragraph, in our cation exchange approach, this nonvolatile Re element can serve as lattice pins that can form a collapse-proof matrix. When mass Tl cations escape from their sites simultaneously due to higher processing temperature, the matrix can serve as framework preventing collapse in large scale.

It is also worthwhile to mention here our selection is inspired by the reported results that have shown the Re-doping can prevent contaminating of CO_2

and moisture. Indeed, the material stability of Hg-based films has been remarkably improved through doping Re to the Hg sites, and the sensitivity of precursors and superconducting phases against CO_2 has also been reduced. In addition, the irreversibility field was improved in Re-doped Hg-1223, this actually agreed with the shortening of the blocking layer, despite a slightly lower T_c.

In this cation exchange process, the nonvolatile dopants need to be inserted in the precursor lattice. This is illustrated schematically in Fig. 3.1 with Re taken some of the Tl sites in the Tl-2212 unit cells. During the Tl-Hg cation exchange, the Re cations will remain on the lattice to pin the lattice and to minimize macroscopic lattice deformation. In another words, the "pinning lattice" formed with Re can prevent macroscopic collapse even when the Tl atoms escape rapidly. A plan view of the model is shown on the left side [Fig. 3.1(a)], the solid dots represent Re ions. A cross-section view is shown on the right side [Fig. 3.1(b)]. You might notice that we have marked that Tl-2212 and Re-1212 with different phases. We'll discuss this in more details later on at experimental parts. In this work, we have successfully synthesized the doped $(Tl_{1.88}Re_{0.12})$-2212 [(Tl,Re)-2212 in the rest of the text] films on $LaAlO_3$ substrate and converted them to $(Hg_{0.94}Re_{0.06})$ -1212[(Hg,Re)-1212 in the rest of the text] using the cation-exchange process. Indeed, a dramatic improvement in the film microstructure was observed on Re-doped Hg-1212 films.

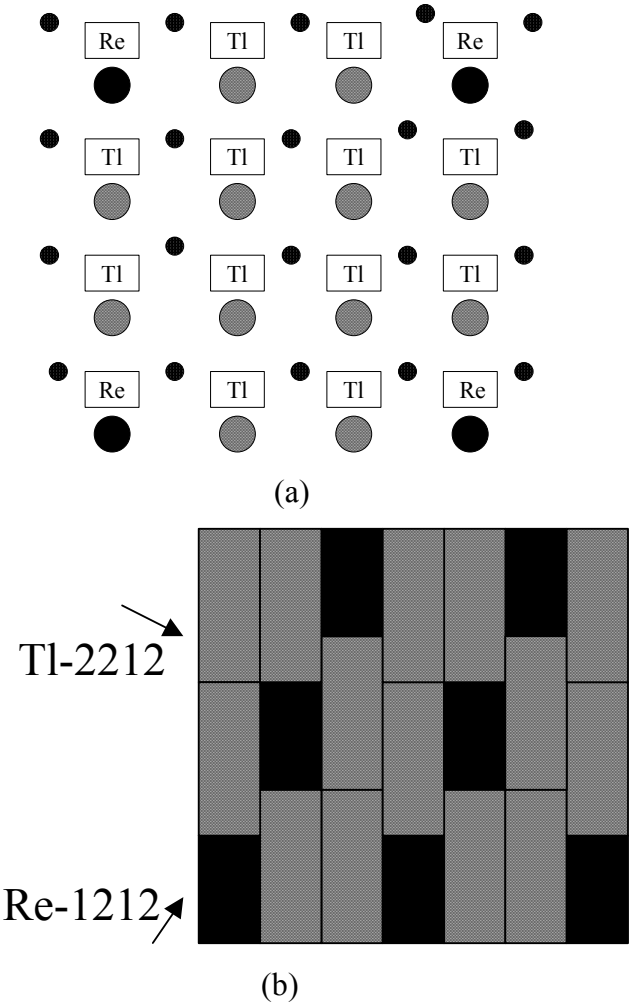

Fig 3.1 Schematic diagrams of the lattice structure of (Tl, Re)-2212 film when 6% of Tl-2212 unit cells (textured symbols) are replaced with Re-1212 ones (solid): (a) a plan view, and (b) a cross-sectional view

3.2 Experiments and Results

Sample fabrication consisted of two steps: preparation of epitaxial (Tl,Re)-2212 precursor films was followed by conversion to epitaxial (Hg,Re)-1212 films via Tl-Hg cation exchange. In the first step, the precursor (Tl,Re)-2212 thin films were deposited on single crystal (100) $LaAlO_3$ substrate at room temperature

using dc magnetron sputtering from a pair of $(Tl_{1.88}Re_{0.12})$-2212 superconducting targets. The rest of condition is the same as that described in previous chapter.

3.2.1 Crystalline Structure

The crystalline structure and phase purity of the films were analyzed using x-ray diffraction (XRD). Fig. 3.2 depicts the XRD θ-2 θ spectra of (a) Hg-1212, and (b) (Hg, Re)-1212 films and their precursor (c) Tl-2212, and (d) (Tl,Re)-2212 films, respectively. All films are *c*-axis oriented and the amount of impurity phases is negligible. The (Hg, Re)-1212 film has a nearly identical structure to the undoped Hg-1212 as shown in Figs. 3.2(a) and 3.2(b). Interestingly, their precursor films had a subtle difference in structure. Without doping, only "2212" lattice structure is visible [see Fig. 3.2(c)]. In the case of Re doping [see Fig. 3.2(d)], some additional peaks marked with * are clearly visible. A comparison of Fig. 3.2(d) with Figs. 3.2(a) or 3.2(b) suggests that these peaks are from "1212" phase. This means that certain amount of 1212 phase was formed in the Re-doped Tl-2212 precursor films. Theoretically speaking, both Tl-1212 and Re-1212 structures are possible. We, however, argue that the latter may occur at a much higher probability based on the following reasons. First, the processing condition used was favorable to Tl-2212, which has been confirmed by the fact that no Tl-1212 was formed in the undoped case [see Fig. 3.2(c)]. On the other hand, Re-2212, similar to Hg-2212, is much less stable than Re-1212 (Hg-1212) and special processing condition, such as high vapor pressure plus chemical replacement on

the Hg or/and Ca sites, is required to form "double-layer" structure.[3.6, 3.7] Based on these considerations, we propose that the Re-doped Tl-2212 is composed of pure Tl-2212 and Re-1212 phases. If no phase segregation occurs, Re-1212 unit cells should be present uniformly in the lattice of Tl-2212. Since the *c*-axis lattice constant of Re-1212 is 1.27 nm while that of Tl-2212 is 1.48 nm, the mixing of the Re-1212 phase in Tl-2212 lattice will result in antiphase grain boundaries, as schematically illustrated in Fig. 3.1(b), in the first several to several tens of monolayers. These antiphase grain boundaries have been observed on $YBa_2Cu_3O_7$ films grown on miscut substrates and they later develop into dislocation type of growth defects at larger film thickness [3.8, 3.9].

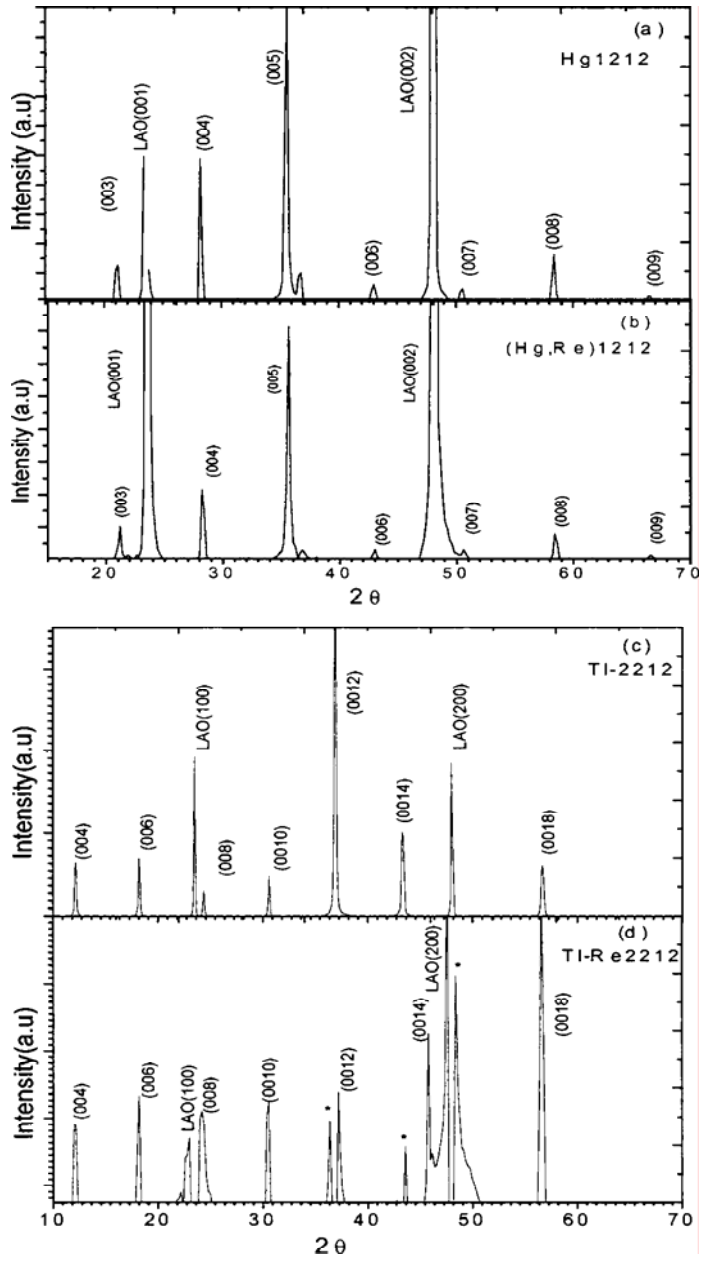

Fig 3.2. XRD θ−2θ spectra of (a) A Hg-1212 film fabricated using cation exchange process; and (b) a (Hg, Re)-1212 film made under the same condition as (a). The XRD θ−2 θ spectra of their precursor films are also shown, respectively, in (c) and (d). Both precursor films were about 0.25 mm thick. After cation exchange, the film thickness reduced to 0.21 mm when the 2212 unit cells (c=1.48 nm) were transferred to 1212 cells (c=1.27 nm). All films were on (100) $LaAlO_3$ substrates.

3.2.2 Surface Morphology

The scanning electron microscopy (SEM) micrographs of the Tl-2212 and (Tl,Re)-2212 precursor films are shown in Figs. 3.3(a) and 3.3(b), respectively. The surface morphology of the latter [Fig. 3.3(b)] is nearly featureless, much smoother than that of the undoped Tl-2212 film [Fig. 3.3(a)]. In addition, the impurity phases (mostly the intermediate oxide compounds) typically observable on undoped Tl-2212 films due to contamination of the simple oxides precursor materials in air [see Fig. 3.3(a)] disappeared in the case of Re doping. This suggests Re doping reduces air contamination of the Tl-2212, which is similar to what has been observed for Hg-1212 and Hg-1223 cases. On Fig. 3.3(b), many small size "holes" of tens of nanometers in diameter can be clearly seen.

By carefully examining the surface of undoped Tl-2212 [Fig. 3.3(a)], we conclude that this is unlikely related to Re doping since the holes are present also on the undoped Tl-2212 films. Nevertheless, those holes are not as obvious on the undoped Tl-2212 films simply because they are covered by many surface impurity particles. The mechanism of the hole formation remains unclear at this point. One possibility is that they may be the pathways for Tl diffusion during the Tl vapor processing. Further experiments are necessary to pinpoint this mechanism.

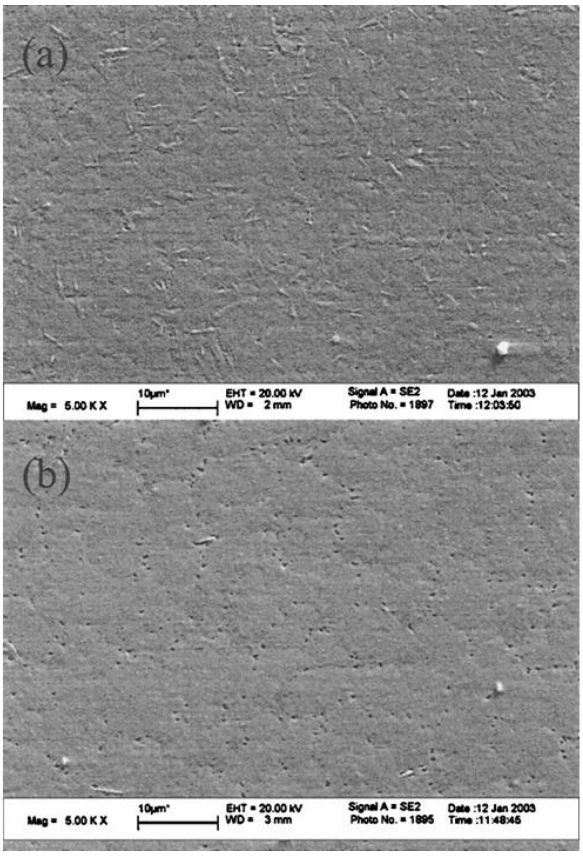

Fig 3.3. SEM micrographs of (a) a superconducting Tl-2212 precursor film; and (b) a (Tl,Re)-2212 precursor of film both annealed in thallium vapor at 820 °C for 1 h in an Al_2O_3 crucible in flowing oxygen gas.

Figures 3.4(a) and 3.4(b) depict the SEM micrographs of Hg-1212 and (Hg, Re)-1212 films obtained via cation exchange process from Tl-2212 and (Tl, Re)-2212 precursor films, respectively. A remarkable difference between these two films is the reduced void dimension with Re doping, suggesting that the crystalline lattice deformation pattern was indeed modified by doping Re on Tl-2212 lattice. In the undoped case, the dimension of the voids is in the range of submicrometer to several micrometers [see Fig. 3.4(a)] while with Re doping, the average dimension of the voids is in the range of tens of to 3 hundreds

nanometers, and the average size of the voids is about 150 nm. It reduced by an order of magnitude [see Fig. 3.4(b)]. The void density of the (Tl, Re)-2212 precursor film is 0.6 on a 10 μm^2 area, while that of the (Hg, Re)-1212 is 4.6 on a 10 μm^2 area. However, it is hard to tell if the voids on the precursor are inherited to the (Hg, Re)-1212 film. It should be realized that this reduced void dimension is two orders of magnitude larger than what is expected theoretically. When 6% of unit cells of Tl-2212 are replaced with Re-1212 ones, the void dimension should be less than 1.6 nm (both Re-1212 and Tl-2212 have their *an* axes around 0.4 nm) if the two types of unit cells formed an alloy. The observation of the much larger dimension of the voids suggests that phase segregation may occur in (Tl, Re)-2212. This argument is supported by the observed Re-1212 phase in XRD data [Fig. 3.2(b)]. This phase segregation is in fact not unexpected because of large lattice mismatch between Tl-2212 and Re-1212 along the *c* axis. The strain generated by this lattice mismatch may serve as the driving force for the phase segregation.

Another fact consistent with this argument is the difficulty we have encountered in doping higher percentage Re in Tl-2212 lattice. Dramatically roughened surface morphology was observed when the Re-doping level was doubled. The size of Re-1212 colonies after the phase segregation can be estimated by assuming that the collapsed Tl-2212 colonies are a hundred times bigger in dimension than the theoretically expected value of 1.6 nm. A simpleminded calculation suggests 10^4 unit cells of Re-1212 in each Re-1212

colony with dimension of 40 nm along each side if the colony is a square. Transmission electron microscopy with adequate spatial resolution would be ideal to confirm this and will be certainly a topic of future research (unfortunately, such a facility is not available locally at this point).

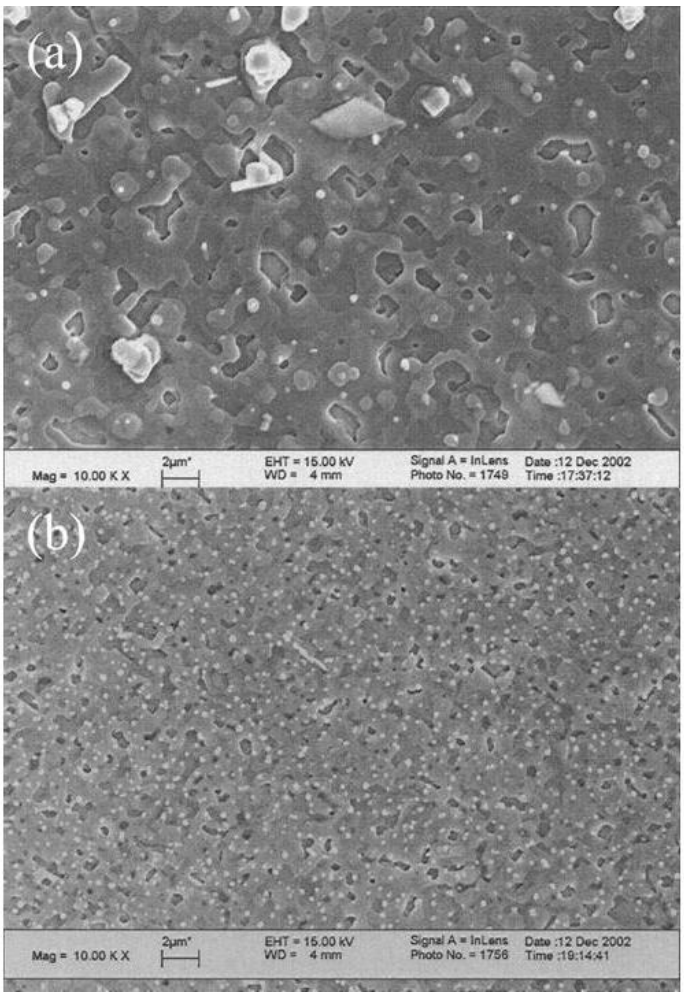

Fig 3.4 SEM micrographs of (a) Hg-1212 film, and (b) (Hg, Re)-2212 film both made using cation-exchange process in Hg vapor at 700 °C for 12 h.

3.2.3. Superconducting Properties

Figure 3.5 depicts the temperature dependence of the magnetic susceptibility of Hg-1212 (solid squares) and (Hg, Re)-1212 (solid triangles) films measured in a 10 Oe magnetic field (H) applied along the normal of the film. Both films showed superconducting transition above 110 K. The T_c of (Hg, Re)-1212 films was typically in the range of 114−118 K, slightly lower than that of the undoped Hg-1212 film (120−124 K). Interestingly, lower T_c's were also reported previously on most chemically doped Hg-1212, including Re-doped ones.

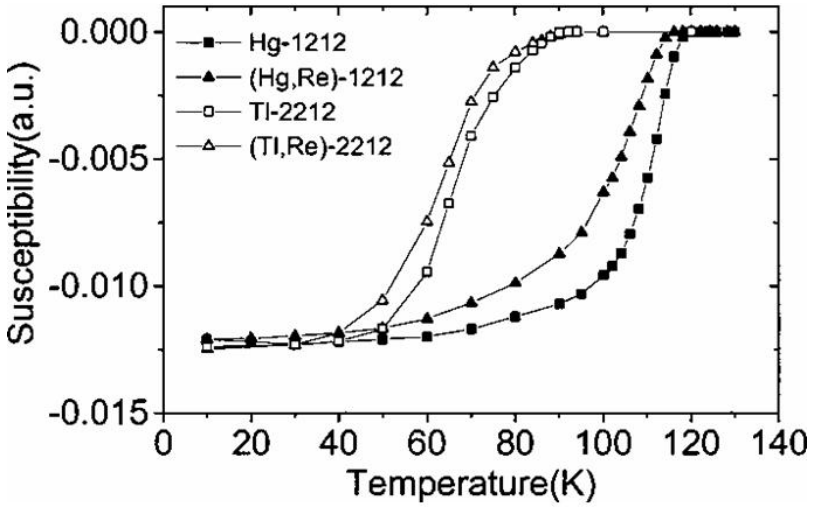

Fig 3.5 Magnetic susceptibility as a function of temperature measured in zero-field-cool mode on Hg-1212, (Hg, Re)-1212 films, and their precursor films. The magnetic field was 10 Oe applied along the normal of the film.

The susceptibility vs. temperature curves for the Tl-2212 (open squares) and (Tl, Re)-2212 (open triangles) measured under the same experimental conditions were also included in Fig. 3.5. It has been noticed that T_c's of the Tl-2212 films were also slightly higher than that of (Tl, Re)-2212 films. Since post oxygen anneal did not improve the T_c's of Re-doped Tl-2212 and Hg-1212 films,

we speculate that Re dopants may disturb the local oxygen distribution in both the 2212 and 1212 lattice, which in turn lowers the T_c of the material.

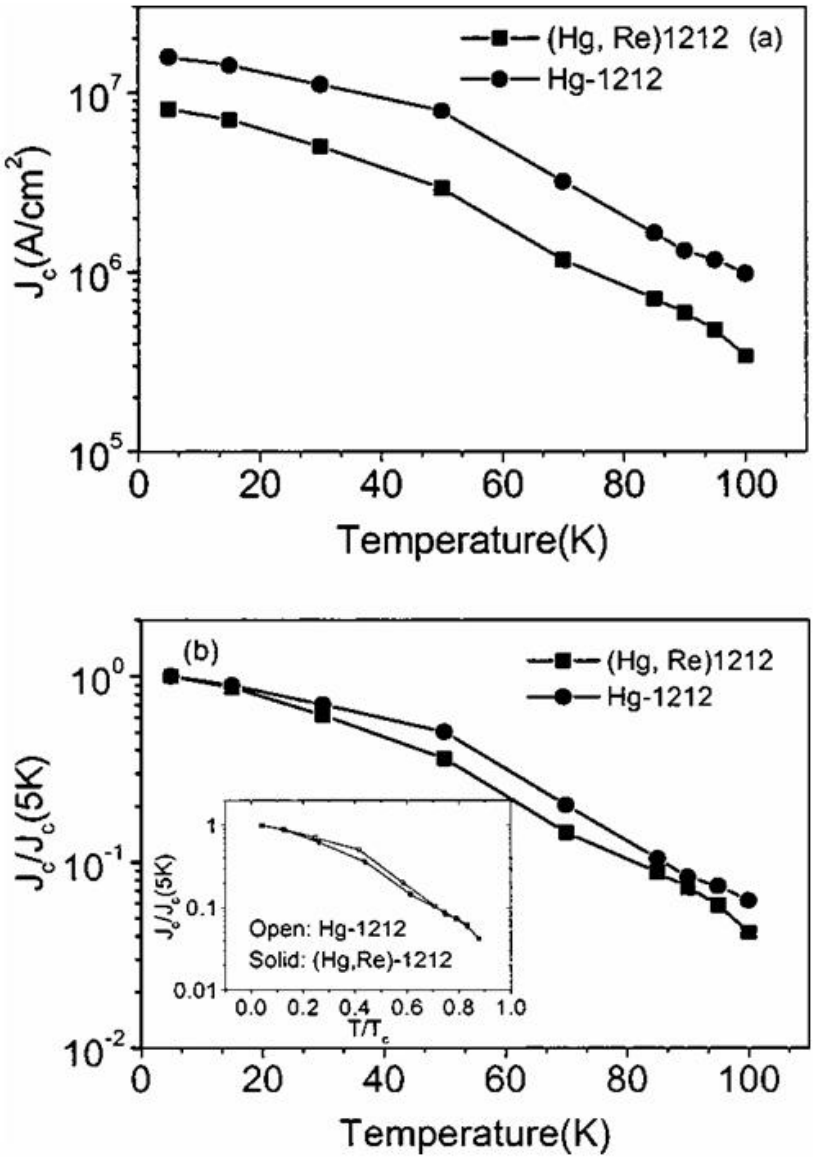

Fig 3.6 Temperature dependence of J_c of the Hg-1212 film (circle solid symbol) and the (Hg, Re)-1212 film (square solid symbol) plotted (a) in the original J_c scale and (b) normalized J_c scale [J_c /J_c(5 K)]. The inset of (b) replots the data in (b) on the normalized temperature scale [T/T_c].

J_c's were calculated using the Bean model from the magnetization vs. magnetic field hysteresis loops measured at different temperatures. The magnetic field was applied along the normal of the film. Figure 3.6 shows a typical comparison of the self-field J_c as function of temperature for a pair of representative Hg-1212 and (Hg, Re)-1212 films. The J_c in the former is typically higher by a factor of 1.5–3 than that of the latter in the whole temperature range from 5 K to 100 K. For example, the J_c's of the undoped Hg-1212 are 15.6, 3.2, and 1.0 MA/cm^2 at 5 K, 77 K, and 100 K respectively, while those for the (Hg,Re)-1212 are 8.0, 1.2, and 0.38 MA/cm^2 at the same temperatures [see Fig. 3.6(a)]. This represents the typical behavior among all the films we have studied. The J_c ratio between the Hg-1212 and (Hg, Re)-1212 films increases slightly with increasing temperature, as shown in Fig. 3.6(b). This slightly higher J_c ratio at higher temperature may be attributed to the lower T_c of the (Hg, Re)-1212. Indeed, the two J_c curves almost coincide when Fig. 3.6(b) is replotted on the normalized temperature scale (T/T_c) as shown in the inset of the Fig. 3.6(b). It is, however, unclear why the overall J_c is lower in the Re-doped Hg-1212 films.

Figure 3.7 compares the magnetic field dependence of J_c in the two types of films at 5 K, 77 K, and 100 K. Subtle difference is visible. Despite an overall higher values as shown in Fig. 3.7(a), the J_c in the undoped Hg-1212 film decreases faster with increasing field in the low field range. This can be better demonstrated when the same curves are plotted on the normalized scale ($J_c/J_{c,0}$) in Fig. 3.7(b). This indicates the magnetic flux pinning is enhanced with Re doping,

consistent with what was previously reported by other groups. At higher field, the two J_c -H curves cross over and both drop sharply when the field is further increased.

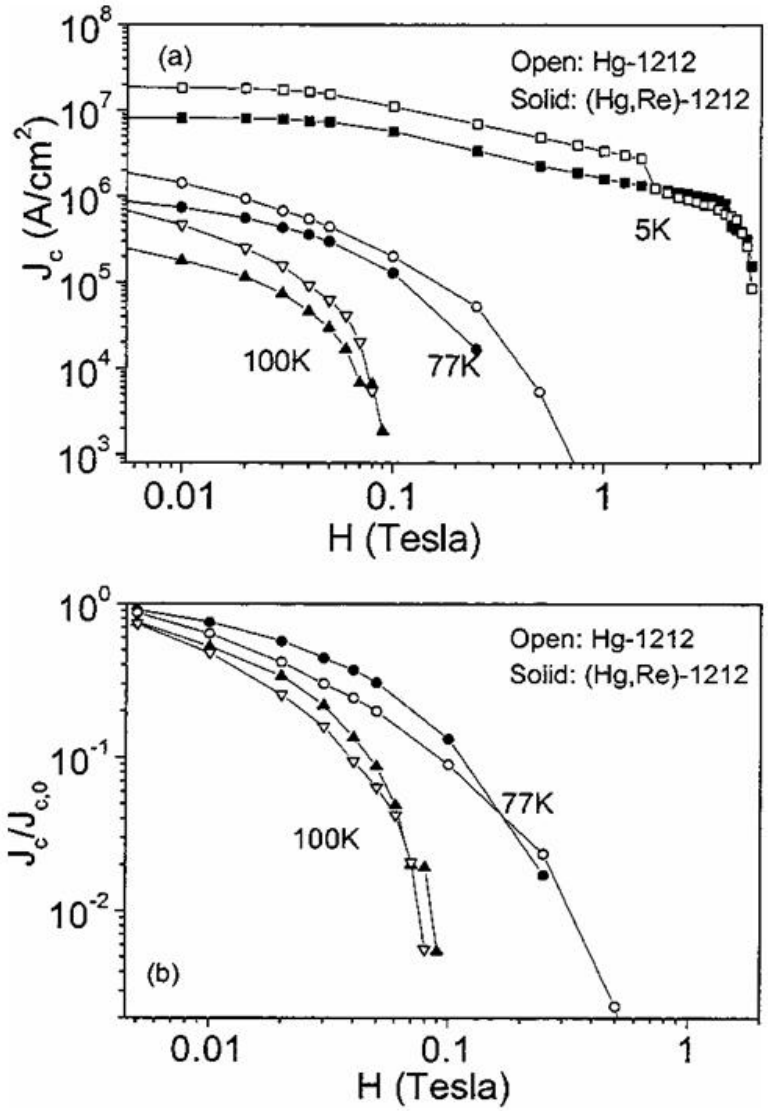

Fig 3.7 (a) $Jc-H$ curves at different temperatures of 5 K, 77 K, and 100 K for Hg-1212 and (Hg, Re)-1212 films. (b) replots the same J_c's at 77 K and 100 K on the normalized Jc scale (J_c /$J_{c,0}$) . $J_{c,0}$ is the J_c at zero applied magnetic field.

3.3 Conclusion of This Chapter

In conclusion, we have fabricated epitaxial c-axis oriented $(Hg_{0.94}Re_{0.06})Ba_2CaCu_2O_6$ films by replacing the Tl cations from an epitaxial $(Tl_{1.88}Re_{0.12})Ba_2CaCu_2O_x$ precursor films in the cation-exchange process. It was found that the presence of nonvolatile Re on the precursor lattice pins the lattice locally so as to reduce the large-scale lattice collapse, which occurs on undoped Tl-2212 precursor lattice and typically results in micrometer size voids in Hg-1212 films after the cation exchange processing. By pinning the lattice with Re doping, the void size has been reduced by an order of magnitude and the surface morphology has been improved dramatically. In addition, this result has also demonstrated for the first time that Tl-2212 precursor lattice doped with nonvolatile elements on the volatile Tl sites can be employed for epitaxy of chemically doped Hg-1212 films in cation exchange process, enabling tailoring microstructure and physical properties of Hg-1212 films in a much controllable fashion.

Chapter 4

Reversibility of the Cation Exchange Process

As already reviewed earlier, using the cation exchange methodology, epitaxial thin films of $HgBa_2CaCu_2O_6$ (Hg-1212) exhibiting superior physical properties have been obtained from epitaxial precursor films of Tl-1212 (y = 1 and z = 1) or Tl-2212 (y = 2 and z = 1)[4.1–4.6]. Despite the exciting results obtained, the mechanism of the cation exchange has been the subject of debate ever since it was developed. Understanding this mechanism is important not only because cation exchange has provided a vital scheme for the epitaxy of Hg-HTS films, but also because it may be developed into a generic "atomic surgery" scheme for the synthesis and epitaxy of other volatile materials. So, a genetic question rises: is cation exchange process reversible? If the answer is a yes, what is the underlying mechanism? Motivated by this, we have recently carried out a study on the cation-exchange mechanism. It has been found that within the '1212' structure (between Tl-1212 and Hg-1212), the cation exchange process is completely reversible and the direction of the process is determined by the relative population ratio of Tl and Hg cations. The cation exchange is bidirectional since Tl (or Hg) cations are only weakly attached to the "1212" lattice (see Fig. 4.1). The lattice decomposition temperature for Tl-1212 (or Hg-1212) may represent the binding energy of Tl (or Hg) cations to the "1212"

lattice. This result suggests that the cation exchange could be completely reversible and the direction of the process is controlled by the population ratio of the new cation and the one to be replaced. The final material after the cation exchange may be an alloy of the precursor and the targeted material if a finite ratio is selected.

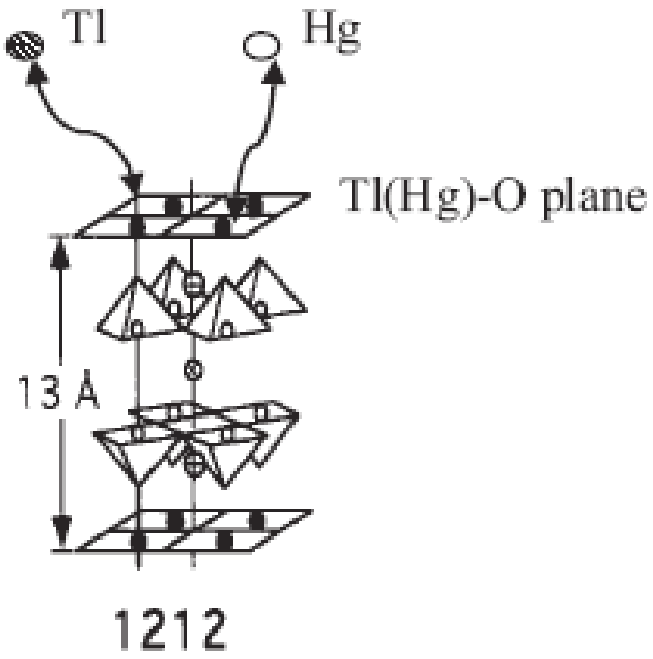

Fig 4.1 Schematic description of the Tl–Hg cation exchange occurring on the "1212" structure. The crystal lattice remains nearly unchanged while the superconducting transition temperature is altered between 85 and 90 K for Tl-1212, and 120 and 125 K for Hg-1212.

The high J_c of Hg-1212 film made from Tl-2212 film has been obtained by generating micro-channels to facilitate Tl-Hg cation exchange on "1212" lattice using reversible cation-exchange. We have also investigated the conversion from Hg-1212 to Tl-2212 at temperatures for which recrystallization of the Hg-1212

lattice is unlikely to happen. We have found that this conversion can be completed under high Tl vapor pressure via two steps: Hg-1212 to Tl-1212 through Tl–Hg cation exchange followed by Tl-1212 to Tl-2212 through Tl cation intercalation. The experimental results are reported in this chapter.

4.1 Generating Micro-Channels to Facilitate Tl-Hg Cation Exchange on "1212" Lattice

I. Introduction

During the Tl and Hg cation exchange process, one particular remaining question is on diffusion pathways. It is unclear whether the diffusion occurs layer-by-layer along the c-axis of the film, which is normal to the film, or through the film along certain channels of growth defects such as voids and then followed by the a-b plane diffusion. The answer for this question may not be unique when different precursor matrices are employed. For Hg-1212 films, either Tl-1212 (y=1 and z=1) or Tl-2212 (y=2 and z=1) can be used as the precursor films. The precursor Tl-2212 has two Tl-O planes that collapse into one Hg-O plane during cation exchange, resulting in lattice shrinkage of ~14% along the c-axis. Many voids form during cation exchange from Tl-2212 to Hg-1212, in contrast to the nearly unchanged dense and smooth film morphology in the process from Tl-1212 to Hg-1212 since Tl-1212 and Hg-1212 have nearly the same crystalline structure. Interestingly, the Hg-1212 films obtained from Tl-1212 always have broader superconducting transition and lower J_c as compared to the ones from Tl-2212

precursor films. It was hence suspected that the voids actually serve as diffusion channels through the film thickness and therefore enables dominance of a-b plane cation diffusion as shown in Fig. 4.2(b). In the case of Tl-1212 to Hg-1212 cation exchange, the diffusion of the Tl and Hg cations may have to follow a layer-by-layer pattern, as shown in Fig. 4.2(a), due to lack of vertical channels through the film thickness. It is well known that the c-axis diffusion speed of oxygen is several orders of magnitude lower than that along the a-b plane because of the layered structure of HTS materials. If Hg and Tl cation diffusion is similarly anisotropic for the same reason, the efficiency of Tl-Hg cation exchange is much higher in the case of Tl-2212 to Hg-1212. Given the time frame for cation exchange from Tl-2212 to Hg-1212 is on the order of 45-60 minutes, the conversion from Tl-1212 to Hg-1212 may be only partially completed. The mixed phase of Tl-1212 and Hg-1212 may be responsible for the observed broad superconducting transition as well as the lower J_c values as we discussed earlier.

It is important to confirm the role of the micro-channels in the cation exchange process. Motivated by this, we have developed a high-pressure annealing process. Using this process, micro-channels can be generated in the "1212" films. We have found that the Tl-Hg cation exchange process from Tl-1212 to Hg-1212 or vice versa can be significantly expedited in the presence of these micro-channels. Consequently, the Hg-1212 films obtained from Tl-1212 precursor contained the micro-channels show comparable superconducting

properties to that from Tl-2212. In the next section, we will discuss our experimental results in details.

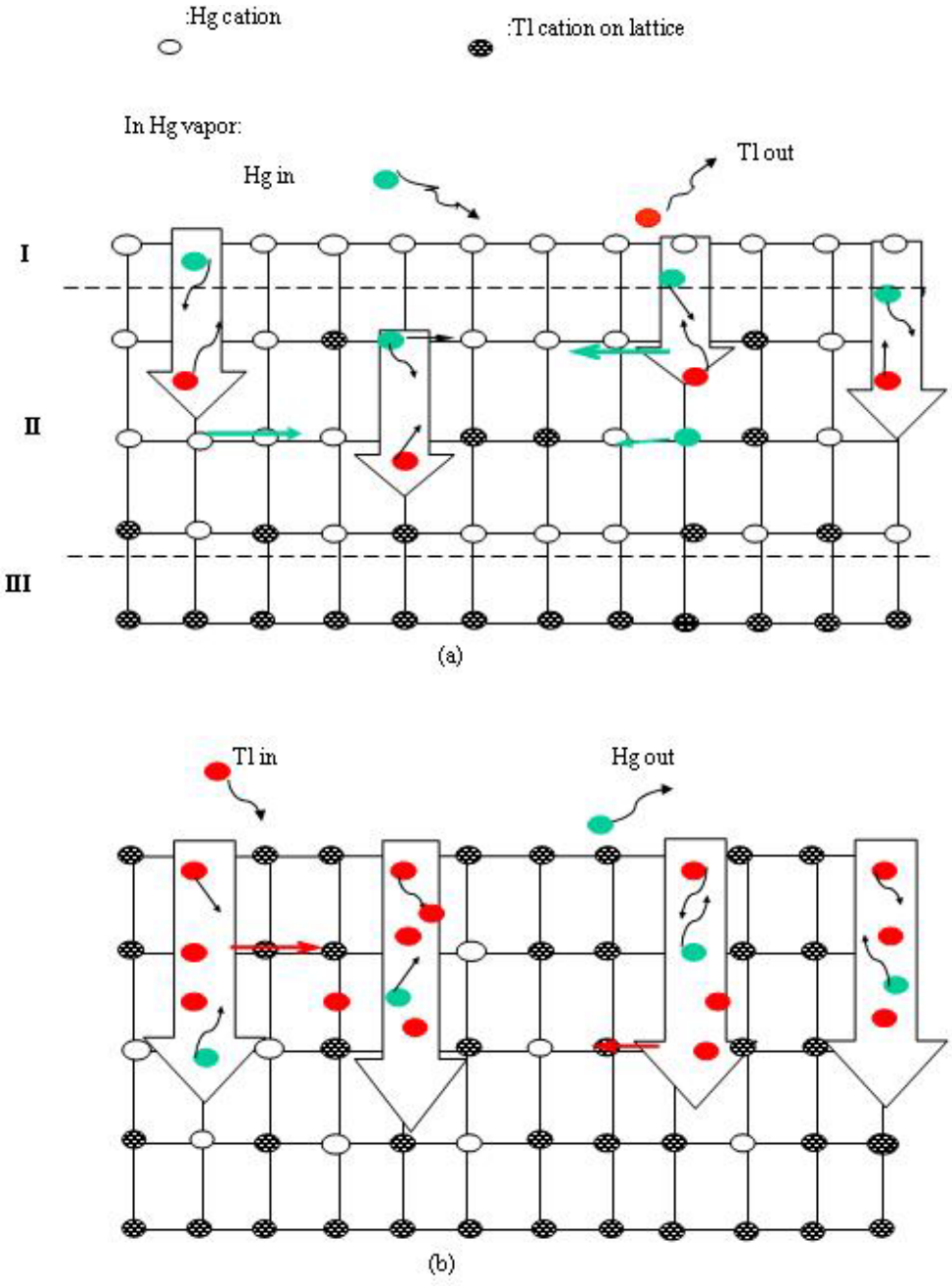

Fig 4.2 Diffusion channel of "1212" structure (a) the diffusion of the Tl and Hg cations may have to follow a layer-by-layer pattern. (b) The voids actually serve as diffusion channels through the film thickness and therefore enable dominance of ab-plane cation diffusion.

II. Experiment and Discussion

1. Sample preparation

Two types of Tl-1212 precursor films were prepared with one containing no micro-channels (set A) and the other, micro-channels. A big piece of Tl-1212 thin film was deposited on single crystal (100) $LaAlO_3$ substrates at room temperature using dc magnetron sputtering, and then annealed at 840 ºC for 1 hr in flowing oxygen using crucible technique. At this stage, there were no micro channels on both films. The Tl-1212 film prepared was then cut into two pieces in the middle. One piece of film was kept in its primitive state, marked with precursor Tl-1212A, the so-called set A. We then purposely processed another piece of Tl-1212 film in order to introduce micro channels by following two-step cation exchanges. In the first step, the sample was sealed in an evacuated quartz tube together with two pellets. One of the pellets was an unreacted fine ground and mixed $HgBa_2Ca_2Cu_3O_x$, and the other, a $Ba_2Ca_2Cu_3O_x$ pellet. The first pellet served as cations vapor source, and the second vapor absorber. The weight ratio of the former to the latter was 3:1. They worked together to establish stable pressure of the desired cations (atoms) that can be diffused into the lattice. The whole assembly was kept in a furnace at 700 °C for 12 hr. In the second step, the film was processed at Tl-rich environments of the evacuated quartz tube at 730 °C for 2hr. Similarly, the Tl-rich environment was established by putting an

unreacted $TlBa_2Ca_2Cu_3O_x$ with a $Ba_2Ca_2Cu_3O_x$ pellet. Later on by SEM micrograph, one will observe that micro channels had been introduced by this film that came out these two step cation exchange processing. This film, which is mainly in Tl-1212 state, will serve as second precursor, marked with Tl-1212B, the so-called set B.

After all proceeding preparation of the two precursors, i.e., Tl-1212A and Tl-1212B, they were put into the sealed evacuated quartz tube together at 700 °C for 12 hr. The outcome films were marked by Hg-1212A and Hg-1212B accordingly.

2. Crystalline Structure

The crystalline structure and phase purity of the films were analyzed using x-ray diffraction (XRD). Fig. 4.3 illustrated the XRD θ-2θ spectra of the films described in the previous section. All films were all c-axis oriented. Fig. 4.3 (a) is corresponding to the regular precursor Tl-1212A film; (b) Tl-1212B film with micro-channels; (c) Hg-1212A film made from Tl-1212 film (d) Hg-1212B film made from Tl-1212B. Comparing Fig. 2 (a) through (d), one can see only "1212" phase existed for all four films, judging from their nearly identical structure. This outcome was indeed very encouraging in terms of layer structure, although it was unclear about the completion of the Hg-Tl cations conversion in each status by checking XRD data alone. The data of measured T_cs and scanning electron

microscopy (SEM) micrographs taken respectively will unveil more interesting features during the transformation of the films.

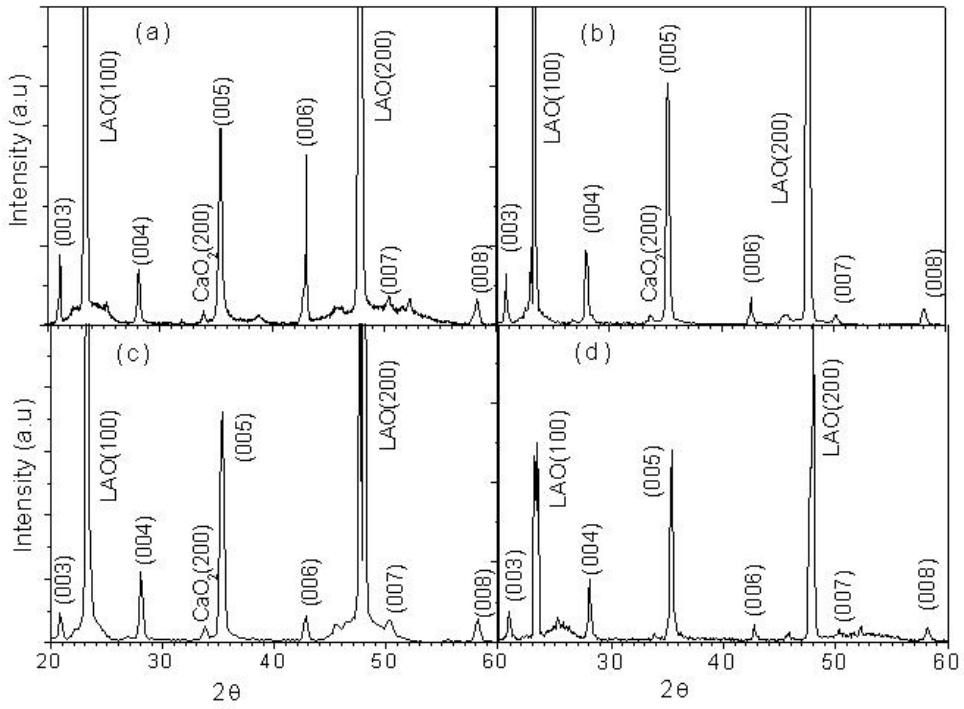

Fig. 4.3 XRD θ-2θ spectra of the sample films (a) a regular Tl-1212A film annealed in an Al_2O_3 crucible in Tl vapor at 840ºC for 1 hour; (b) the Tl-1212B film with micro-channels ; (c) the Hg-1212A film made from the Tl-1212A film; (d) the Hg-1212B film from Tl-1212B film; All films except Tl-1212A made in a sealed quartz tube in Hg vapor at 700º C for 12 hours to get target Hg-1212 films or in Tl vapor at 730º C for 2 hrs to achieve target Tl-1212B films.

3. Surface Morphology

Along the lines of the expectation based on the model established for cation exchange processing technique, far better surface morphology was seen in all the films generated from the cation exchange between Tl-1212 and Hg-1212, compared with that of the films prepared from Tl-2212 precursors. The SEM

micrographs taken from all the four films were exhibited in Fig.4.4 (a) to 4.4(d), respectively. The surface morphology of the precursor Tl-1212A shown in Fig. 4.4(a) is very smooth. After cation exchange at 700 °C for 12 hr, the surface morphology of Hg-1212A inherited the excellent quality from its precursor [see Fig. 4.4(c)]. Only a few small voids have been seen. It was no surprise to see this outcome, according to the diffusion mechanism model established in our previous work, simply because of no double- to single-layer transition involved. Precursor Tl-1212B possessed also good surface morphology [Fig. 4.4(b)]. Interestingly, some micro channels of submicrometer dimension had been introduced successfully, in line with the expectations based on the diffusion model established previously. After final cation exchange in the Hg-rich environment, the sizes of micro channels on Hg-1212B film increased (Fig. 4.4(d)). The evolution of these vertical channels indeed evidenced the diffusion mechanism governing the cation exchange process. The addition of these microchannels could benefit high field applications by providing flux pinning. We will come back to this point soon regarding the current density of the Hg-1212 films.

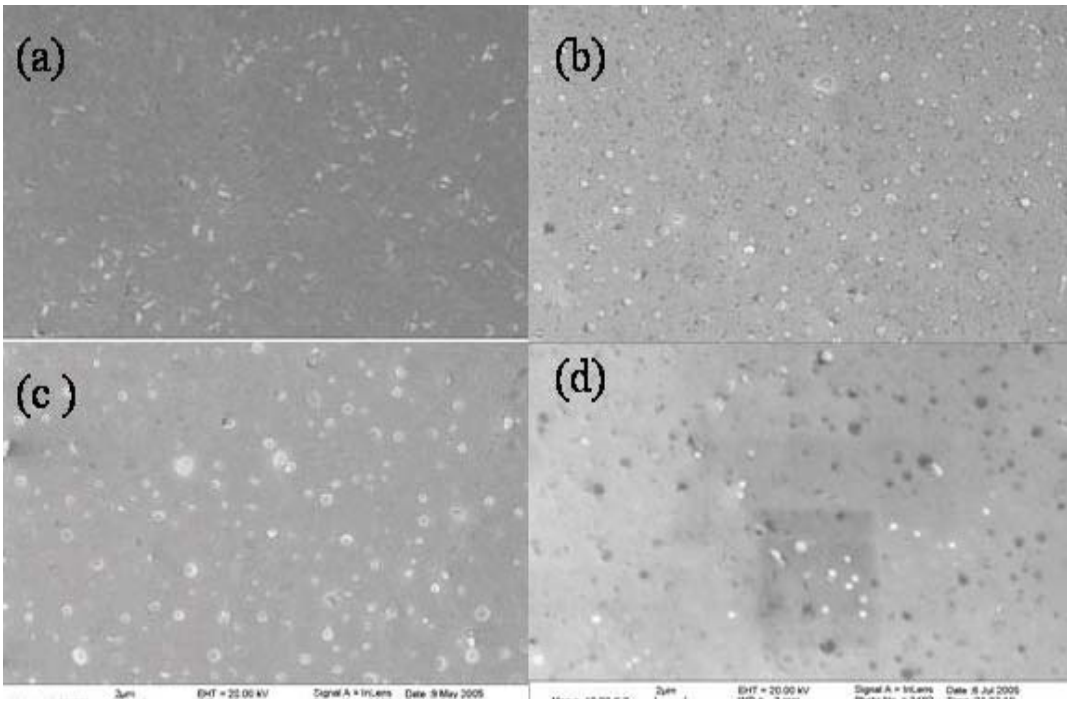

Fig. 4.4 scanning electron microscopy images of: (a) the regular Tl-1212A; (b) The Tl-1212B film; (c) The Hg-1212A film made from Tl-1212A; (d) The Hg-1212B film from Tl-1212B. (e) The Hg-1212AA film from Hg-1212A film

4. Superconducting Properties

Fig. 4.5 depicted the temperature dependence of the magnetic susceptibility of Hg-based and Tl-based films measured in a magnetic field (H) applied along the normal of the film. In the precursor status (see the curve marked with Tl-1212A in Fig. 4.5), the measured T_c value was 84 K. After first cation exchange in Hg vapor surrounding, the outcome film should be Hg-1212 by original design. The measured T_c value was 116 K, in the typical range of Hg-1212 films. However, the transition edge was much broader than a typical one in an HTS film, but no visible double shoulder shown in this case, which hints an

interesting mixture status of the film, i.e., an alloy phase of Hg-1212/Tl-1212 was formed (refer to the curve marked with Hg-1212A in Fig. 4.5), consistent with the theoretical prediction previously. For Tl-1212B, the surprisingly higher T_c value implies another mixture of Tl-1212 with Hg-1212, but Hg concentration was not high, judging from the transition edge. A typical Hg-1212 T_c-H curve was achieved and the unwanted Tl-1212 phase was diminished to be negligible in Hg-1212B film. This suggested the multiple-run trip between Tl-1212 and Hg-1212, and consequent formation of the micro channels, was crucial for fabricating a purer Hg-1212 film.

One may argue that solely extending the processing time of the first cation exchange could work the same way. To answer this question, another experiment had been conducted employing the identical setup and conditions with the sample Hg-1212A, only helping us to conclude that the purity of the outcome Hg-1212AA film did not show any improvement even the processing time doubled. Actually, both T_c and J_c properties became even worse if purely doubled the processing time. One can see this clearly from the curves marked with Hg-1212AA in Fig. 4.5 and Fig. 4.6, i.e., no improvement see after doubling the processing time in Hg-rich environment. By SEM micrograph, merely doubling processing time in Hg vapor was unable to introduce micro channels.

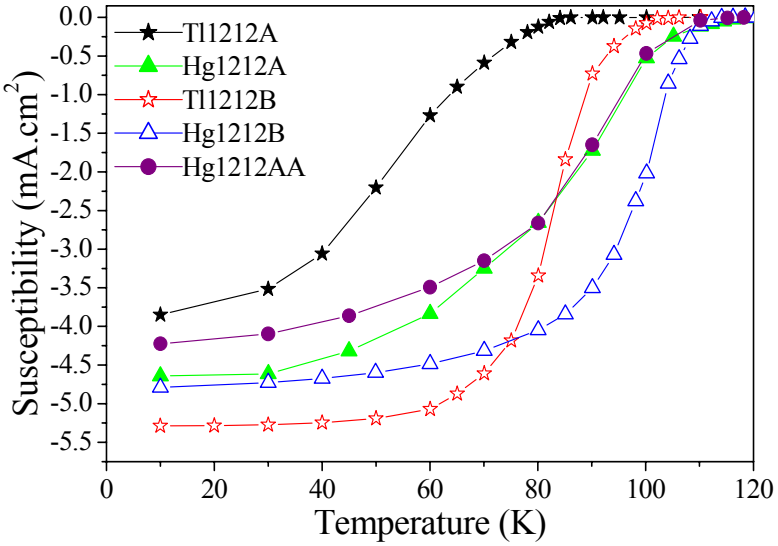

Fig. 4.5 Magnetic susceptibility as a function of temperature measured in zero-field-cool mode for the superconducting films. The applied field is 10 gauss and perpendicular to the film.

Then one may ask: what was major cause for this big difference? Let us look back closely to all the processing parameter to answer this question. When we converted Hg-1212 into its Tl-1212 target film, the temperature was set at 730 °C for 2 hr. At this temperature, the Hg cations as well as Tl ones can escape from their equilibrium sites easier for the reason of higher stimulating energy. Owing to the dominant Tl surrounding, the Hg cations tended to make their way out and resulted in channels vertically, according to the diffusion mechanism of cation exchange processing. J_cs were calculated using the Bean model from the magnetization vs. magnetic field hysteresis loops measured at different temperatures. The magnetic field was applied along the normals of the films. Fig. 4.6 showed comparative data of J_c as function of field at different temperatures for the pair of representative Hg-1212A Hg-1212B films.

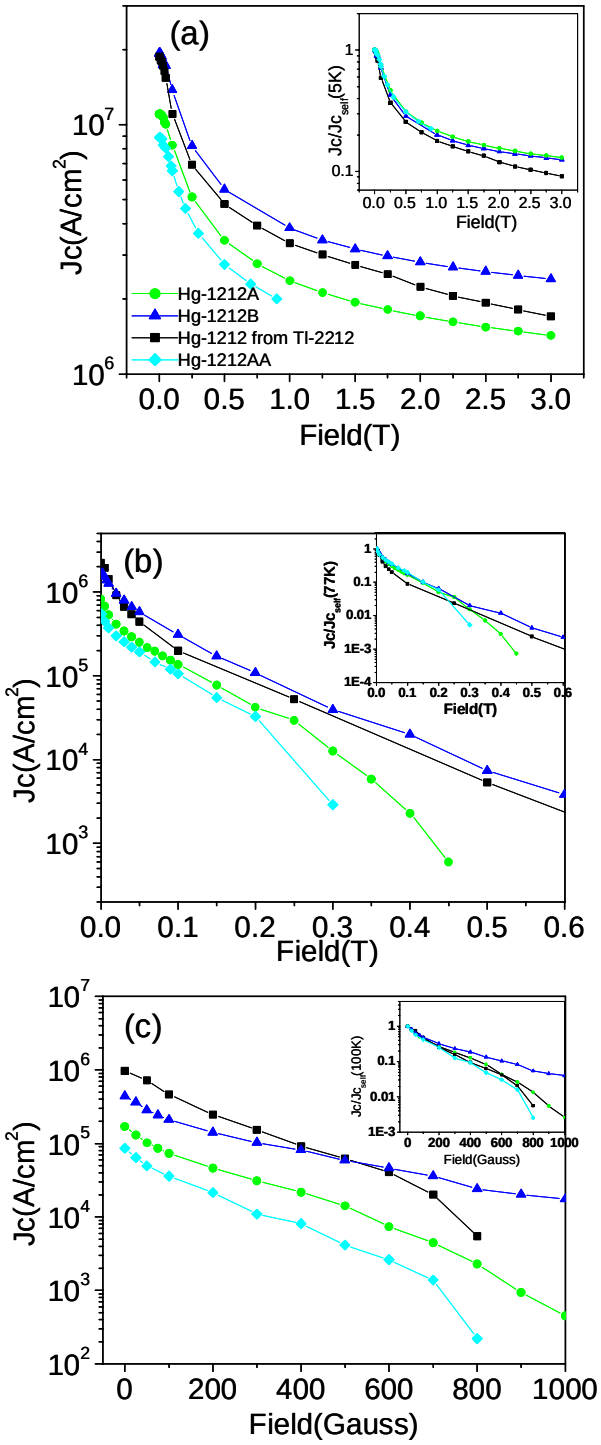

Fig 4.6 The J_cs of all Hg-1212 films at different temperatures (a) at 5K, (b) at 77K and (c) 100K and the inlets are the normalized J_c

Three typical surrounding temperatures were set at 5 K, 77 K, and 100 K, respectively. Two striking features were seen from the graphs. Firstly, remarkable increase of J_c values obtained in Hg-1212B compared with that from Hg-1212A. Based on the analyses early on, the film Hg-1212A consisted of a mixture of Hg-1212 with Tl-1212. The ionic radius of Tl element was reported as 1.50 Å, whereas ionic radius of Hg element was 1.02 Å. This might result in mismatch of the lattice, consequently strains of the grain boundaries thus misorientation between them. This could limit the current density of the film [18]. When the phase of the film was purer, the strains lesser, thus higher the J_c value.

Another striking feature in all three cases was the superior J_c values for higher magnetic field, especially in the film Hg-1212B. One can see this from the crossover of the J_c curve at certain field values in 77 K and 100 K. In order to see this clearer, we normalized J_c values for all the three cases and included them in the insets. A great advantage of type-II superconductors is the large magnetic fields. In our layered structure HTS film, the vertical channels (voids) of micrometer dimension, though undesirable for the microwave related applications, served here as parking spots to trap the fluxes in the film when the Lorenz force to push them out of the film to reach diamagnetic state. These naturally developed columnar defects in the multiple-run cation exchange processing remarkably enhanced the current density in the high magnetic field, which other techniques need a lot extra efforts to do the job.

Previously, Hg-1212B film suggested purer phase, thus sharper transition edge and clean surface morphology seen. This deduction can be confirmed further by R-T curves of the Hg-1212 films. In Fig. 4.7, the upper curve was corresponding to Hg-1212A film, the lower one the Hg-1212B.

One can see although the T_c value in film Hg-1212B was little lower than that of Hg-1212A, the much lower resistivity hinted high phase purity in the film Hg-1212B. This was consistent with the explanation of the purer Hg-1212 phase formation previously. In film Hg-1212A, the coexistence of Tl-1212 and Hg-1212 increased the discontinuity (inhomogeneity) possibly in unit cell scale, thus the number of extra barriers the carriers need to jump across, like we mentioned briefly

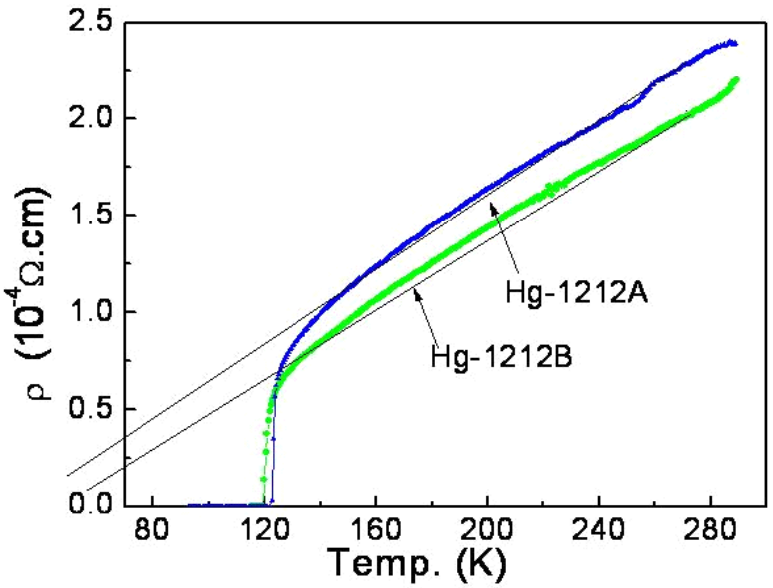

Fig. 4.7 Temperature dependence of resistivity (ρ) of Hg-1212A and Hg-1212B films

III. Conclusion of This Section

To conclude, we have successfully conducted three-runs of reversible cation exchange between epitaxial c-axis oriented Hg-1212 film and Tl-1212 film, starting from Tl-1212 precursor film and elucidated the diffusion mechanism governing the cation exchange processing. Furthermore, the vertical channels developed during consecutive cation exchange processing functioned as flux pinning centers, which are responsible to the obviously increasing of the J_c values in higher magnetic field as well as the overlapping structure in the normalized J_c – H curves of Hg-1212 films. Apparent formation of the alloy Hg-1212 with Tl-1212 had been seen for two intermediate states during the three runs of cation exchange processing. The remarkable increase of critical current density J_c of Hg-1212 film from third cation exchange conversion hinted the better phase purity achieved after three cation exchange conversions, which was supported by the corresponding R-T curves from the same films. The reversible cation exchange might be a good way to fabricated Type II High T_c superconductors, useful for the high field applications, without extra efforts and hence extra cost.

4.2 Converting Hg-1212 to Tl-2212 via Tl–Hg Cation Exchange in Combination with Tl Cation Intercalation

I Motivation

It is confirmed that the cation exchange is reversible between “1212” lattice in last section. This result raises an interesting question of whether the

same or a similar mechanism applies to the cation exchange between Tl-2212 and Hg-1212. An obvious complication in this case is the lattice variation along the *c* axis. In the cation exchange from Tl-2212 to Hg-1212, two Tl–O planes in each unit cell collapse into one Hg–O plane, leading to about 14% reduction in the *c*-axis lattice constant from 1.48 to 1.27 nm. To convert the Hg-1212 back to Tl-2212 via cation exchange the *c*-axis expansion is anticipated, which may be prevented if the forward process from Tl-2212 to Hg-1212 involves a phase transition. To pinpoint the cation exchange mechanism between Tl-2212 and Hg-1212, we have investigated the conversion from Hg-1212 to Tl-2212 at temperatures for which recrystallization of the Hg-1212 lattice is unlikely to happen. We have found that this conversion can be completed under high Tl vapor pressure via two steps: Hg-1212 to Tl-1212 through Tl–Hg cation exchange followed by Tl-1212 to Tl-2212 through Tl cation intercalation. In this paper, we report our experimental results.

II. Sample Preparation

The starting epitaxial Tl-2212 films were fabricated on $LaAlO_3$ (LAO) substrates using the crucible technique and the experimental details have been reported previously [4.7]. Briefly, an amorphous Tl–Ba–Ca–O film with nominal composition of 2.1:2:1:2 was deposited using dc sputtering and annealed at 820 ◦C for 1.0 h in flowing oxygen in a closed crucible. The thickness of these Tl-2212 films was around 300 nm. These samples were then subjected to single or

multiple cation exchanges in either Hg or Tl vapour. In each cation exchange step, the sample was sealed in an evacuated quartz tube together with two pellets to reach a controlled vapor pressure. One of the pellets was an unreacted $HgBa_2Ca_2Cu_3O_x$ one for conversion from Tl-2212 to Hg-1212 (or an unreacted $TlBa_2Ca_2Cu_3O_x$ one for conversion from Hg-1212 to Tl-2212) and the other, a $Ba_2Ca_2Cu_3O_x$ pellet. The first pellet served as the Hg (or Tl) cation vapor source and the second, a vapor absorber to stabilize the pressure during the processing. The weight ratio of the former to the latter was 3:1 and the total pressure inside the quartz tube was estimated at ~5–10 atm. The whole quartz-tube assembly was kept in a furnace at 700 °C for 12 h for the conversion from Tl-2212 to Hg-1212. For the reverse cation exchange from Hg-1212 to Tl-2212, processing in Tl vapor at 760 °C for 2.0 h was employed. It should be mentioned that the crystal lattice decomposing temperature T_{th} is 770–790°C for Hg-1212 films in 0.9 atm pure oxygen. At high Hg vapor pressures of several atmospheres employed in this experiment, much higher T_{th} is anticipated for the Hg-1212 lattice. This means that lattice decomposition and recrystallization at 760 °C is unlikely to occur.

III. Results and Discussion

1. Crystalline Structure

Figure 4.8 shows the x-ray diffraction (XRD) θ–2θ spectra taken on a representative sample at different processing stages in two complete cycles of conversion between Tl-2212 and Hg-1212 structures with (a) the starting Tl-2212

film; (b) after its first cation exchange in Hg vapor at 700 °C for 12 h; (c) after a half-time of the second cation exchange in Tl vapor at 760 °C for 1.0 h (marked with Tl-Interphases); (d) after completion of the second cation exchange in Tl vapor at 760 °C for a total period of 2.0 h; (e) after the third cation exchange in Hg vapor at 700 °C for 12 h; and (f) after the fourth cation exchange in Tl vapor at 760 °C for 2.0 h. The conversion from Tl-2212 to Hg-1212 is nearly complete except for a small volume per cent of remaining Tl-2212 phase, which is 6% and 12%, respectively, from Fig. 4.8 (a) to (b) and from Fig. 4.8(d) to (e). In a similar way, the reverse conversions from Hg-1212 to Tl-2212 [Fig. 4.8(b)–(d) and (e)–(f)] are also nearly 100% with negligible trace of any remaining Hg-1212 phase. This observation, together with our recent result on the reversibility of cation exchange between Tl-1212 and Hg-1212 [4.10], suggests that the cation exchange is a simple perturbation over the volatile cations on the existing lattice and the process is bidirectional, with its direction determined by the population ratio between the two cations involved.

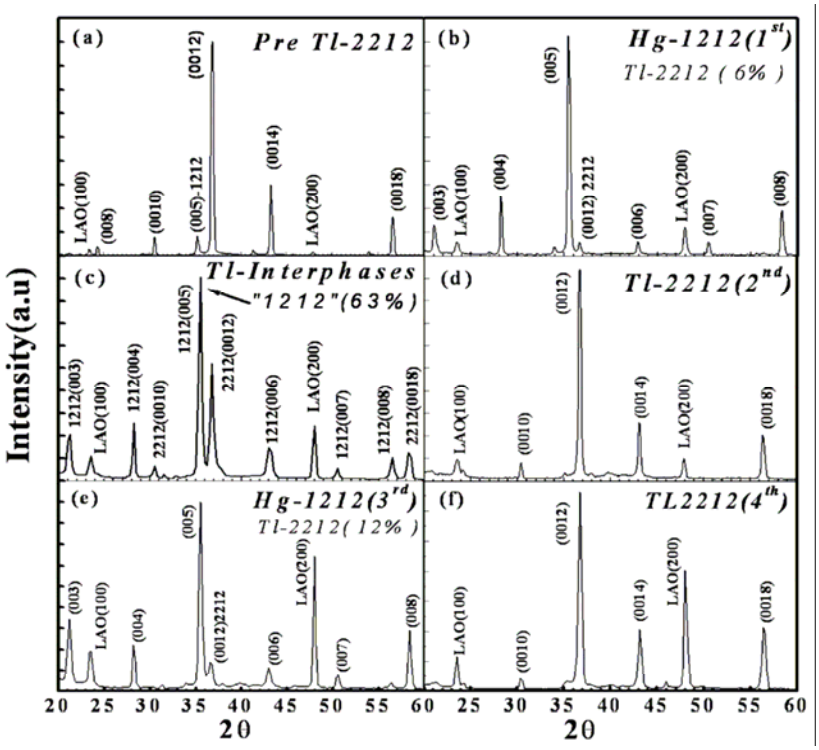

Fig. 4.8 XRD θ–2θ spectra of the sample films: (a) the starting Tl-2212 film; (b) after its first cation exchange in Hg vapor at 700 °C for 12 h; (c) after a half-time of the second cation exchange in Tl vapor at 760 °C for 1.0 h; (d) after completion of the second cation exchange in Tl vapor at 760 °C for 2.0 h; (e) after the third cation exchange in Hg vapor at 700 °C for 12 h; and (f) after the fourth cation exchange in Tl vapor at 760 °C for 2 h. All films were made in sealed quartz tubes except the starting Tl-2212 film.

The conversion between Tl-2212 and Hg-1212, however, differs from the conversion within the '1212' structure because of the *c*-axis lattice variation. From Fig. 4.8, the *c*-axis lattice constant was 1.48 nm for Tl-2212 and 1.27 nm for Hg-1212. To understand how the structural change occurred during the conversion from Hg-1212 to Tl-2212, some samples were processed at shorter time in Tl vapor before the conversion was completed. One distinctive observation on these samples was the large volume portion of the '1212' phase. As shown in Fig. 4.8(c) for an Hg-1212 sample processed in Tl vapor at 760 °C

for 1.0 h, the remaining '1212' phase was 63%. It should be noted that Hg-1212 films can be converted completely to Tl-1212 ones at this same processing condition in Tl vapor of ~1 atm. This leads one to suspect, which was later confirmed in the study of the electromagnetic properties (details in the following), that this '1212' phase is a Tl-1212 phase. This means that the conversion from Hg-1212 to Tl-2212 involved two steps as shown in Fig. 4.9. First, Hg cations on the '1212' lattice was replaced by Tl ones, which can be completed in about 1.0 h at 760 °C and in Tl vapor of ~1 atm and a much shorter period at higher Tl vapor pressures. This Hg-1212 to Tl-1212 conversion was then followed by intercalation of Tl cations into the '1212' lattice for the '2212' lattice to form. The high Tl vapor pressures played a critical role in facilitating the intercalation. It should be mentioned that a similar intercalation process has also been reported for iodine in Bi-based HTS with similar layer structure [4.7-4.9].

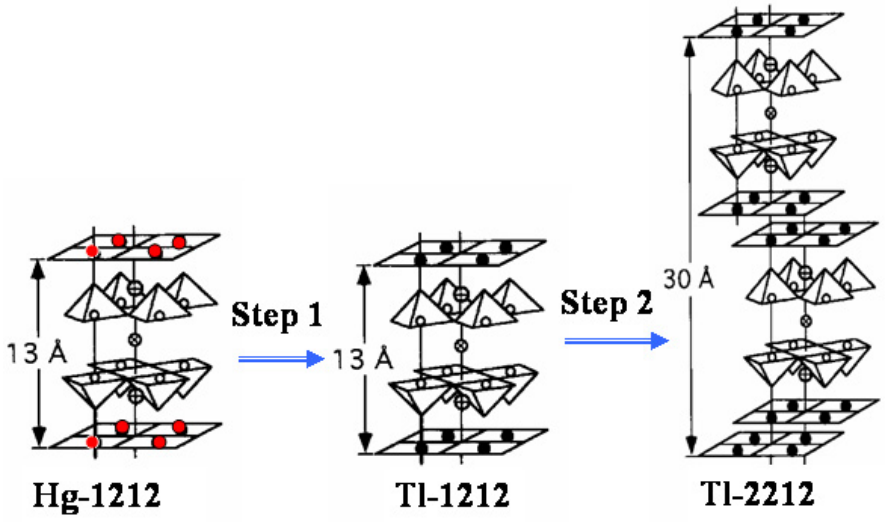

Fig. 4.9 Schematic description of the two steps of the conversion from Hg-1212 to Tl-2212.

2. Surface Morphology

The surface morphology of the samples after each consecutive processing step was analyzed using scanning electron microscopy (SEM). Fig. 4.10 includes the SEM micrographs taken on a Tl-2212 sample through two round trips of conversions: (a) after the first cation exchange in Hg vapor; (b) after the second cation exchange in Tl vapor; (c) after the third cation exchange in Hg vapor; and (d) after the fourth cation exchange in Tl vapor, corresponding to the steps shown in Fig 4.8(b), (d), (e) and (f), respectively.

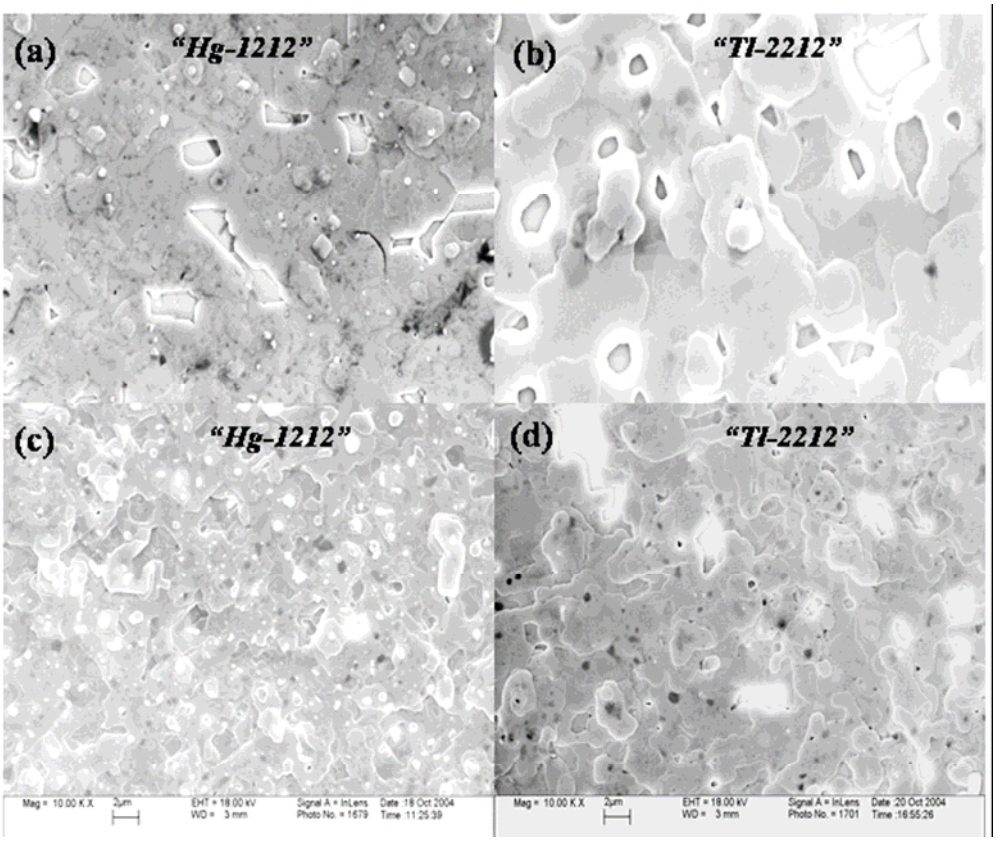

Fig. 4.10 SEM images of a representative sample after several cation exchanges: (a) after the first cation exchange in Hg vapor from a Tl-2212 precursor film; (b) after the second cation exchange in Tl vapor; (c) after the third cation exchange in Hg vapor; and (d) after the fourth cation exchange in Tl vapor.

Overall, the surface morphology experienced minimal changes after two cycles of conversions between Tl-2212 and Hg-1212 except getting slightly denser with each additional processing step. Besides many terrace-like surface steps of increasing dimension with further processing, negligible impurity phases were observable on the surface of the sample, suggesting that phase decomposition during the processing was unlikely.

3. The Superconducting Properties

The superconducting properties of the sample were measured using a Quantum Design SQUID magnetometer. The magnetic moment (M) as a function of temperature (T) on the same sample shown in Fig. 4.10 after each corresponding processing step is plotted in Fig. 4.11(a). The applied magnetic field was 5.0 Oe along the normal of the film and the M–T curves were taken in the zero-field-cooling mode. The two curves measured after the first (solid squares) and third (open squares) cation exchange both in Hg vapor showed a superconducting transition temperature T_c around 120 K, which is consistent with the value expected for Hg-1212 film. This, on the other hand, excludes the possibility of Tl-1212 being the dominant phase. The transition width of the M–T curve for the latter is slightly broader possibly due to the higher remaining Tl-2212 phase (12%) in the sample after this run [Fig. 4.8(e)] as compared to 6% Tl-1212 remaining phase in the first run [Fig. 4.8(b)]. On the other hand, the two M–T curves after the second (solid triangles) and fourth (open triangles) conversion

in Tl vapor nearly coincide with T_c = 105 K as expected for the Tl-2212 phase. Also included in figure 4.11(a) is the *M–T* curve (solid circle) for the sample shown in Fig. 4.8(c). The lower T_c = 100 K indicates the predominant Tl-1212 and Tl-2212 phases, instead of the Hg-1212 one in this sample. This confirms that the conversion from Hg-1212 to Tl-2212 takes a two-step scheme with a cation exchange from Hg-1212 to Tl-1212 followed by Tl cation intercalation in a Tl-1212 lattice to form the Tl-2212. Fig. 4.11(b) compares critical current density J_c as a function of magnetic field (applied along the normal of the film) at T = 5 and 77 K, respectively, for the same sample in Fig. 4.8(b) and (e). At 5 K, the *J*c value was nearly unchanged after a round trip of conversion from Hg-1212 to Tl-2212 and back to Hg-1212. At 77 K, the slightly reduced J_c in lower fields after this round trip may be attributed to the slightly higher volume portion of the Tl-2212 remaining phase.

The reduction of pore (or voids) population may also contribution to the J_c decrease in low magnetic fields since pores serve as strong pinning centers for magnetic vortices. Nevertheless, the J_c values observed in this sample are in the range for our high-quality Hg-1212 films. A similar trend was observed for the same precursor Tl-2212 sample (stars) after the second (solid triangles, after one cycle from the precursor Tl-2212 to Hg-1212 and back to Tl-2212 conversion) and fourth (open triangles, after an additional cycle from Tl-2212 to Hg-1212 and back to Tl-2212) conversion in Tl vapor.

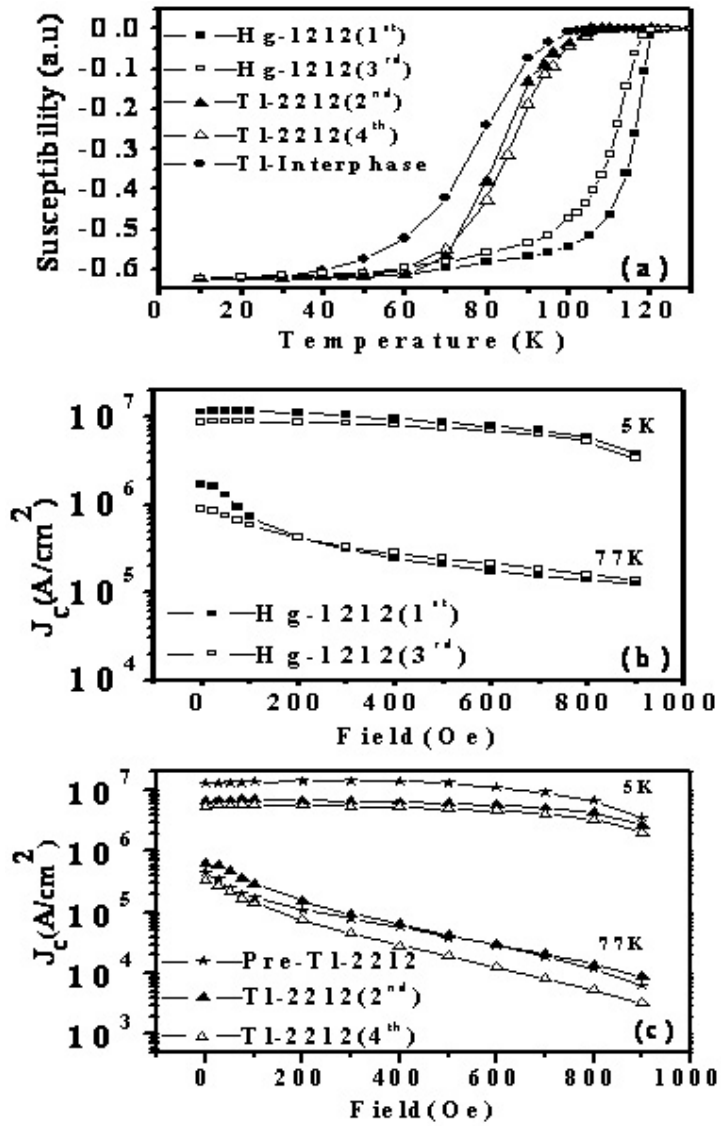

Fig 4.11 (a) Magnetic susceptibility as a function of temperature measured in zero-field-cooling mode for a sample experiencing several cation exchanges. (b) Comparison of the J_c values of the same sample in Hg-1212 phase after the first and third cation exchange from Tl-2212. (c) Comparison of J_c values of the same sample in Tl-2212 phase before any cation exchange (marked with Pre-Tl2212) and after the second and fourth cation exchange from Hg-1212.

The result is shown in Fig. 4.11(c). At 5 K, the precursor Tl-2212 film has the highest *J*c value, which decreases slightly after the first cycle while it does not change much after the second cycle. At 77 K, on the other hand, a minimal *J*c

change was observed after the first cycle, while some noticeable reduction was seen after the second cycle. Since J_c sensitively dictates the changes occurring to the sample microstructure, these minor changes in J_c values suggest that some defect structural variation may occur during the processing.

IV. Conclusion of This Section

In summary, we have demonstrated the conversion from Hg-1212 to Tl-2212 structure can be achieved at relatively higher Tl vapor pressure and the conversion consists of two steps: from Hg-1212 to Tl-1212 via Tl–Hg cation exchange on the '1212' lattice followed by Tl-1212 to Tl-2212 via Tl cation intercalation. We have shown that the changes in the sample's physical properties are minimal after the sample underwent two full cycles of cation exchange processes. This result, together with our recent demonstration of reversibility of cation exchange within the '1212', suggests that the cation exchange is a simple perturbation over the volatile cations on the existing lattice and the process is bidirectional with its direction determined by the population ratio between the replacing cation and the one to be replaced.

Chapter 5

Third-Order Intermodulation in Two-Pole X-Band $HgBa_2CaCu_2O_{6+\delta}$ Microstrip Filters

HTS microwave filters hold a great promise for applications because of the significantly lower surface resistance (R_s) as compared to that of their normal metal counterparts [5.1, 5.2]. This has prompted intensive studies in recent years on the improvement of HTS microwave device performance particularly in the high power range. Among many different materials studied, such as $YBa_2Cu_3O_7$ (YBCO), $Tl_2Ba_2CaCu_2O_8$ (Tl-2212) and $HgBa_2CaCu_2O_{6+\delta}$ (Hg-1212) [5.3-5.6], Hg-1212 is of special interest because of its high transition temperature (T_c) above 120 K. Since a higher T_c allows higher device operation temperatures, a lower cost is projected considering higher efficiency of commercial cryogenic systems. In our previous study, we have observed low microwave surface resistance (R_s) and high power handling capability in Hg-1212 films and microstrip resonators up to 110 K [5.7]. More recently, we have fabricated Hg-1212 two-pole X-band microstrip filters using a cation exchange process[5.8] and observed a low insertion loss of 0.70 dB at 110 K, which is better than that of YBCO and Cu at 77 K[5.6]. These results have demonstrated that Hg-1212 is a promising alternative material for passive microwave applications at operation temperatures

above 77 K.

5.1 Nonlinearity in HTS Passive Microwave Devices

Nonlinear effects in HTS passive microwave devices are considered to be the major cause that limits the power handling capability of the devices. Therefore, understanding the nonlinearity is of great importance to the application of the HTS microwave devices. The nonlinear effects appear in various different ways including:

I. Nonlinear surface impedance [5.20]

The HTS nonlinearity is believed to originated either from the RF magnetic field or from RF current dependence of surface impedance, $Z_s = R_s + jX_s$, of HTS materials. In the low field region ($H_{rf} < 10$ Oe), the weak links is regarded as governing role for nonlinearity in the HTS film [5.9], whereas in the intermediate field (10 Oe to 50 Oe at 77K), the measured R data for YBCO can be fitted well with the following expression:

$$R_s\left(H_{rf}\right) = a(f,T) + b(f,T)H_{rf}^2, \qquad (1)$$

Where f is the frequency, T the temperature, b (f, T) is proportional to f^2. The expression of the surface resistance above is consistent with the postulation that the RF field is breaking Cooper pairs. Interestingly, R_s increases faster than H^2 in the high field (50 Oe to 300 Oe), suggesting that the losses in the high power region may be determined by hysterestic losses.

II. Generation of harmonics

Like any other nonlinear elements in an RF circuit, harmonics can be generated from a HTS device, especially for high incoming microwave intensity. Macroscopically, the nonlinear effect can be treated by a nonlinear resistance.

$$I(V) = I(0) + (\tfrac{dI}{dV})_{V=0}\delta V + \frac{1}{2!}(\frac{d^2I}{dV^2})_{V=0}\delta V^2 + \frac{1}{3!}(\frac{d^3I}{dV^3})_{V=0}\delta V^3 + O(\delta V^4) \tag{2}$$

Since I (-V) = -I (V), the lowest harmonic is the third order one. Consider a sinusoidal signal:

$$\delta V = v\sin\omega t \tag{3}$$

Substituting (3) into (2), the third harmonic term is

$$-\frac{1}{24}(\frac{d^3I}{dV^3})_{V=0}v^3\sin 3\omega t \tag{4}$$

Take the logarithm of the amplitude:

$$y = \log[\frac{1}{24}(\frac{d^3I}{dV^3})_{V=0}v^3] = \log[\frac{1}{24}(\frac{d^3I}{dV^3})_{V=0} + 3x, \tag{5}$$

where $x = \log v$. In the x-y plane, (5) gives a straight line with a slope that equals to 3.

III. The third-order intermodulation (*IM3*) [5.9].

When two signals at frequencies f1 and f_2 with the same amplitude are applied to a device, such as filter, the initial phase can be expressed as:

$$\delta V = v(\sin\omega_1 t + \sin\omega_2 t) \tag{6}$$

Instituting (6) into (2), a signal with frequency $2f_1$ - f_2 will be generated by nonlinearity. The third-order intermodulation frequency ($2\omega_1 - \omega_2$) term is

$$-\frac{1}{8}\left(\frac{d^3 I}{dV^3}\right)_{V=0} v^3 \sin(2\omega_1 - \omega_2)t \qquad (7)$$

The amplitude of the third-order intermodulation frequency (*IM3*) signal increases with the amplitudes of the two input signals.

Although they are all related to the nonlinear surface impedance [5.10], their relative impacts on the performance of microwave devices may vary greatly in each special case. For example, in passive rf filters, *IM3* is perceived to be the most serious problem to deal with due to the generation of spurious signals within the passing band of the filter, which consequently deteriorates the device performance. The origin of the nonlinearity has been a debate and various mechanisms have been proposed. Two popular models proposed explain the mechanism of the nonlinearity in passive microwave devices based on field-driven[5.11] or current-driven.[5.12] In the former, the nonlinearity was attributed to the penetration of magnetic vortices while in the latter, the exceeding limit of the rf current density. Since inconsistency was observed in devices of different magnetic field configuration[5.13], the field-driven mechanism may have strong limitations in explaining the nonlinearity. The current-driven mechanism has also been investigated in HTS devices and the difficulties associated to this study are caused by multiple current limiting factors, intrinsic and extrinsic, including grain-boundary Josephson junction behavior [5.14, 5.15], pair breaking[5.16, 5.17], and vortex depinning[5.12]. Although some of the extrinsic effects can be

minimized by improving the HTS materials, it remains an intensive research topic to untangle the intrinsic current-limiting factors, which may behave differently at different temperatures [5.12, 5.18].

The microwave nonlinearity has not been investigated so far in Hg-1212 devices, despite its importance to the device applications and also to the understanding of the nonlinearity mechanism. Motivated by this, we have studied the *IM3* in two-pole Hg-1212 X-band microstrip filters. We have made comparisons between the dc critical current density J_c and the rf current density J_{IP3} derived from the third-order intercept at a reduced temperature scale for both Hg-1212 and YBCO filters of the same configuration. Our results suggest that the nonlinearity *IM3* correlates intimately with the magnetic vortex depinning in HTS materials, which is consistent with the current-driven model. In this paper, we report our experimental results and theoretical analysis.

5.2 Fabrication and Characterization of Two-Pole Hg-1212 Filters

5.2.1 Fabrication and Transmission Properties of Hg-1212, YBCO and Tl-2212 filters

Two-pole X-band Hg-1212 microstrip filters were prepared in a two-step process: photolithographically patterning the Tl-2212 precursor films into two-pole band-pass filters followed by Hg vapor-annealing of the resulting superconducting filters using the cation exchange process [5.8]. The thickness of the Hg-1212 filters is around 0.44 μm. For comparison, filters of the same

geometry and configuration were also fabricated on YBCO and Tl-2212 films of 0.5 μm thickness. Silver electrodes were laid on the feedlines of the filters via a shadow mask using dc magnetron sputtering. For YBCO and Tl-2212 filters, the Ag contacts were deposited before lithography while for Hg-1212 filters, after the cation exchange. All filters were fabricated on 5 mm (width) × 10 mm (length) × 0.5 mm (thickness) single crystal (001) $LaAlO_3$ (LAO) substrates. Fig. 5.1 shows the normalized magnetic susceptibility of the Hg-1212, Tl-2212 and YBCO films (before lithography) as function of temperature measured by a Quantum Design superconducting quantum interference device magnetometer in zero-field-cooled mode in 10 Oe magnetic fields applied along the normal of the film. The T_c values are 118 K for Hg-1212, 88 K for YBCO and 102K for Tl-2212. A plot of the dc critical current density J_c against the temperature is shown in Fig. 5.2 for Hg-1212, Tl-2212 and YBCO films, respectively. At 77 K, the J_c values are ~1.15 MA/cm^2 for Hg-1212, ~0.47 MA/cm^2 for Tl-2212 and ~1.16 MA/cm^2 for YBCO. These values fall into both the T_c and J_c range, respectively, for high-quality Hg-1212, Tl-2212 and YBCO films of the thickness of 0.5 μ m.

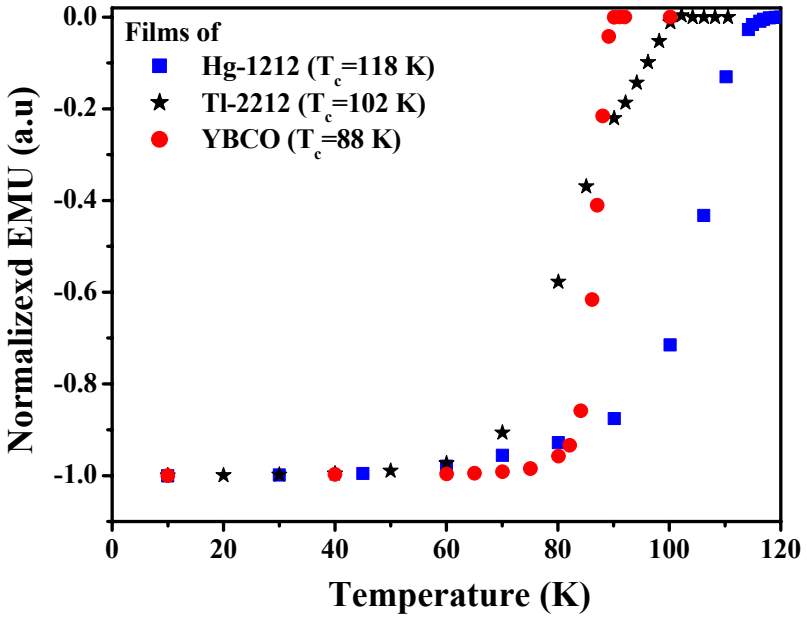

Fig. 5.1 Magnetic susceptibilities as a function of temperature of the Hg-1212 and YBCO films measured in zero-field-cooled mode. The magnetic field was 10 Oe applied along the normal of the film.

Fig. 5.3 plots the frequency dependence of the S_{21} transmission for all three types of filters. The insertion losses measured at 77 K are 1.7 dB for YBCO filter, 2.2 dB for Tl-2212 filter. They are plotted against the Hg-1212 result of 110 K where the insertion loss is approximately 0.6 dB. Overall, the Hg-1212 filter provides better performance over both the Tl-2212 and YBCO filters at an operating temperature 33 K higher.

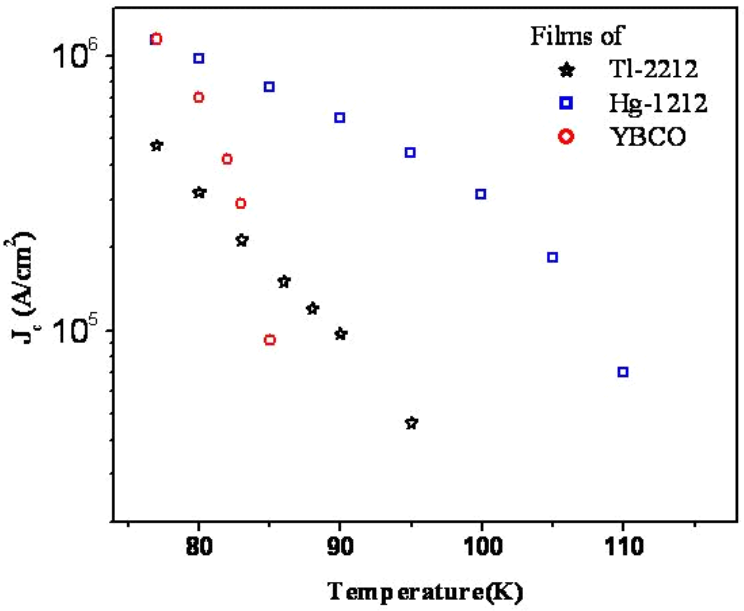

Fig. 5.2 Temperature dependence of critical current density (J_c) for all three types of films.

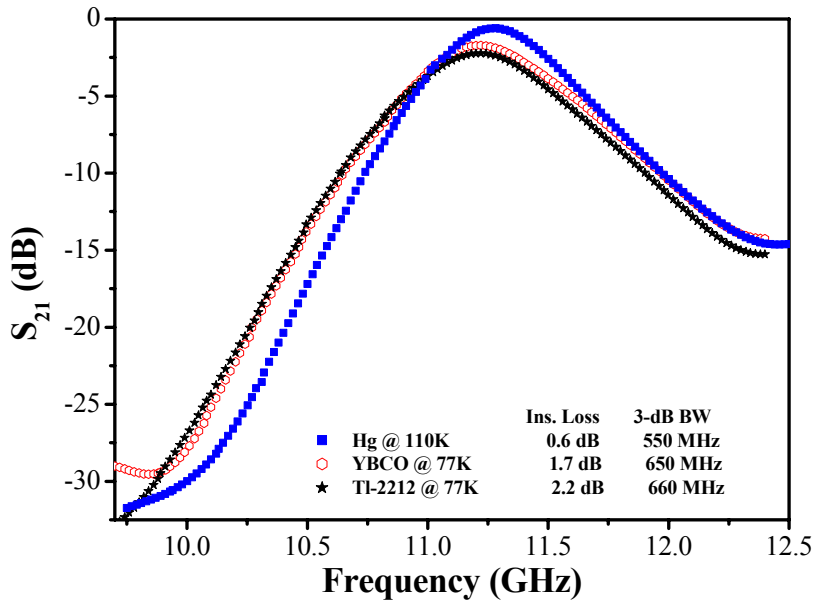

Fig. 5.3 Comparison of plots of S_{21} vs. frequency for three types of filters: Hg-1212, Tl-2212 and YBCO.

5.2.2 Comparison of Third Order Intermodulation of Hg-1212 Filters with YBCO and Tl-2212 Filters

The *IM3* signals were measured at several different temperatures in the range between 77 K and 110 K. The third-order intercept point (*IP3*), which is defined as the input power at which extrapolations of the fundamental and the *IM3* curves intersect, was extracted from the measurement. In general, a higher *IP3* value corresponds to a weaker nonlinearity and hence greater power-handling capability. Fig. 5.4(a) illustrates a schematic of the experimental set-up for measurement of the fundamental and *IM3* signals. Microwave signals were generated using two sources: Agilent signal generators E8257D and E8251A. An Agilent microwave network analyzer E8362B was utilized as a spectrum analyzer with its receiver function. Two inputs with the same power at different frequencies (f_1=11.105 GHz) and f_2=11.110 GHz) were chosen near the resonant frequency. The inset of Fig. 5.4(a) shows the layout of the two-pole microstrip filter and the details of the dimension have been described elsewhere [5.6, 5.19]. Fig. 5.4(b) exhibits the input versus the output power at different temperatures for a representative Hg-1212 filter. The measured output powers for both fundamental and *IM3* signals were linearly proportional to the input power within the measurement range up to 25 dBm (the upper limit of our instrument). Extrapolating both the fundamental and the *IM3* signals to higher input powers reveals the intersection point of the two curves and allows determination of the *IP3* value. At 77 K, the *IP3* value is around 58 ± 1 dBm and it decreases with increasing temperature. At 90 K, the *IP3* is about 55 ± 1 dBm and at 110 K, 38 ± 1

dBm. It should be noticed that the *IP3* value obtained at 110 K represents the best reported so far for superconducting microwave filters. The observed slopes of the *IM3* signals in Fig. 5.4(b) were 2.7 at 77 K, 3 at 90 K, and 3.4 at 110 K, respectively, which differ slightly from the constant theoretical value of 3[5.20]. Interestingly, a weak temperature dependence of the slope has also been observed on the YBCO filters and the slope decreases with increasing temperature, in agreement with what reported by other groups [5.21, 5.22]. It has been noticed that at 77 K, the Hg-1212 and YBCO filters have comparable slopes on the *IM3* curve (2.8 at 77 K for YBCO). However, the values of the slopes in YBCO filter were systematically lower than that in Hg-1212 filter at the same reduced temperatures [see the inset of Fig. 5.4(b)]. Since higher slope of the *IM3* curve leads to lower interception point between the fundamental and the IM3 curve, lower *IP3* or power handling capability is then expected from Hg-1212 at a given reduced temperature. This difference between Hg-1212 and YBCO may be attributed to the different magnetic vortex pinning strength of these two materials, as we will discuss in detail later in this paper. Fig. 5.5 compares the *IP3* values of the Hg-1212, Tl-2212 and YBCO filters as function of temperature. In the temperature range of 77 K to 110 K, the Hg-1212 filter exhibited higher *IP3* than that of the Tl-2212 and YBCO filter and the difference between the *IP3* values of three types of filters increases with temperature. At 77 K, the *IP3* for Hg-1212 filter is 58 dBm, 1 dBm higher than that of YBCO (57 dBm) and 4 dB higher than that of Tl-1212(54 dB), respectively. At 110 K, the Hg-1212 filter has a similar

IP3 of 38 dBm to that of YBCO at 85 K and Tl-2212 around 90 K. The higher *IP3* values of Hg-1212 filters are more or less expected and are attributed to the higher T_c of Hg-1212 and suggest that Hg-1212 is indeed an alternative for passive microwave devices operating at higher temperatures.

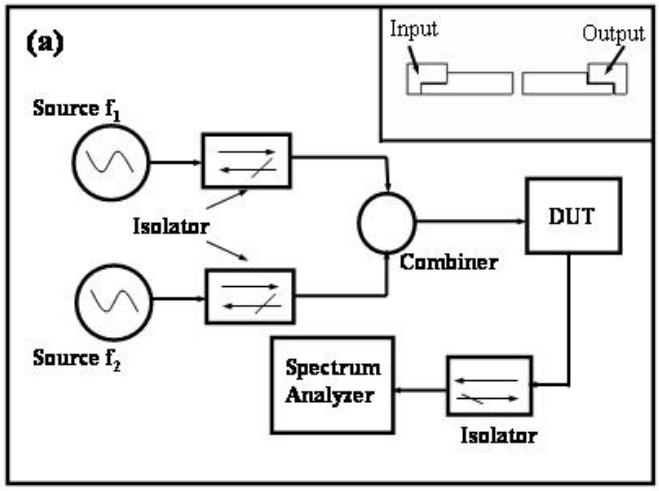

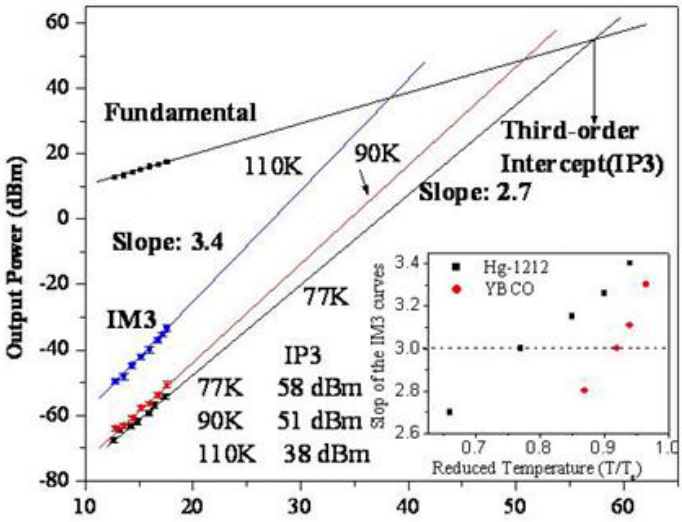

Fig. 5.4 (a) Schematic diagram of the experimental set-up for measuring *IMD* signals. Inset: Design layout for the two-pole half-wavelength filter with width of 0.7 mm. (b) Input power versus the output power at different temperatures for the Hg-1212 filter. Inset: the slop of the *IM3* curves against reduced temperature.

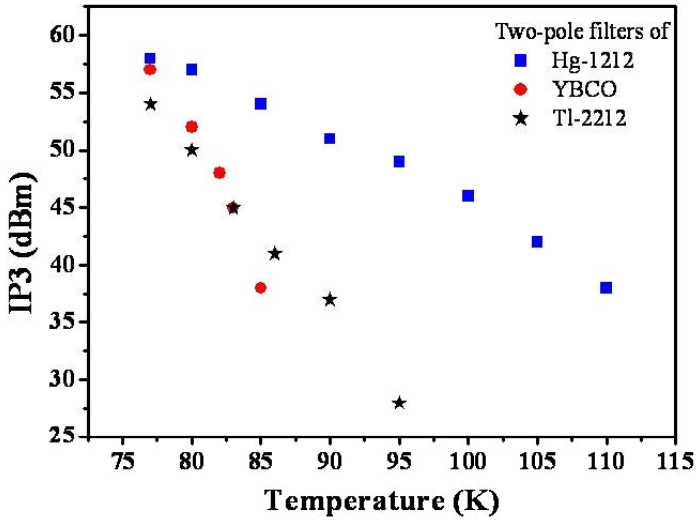

Fig. 5.5 Plot of the *IP3* values for Hg-1212, Tl-2212 and YBCO filters

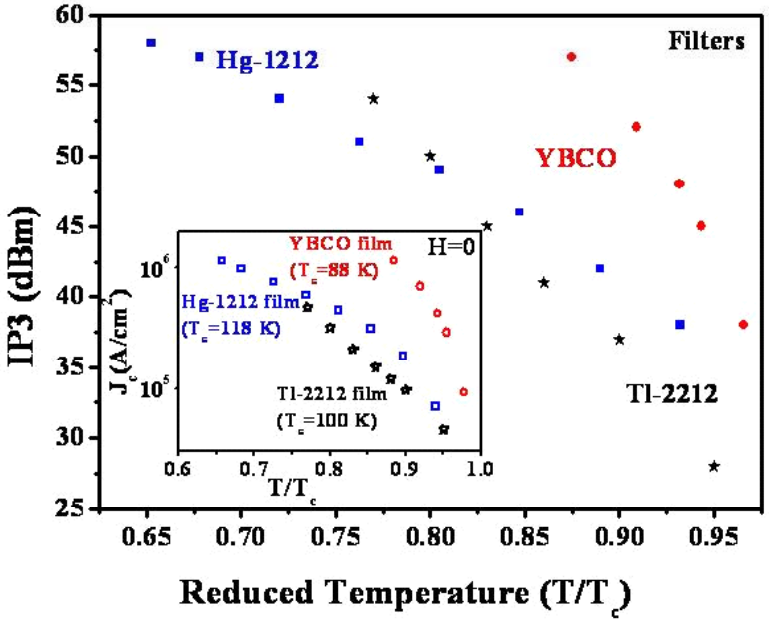

Fig. 5.6 Plot of the IP3 values for Hg-1212, Tl-2212 and YBCO filters at reduced temperature scale. Inset: Temperature dependence of the dc critical current density (J_c) for the three types of films before patterning.

Also worth mentioning is the 0.44 μm thickness of the Hg-1212 filter which is slightly smaller than that of YBCO (0.50 μm). It has been reported that the transmission properties of the microwave filters improve as the thickness increases up to a certain range (0.8 μm) [5.3]. This implies that the *IP3* values of the Hg-1212 filter could be higher if the *IP3* value scales with film thickness.

Since the higher T_c of Hg-1212 is the main reason for the higher *IP3* values observed in Hg-1212 filters, the *IP3* curves were replotted on the reduced temperature (T/T_c) scale to eliminate the T_c effect and to facilitate a direct comparison between Hg-1212, Tl-2212 and YBCO filters. As shown in Fig. 5.6, better power-handling performance can be obtained from the YBCO filters at a given reduced temperature. To understand the mechanism underlying this performance difference, a plot of the dc critical current density (J_c) against the reduced temperature is included in the inset of Fig. 5.6 for Hg-1212, Tl-2212 and YBCO films, respectively. Interestingly, the J_c vs. T/T_c curves for these three different materials show qualitatively similar trends to their *IP3* vs. T/T_c curves. Since J_c is determined by the strength of the magnetic pinning in a specific material, the difference in the J_c vs. T/T_c curves of YBCO, Tl-2212 and Hg-1212 films has been attributed to the different magnetic vortex pinning strength of these three materials. Tl-2212 is extremely two-dimensional. The magnetic vortices formed in Hg-1212 have geometry of “pancakes” that are weakly interacting along the c-axis [5.23]. This is in contrast to the regular vortices formed in the three-dimensional YBCO. The “pancakes” vortices can be depinned much more

easily than the regular ones, which results in weaker magnetic vortex pinning in Hg-1212 and Tl-2212 as compared to YBCO.

In order to make a quantitative assessment of the correlation between the dc and rf properties, the rf current density J_{IP3} was calculated from the measured *IP3* values. The rf current I_{IP3} can be derived from the measurement of the P_{IP3} according to[5.12].

$$I_{IP3} = \sqrt{\frac{2P_{IP3}}{Z_L}}, \qquad (1)$$

Where Z_L is the transmission line impedance. In a microstrip resonator, the rf current density maximizes near the edge of the microstrip and the edge current in the microstrip resonator can be written as: [5.24]

$$J = \frac{j(0)\sqrt{wt}}{2\lambda}, \qquad (2)$$

within roughly λ^2 / t of the edges. Where λ is the penetration depth, *w* is the width and *t,* the thickness of the strip, and the value *j* (0) can be calculated by [5.24]

$$I = \int jds \approx \frac{\pi}{2} j(0)wt. \qquad (3)$$

In the same way, the rf current density J_{IP3} in two-pole microstrip filter can be approximately expressed as:

$$J_{IP3} = \frac{j_{IP3}(0)\sqrt{wt}}{2\lambda} = \sqrt{\frac{2P_{IP3}}{Z_L}} \times \frac{1}{\pi\lambda\sqrt{wt}} \qquad (4)$$

Thus, near the edge, the ratio of the intermodulation current density J_{IP3} to J_{IP3} at 77 K is

$$\frac{J_{IP3}(T)}{J_{IP3}(77K)} = \left[\frac{P_{IP3}(T)}{P_{IP3}(77K)}\right]^{1/2} * \frac{\lambda(77K)}{\lambda(T)}, \qquad (5)$$

where, the $\lambda(T)$ is the magnetic penetration depth that depends on temperature via:

$$\lambda(T) = \lambda_0[1-(\frac{T}{T_c})^4]^{-1/2}. \qquad (6)$$

Fig 5.7 compares the normalized $J_{IP3}/J_{IP3}(77K)$ with $J_c/J_c(77K)$ against the reduced temperature for Hg-1212, Tl-2212 and YBCO filters. It is clearly shown that the normalized J_{IP3} (triangles) and J_c (squares) curves follow a similar trend on the reduced temperature scale for the three types of filters. It is well known that the dc J_c in an HTS film is limited mainly by the depinning of the magnetic vortices. The best J_c value achieved in YBCO, for example, is at least an order of magnitude lower than the theoretical depairing J_c. This differs from the rf case where the nonlinerity or J_{IP3} is determined by different mechanisms at different temperatures. In the low temperature range much below T_c, the dominant mechanism is d-wave intrinsic while at high temperatures near T_c, it has been anticipated that magnetic vortex depinning plays the dominant role [5.18]. The similar reduced temperature dependence observed in the normalized J_{IP3} to that of J_c suggests that the magnetic vortex pinning mechanism indeed determines, or at

least plays the dominant role on, the nonlinearity J_{IP3} in Hg-1212, Tl-2212 and YBCO at elevated temperatures near T_c.

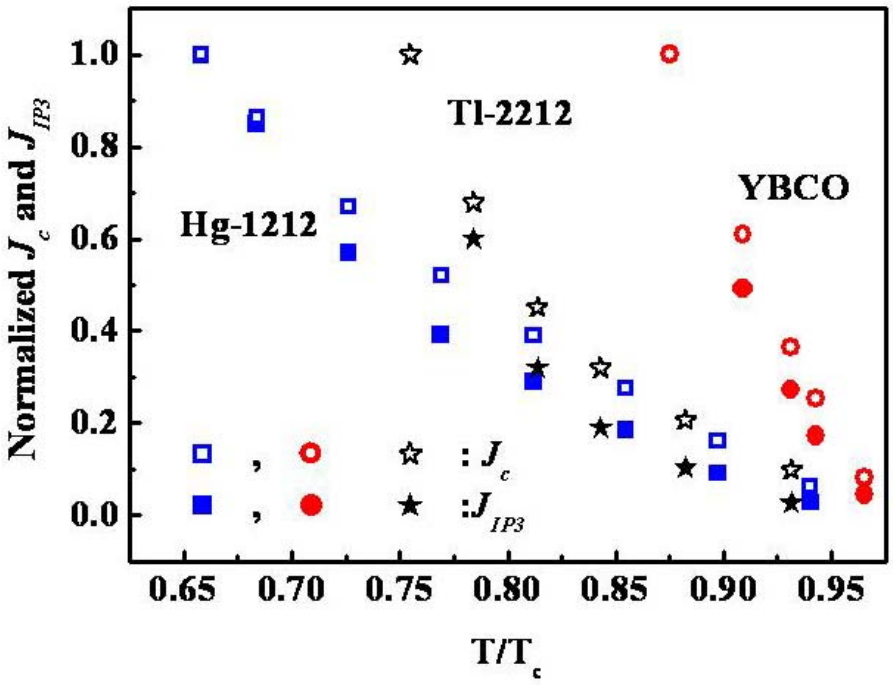

Fig. 5.7 Normalized J_{IP3} /J_{IP3} *(77 K)* with J_c/J_c *(77 K)* against reduced temperature for Hg-1212, Tl-2212 and YBCO patterned into the same type of microstrip filters.

It should be mentioned that the correlation between J_{rf} and J_c has been studied by others [5.4, 5.12] while no consensus has been achieved. On YBCO coplanar resonators, Lahl and Wördenweber reported the same maximum rf current density $J_{rf,\,max}$ derived from the measured breakdown power P_{max} and the dc J_c over the whole temperature range below T_c. They argued that the fundamental limiting mechanism in the absence of thermal and grain-boundary effects is given by dc J_c, which disagrees with observation of intrinsic d-wave nonlinearity in high-quality YBCO films at low temperatures not very close to T_c

[5.18]. It should be noticed that the dc J_c values shown in Ref. 12 are a factor 2-3 lower than that reported for typical high-quality YBCO films of comparable thickness of ~ 300 nm[5.25]. In fact, the normalized J_{IP3} values obtained in this work are consistently lower than the dc J_c. On Tl-2212 hairpin resonators, Willemsen *et al* [5.4] compared the curves of intermodulation critical current density J_{IMD} (derived from the intermodulation power P_{IMD}) [5.24] with J_c at the lower input power (from 0 to -40 dBm). Large discrepancy between the J_{IMD} and J_c was observed. The authors argued that the J_{IMD} and J_c describe different physical regimes with J_{IMD} describes the low-power microwave behavior while J_c characterizes the high-power dc behavior. It should be realized that Tl-2212 is an extremely two-dimensional HTS system in which magnetic vortices form "pancakes" that are weakly interacting along the c-axis. This results in much weak magnetic pinning in Tl-2212 as opposed to the strong pinning in three-dimensional YBCO. Similar to Tl-2212, Hg-1212 is also known as a two-dimensional HTS system. The surprising similarity in the curves of the normalized dc J_c and rf J_{IP3} against reduced temperature in YBCO and Hg-1212 filters strongly supports the current-driven mechanism in HTS microwave filters and the prediction given by Oates[18] that flux pinning plays a major role in the nonlinearity in high temperature region. Indeed, the weaker pinning Hg-1212 shows lower dc J_c and rf J_{IP3} than that of the stronger pinning YBCO as demonstrated in this work.

5.3 Summary of this Chapter

In summary, microwave nonlinearity has been investigated in X-band Hg-1212 two-pole filters and comparisons were made with Tl-2212 and YBCO filters of the same configuration. The power handling capability of the filter was characterized by monitoring the third-order intermodulation signals. Higher *IP3* values were observed in Hg-1212 filters, as compared to that of YBCO and Tl-2212 ones, in the temperature range at and above 77 K. At 77 K, the *IP3* is 58 dBm for Hg-1212, which is higher than that of YBCO filter by ~1 dBm and Tl-2212 filter by ~4 dB. The difference between the *IP3* values for Hg-1212, Tl-2212 and YBCO increases monotonically with increasing temperatures. At 85 K, the *IP3* value for Hg-1212 is about 54 dBm, which is ~18 dBm higher than that of YBCO. At 110 K, a substantial *IP3* of 38 dBm remains in Hg-1212 filter, demonstrating that Hg-212 could be a promising alternative material for microwave passive device applications at temperatures above 77 K. In addition, the curves of the normalized dc critical current density J_c and the normalized rf current density J_{IP3} against the reduced-temperature have a similar trend for Hg-1212, Tl-2212 and YBCO, respectively, suggesting that flux pinning is responsible for the microwave nonlinearity in HTS films at high temperatures.

Chapter 6

Conclusions and Outlook

I. Conclusions

In investigation of underlining mechanism and the improvement of the cation exchange processing, there were three major achievements. Let me summarize them one by one. We have fabricated epitaxial c-axis oriented $(Hg_{0.94}Re_{0.06})Ba_2CaCu_2O_6$ films by replacing the Tl cations from an epitaxial $(Tl_{1.88}Re_{0.12})Ba_2CaCu_2O_x$ precursor films in the cation-exchange process. It was found that the presence of nonvolatile Re on the precursor lattice pins the lattice locally so as to reduce the large-scale lattice collapse, which occurs on undoped Tl-2212 precursor lattice and typically results in micrometer size voids in Hg-1212 films after the cation exchange processing. By pinning the lattice with Re doping, the void size has been reduced by an order of magnitude and the surface morphology has been improved dramatically. In addition, this result has also demonstrated for the first time that Tl-2212 precursor lattice doped with nonvolatile elements on the volatile Tl sites can be employed for epitaxy of chemically doped Hg-1212 films in cation exchange process, enabling tailoring microstructure and physical properties of Hg-1212 films in a much controllable fashion.

Reversibility in cation exchange has been proven by solid experimental work and theoretical analyses. Between 1212 phase of Hg-based and Tl-based HTS films, we have successfully conducted three-runs of reversible cation exchange between epitaxial c-axis oriented $HgBa_2CaCu_2O_6$ film and $TlBa_2CaCu_2O_x$ film, starting from $TlBa_2CaCu_2O_x$ precursor film and elucidated the diffusion mechanism governing the cation exchange processing. Furthermore, the vertical channels developed during consecutive cation exchange processing functioned as flux pinning centers, which are responsible to the obviously increasing of the J_c values in higher magnetic field as well as the overlapping structure in the normalized J_c –H curves of Hg-1212 films. Apparent formation of the alloy Hg-1212 with Tl-1212 had been seen for two intermediate states during the three runs of cation exchange processing. The remarkable increase of critical current density J_c of Hg-1212 film from third cation exchange conversion hinted the better phase purity achieved after three cation exchange conversions, which was supported by the corresponding R-T curves from the same films. The reversible cation exchange might be a good way to fabricated Type II High T_c superconductors, useful for the high field applications, without extra efforts and hence extra cost.

Between Tl-2212 and Hg-1212 phase of the films, we have demonstrated the conversion from Hg-1212 to Tl-2212 structure can be achieved at relatively higher Tl vapour pressure and the conversion consists of two steps: from Hg-1212 to Tl-1212 via Tl–Hg cation exchange on the '1212' lattice followed by Tl-1212

to Tl-2212 via Tl cation intercalation. We have shown that the changes in the sample's physical properties are minimal after the sample underwent two full cycles of cation exchange processes. This result, together with our recent demonstration of reversibility of cation exchange within the '1212', suggests that the cation exchange is a simple perturbation over the volatile cations on the existing lattice and the process is bidirectional with its direction determined by the population ratio between the replacing cation and the one to be replaced.

Regarding characterization of the microwave devices, microwave nonlinearity has been investigated in X-band Hg-1212 two-pole filters and comparisons were made with YBCO filters of the same configuration. The power handling capability of the filter was characterized by monitoring the third-order intermodulation signals. Higher *IP3* values were observed in Hg-1212 filters, as compared to that of YBCO ones, in the temperature range at and above 77 K. At 77 K, the *IP3* is 58 dBm for Hg-1212, which is higher than that of YBCO filter by ~1 dBm. The difference between the *IP3* values for Hg-1212 YBCO increases monotonically with increasing temperatures. At 85 K, the *IP3* value for Hg-1212 is about 54 dBm, which is ~18 dBm higher than that of YBCO. At 110 K, a substantial *IP3* of 38 dBm remains in Hg-1212 filter, demonstrating that Hg-212 could be a promising alternative material for microwave passive device applications at temperatures above 77 K. In addition, the curves of the normalized dc critical current density J_c and the normalized rf current density J_{IP3} against the reduced-temperature have a similar trend for Hg-1212 and YBCO, respectively,

suggesting that flux pinning is responsible for the microwave nonlinearity in HTS films at high temperatures.

II. Outlook

Maintaining momentum accumulating from the substantial works performed in the past pertinent to cation exchange processing and relevant applications in our group, remarkable progress has been achieved through research work activities in my thesis. These achievements kick doors widely open towards fundamental science as well as applications. It is extensively accepted that one of the important driving forces in HTS field is the applications of the superconductors. With the maturity of the cation exchange methodology, application push will be a fruitful direction to go along with Hg-based HTS.

The binding energy of Cooper pairs in a superconductor is of tens μeV to tens of meV, depending on if surrounding temperature (external magnetic field) is at proximity of T_c (H_c) or far away from the value. [6.1, 6.2] The absorption of a single optical photon (energy of 1.2 eV at a wavelength of 1μm) can therefore break a large number of Cooper pairs and hence create quasiparticles. The corresponding changes of microwave properties can be used as a sensing means to detect photon flux ranging from X-rays to THz wave at different temperature [6.1-6.3]. In another end, the combination of the quasiparticles can generate photons with THz frequency. In short, HTS cuprate superconducting materials have drawn great attention in photonics sector due to their excellent transparency and strong photoconductive effect and pyroelectric effect in near-IR through far-

IR waveband (THz) [6.1-6.6]. This intrinsic correlation between THz wave and HTS material family has been envisioned as one of the great potentials of the HTS applications.

Terahertz (THz) electromagnetic (EM) wave, which spans from 100 μm to 1000 μm in wavelength (or $h\nu \approx 1.24 \sim 12.4$ meV in photon energy) has attracted a lot of attentions in recent years due to its broad spectrum of potential applications. [6.1] Among these applications are biological use in many sectors, such as medicine (disease and wound states, skin hydration, plaque, and bone density) homeland security (biological threat detection and explosive materials detection), astronomy exploration (planetary science and life detection), biochemistry (pharmaceutical, DNA analysis), food industry (on-line water content monitoring). Emerging THz wave imaging has become a complement or substitute to X-rays or MRI, particularly for organic substances because of its intrinsically non-ionizing attributes.

In the massive research work related to this rapidly growing field within last decade, tremendous efforts have been made on THz sources developments, while much less efforts on detection side. Although THz imaging is highly promising simply because of their intrinsic match of various fundamental resonances of matters, such as phonons, molecule rotations, intraband electronic transitions, etc, reports regarding detectors development are much less than sources investigation for the rarely explored EM band. It is believed that increasing the sensitivity of the detector would go a long way towards real

applications more efficiently in the standpoint of economics. Currently, most THz detectors can only get intensity of total THz spectrum they see. It is highly desirable to get a detector, which can achieve the entire spectrum of interest to identify the target materials under investigation by comparing against the signature database of THz frequency regime.

Commercial uses for THz sensors and sources are just sprouting as the technology enables new instrumentation and measurement systems. However, generation and detection of THz wave are still of the state of art, particularly, effectively detecting of THz electromagnetic wave is still one of the major roadblocks to the extensive applications of THz technology. The existing THz detection technologies and their availability are as follows: [6.1]

- LHe-cooled detectors
  - Bolometers - commercially available, NEP~10^{-12} - 10^{-13} W/Hz $^{1/2}$
  - Photoconductive Detectors – commercially available, NEP~10^{-15} W/Hz$^{1/2}$
- Room temperature mixers
  - Schottky barrier diodes – ~commercially available, NEP~10^{-19} W/Hz$^{1/2}$
- LHe-cooled mixers
  - SIS mixers – not commercially available, NEP~10^{-20} W/Hz$^{1/2}$
  - Hot-Electron-Bolometers – not commercially available, NEP~10^{-20} W/Hz$^{1/2}$

There are advantages and disadvantages to all of them with much room for improvement and further development.

Among cryogenic detectors, superconducting detectors are especially attractive because thin-film deposition and lithographic patterning techniques may be used to produce large arrays. Recently, a new detector concept based on the microwave measurement of the complex impedance of a thin superconducting film had been demonstrated with low temperature superconductor aluminum deposited on sapphire substrate, allowing a simple frequency-domain approach to multiplexing. [6.2, 6.3] This approach has been proven to have high sensitivity by single X-ray photon detection with a high signal-to-noise ratio and a measurement of the detector noise.

Seeing the broad application potentials of HTS materials and unique properties of Hg-based HTS films, development of the photonics detectors and sources will be one of my research interests in the near future.

Nonlinear resistance dependence is worthwhile to investigate with multi-pole filters, the same as the harmonic generation and intermodulation in these filters. The research work along this line is great significance for applications of the HTS films, as well as fundamental theoretical model, because the devices based on nonlinearity can be derived from investigation activities. The underlining mechanism of the nonlinearity might provide clues about the fundamental interaction that bind the Cooper pairs in HTS, and hence aid the establishment of the theoretical model in HTSs, the counterpart of the BCS theory HTS.

References

Chapter 1

[1.1] M. Tinkham, Introduction to Superconductivity, Dover Publications, Inc. New York, 2004.

[1.2] S. Stavrev, "Modelling of High Temperature Superconductors for AC Power Applications", Dissertation, (2002)

[1.3] J. G. Bednortz and K. A. Muller, "Possible High Tc Superconductivity in the Ba-La-Cu-O System", Zeitschchrift Fur Physik B-Condensed Matter, 64(1986) 189

[1.4] C. W. Chu, "Materials and Physics of High Temperature Superconductors: A Summary, Two Recent Experiments and a Comment", 2002, http://nobelprize.org/physics/symposia/ncs-2001-1/cw-chu.pdf

[1.5] R. Hott, R. Kleiner, T. Wolf and G. Zwicknagl, "Superconducting Materials –A
Topical Overview", Book Chapter of "Frontiers in Superconducting Materials" A. Narlikar (Ed.), Springer Verlag, Berlin, 2005.

[1.6] J. SU, "Fabrication and Characterization of Mercurocuprate Superconductors on Silver Substrates", Dissertation, the Florida State University, 2004

[1.7] E. V. Antivov, A. M. Abakumov, and S. N. Putilin, "Chemistry and structure of Hg-based superconducting Cu mixed oxides", Supercond Sci. Technol.15, 2002 R31-R49

[1.8] R. Hott, R. Kleiner, T. Wolf and G. Zwicknagl, "Superconducting Materials –A Topical Overview", Book Chapter of "Frontiers in Superconducting Materials" A. Narlikar (Ed.), Springer Verlag, Berlin, 2004.

[1.9] S.N. Putilin, E.V. Antipov, O. Chmaissem, M. Marezio – Superconductivity at 94 K in $HgBa_2CuO_{4+\delta}$ – Nature (London) 362 (1993) 226-228.

[1.10] M. Nunez-Regueiro, J.L. Tholence, E.V. Antipov, J.J. Capponi, M. Marezio – Pressure Induced Enhancement of T_c up to 150 K in Hg-1223 – Science 262 (1993) 97-99.

[1.12] P.Schilbe, K.Luders, M.Baenitz, D.A.Pavlov, I.Bryntse, A.Abakumov, and E.V.Antipov, "Irreversibility fields of the high-T_c superconductors Hg-1212 and (Hg, Tl)-1212", Physica C 39, 298-304 (2003)

[1.13] P.Schilbe, K.Luders, M.Baenitz, D.A.Pavlov, A.Abakumov, and E.V.Antipov, "Magnetic investigations of the high-T_c superconductor Hg-1212", Physica C 388-389 247-248 (2003)

[1.14] J. SU, "Fabrication and Characterization of Mercurocuprate Superconductors on Silver Substrates", Dissertation, the Florida State University, 2004

[1.15] E. V. Antivov, A. M. Abakumov, and S. N. Putilin, "Chemistry and structure of Hg-based superconducting Cu mixed oxides", Supercond Sci. Technol 15, 2002 R31-R49

[1.16] J. Z. Wu, S. L. Yan, and Y. Y. Xie, "Cation exchange: A scheme for synthesis of mercury-based high-temperature superconducting epitaxial thin films", Appl. Phys. Lett., 74, 1469-1471 (1999)

[1.17] J. Shwartz and P. V. P. S. S. Sastry, "Emerging Materials, Mercury Superconductors", Handbook of Superconducting Materials, 2004.

[1.18] R. F. Klie, J. P. Buban, M Varela, A. Franceschetti, C. Jooss, Y. Zhu, N. D. , S. T. Pantelides, and S. J. Pennycook, "Enhenced current transpaort at grain boundaries in high-Tc superconductors", Nature (London), 435, 475-478 (2005)

[1.19] I. Braginski, IEEE Trans. Appl. Supercond. **9** 2825 (1999).

[1.20] A. Willemsen, IEEE Trans. Appl. Supercond. **11**, 60 (2001)

[1.21] D. Jing, K. Shao, C. H. Cao, L. X. Zhang, G. Jiao, Z. J. Zhang, S. Q. Li,C. N. Guo, B. C. Yang, X. P. Wang, G. C. Xiong, and Q. J. Lian, Supercond.Sci. Technol. **7**, 792 (1994).

[1.22] J. P. Hong and J. S. Lee, Appl. Phys. Lett. **68**, 3034 (1996).

[1.23] M. Zeisberger, M. Mantel, H. Bruchlos, M. Diegel, F. Thrum, M. Klinger, and A. Abramowicz, IEEE Trans. Appl. Supercond. **9**, 3897 (1999).

[1.24] H. Schneidewind, M. Manzel, G. Bruchlos, and K. Kirsch, Supercond. Sci.Technol. **14**, 200 (2001)

[1.25] R. S. Aga, Jr., S. L. Yan, Y. Y. Xie, S. S. Han, and J. Z. Wu, Appl. Phys.Lett. **76**, 1606 (2000).

[1.26] R. S. Aga, Jr., Y. Y. Xie, S. L. Yan, J. Z. Wu, and S. S. Han, Appl. Phys. Lett. **79**, 2417 (2001).

.[1.27] Y. Y. Xie, J. Z. Wu, T. Aytug, A. A. Gapud, D. K. Christen, D. T.Verebelyi, and K. Song, Supercond. Sci. Technol. **13**, 225 (2000).

[1.28] Z. Y. Shen, *High-Temperature Superconducting Microwave Circuits*_Artech House, Boston, (1994).

Chapter 2

[2.1] M. P. Siegal, E. L. Venturini, B. Morosin, and T. L. Aselage, "Synthesis and properties of Tl-Ba-Ca-Cu-O superfconductors", J. Mater. Res., 12, 2825-2854 (1997)

[2.2] R. Hott, R. Kleiner, T. Wolf and G. Zwicknagl, "Superconducting Materials –A Topical Overview", Book Chapter of "Frontiers in Superconducting Materials" A. Narlikar (Ed.), Springer Verlag, Berlin, 2005.

[2.3] J. Z. Wu, S. L. Yan, and Y. Y. Xie, "Cation exchange: A scheme for synthesis of mercury-based high-temperature superconducting epitaxial thin films", Appl. Phys. Lett., 74, 1469-1471 (1999)

[2.4] Y. Y. Xie, "Epitaxy of Hg-Based High Temperature Superconducting Films on Oxide and Metal Substrates", Dissertation.

[2.5] Y. Y. Xie, J. Z. Wu, S. H. Yun, R. Emergo, R. Aga, and D. K. Christen, "Magnetic flux pinning enhancement in $HgBa_2CaCu_2O_{6+\delta}$ films on vicinal substrates" Appl. Phys. Lett., 84, 2004

[2.6] Y. Y. Xie and J. Z. Wu, T. Aytug D. K. Christen, and A. H. Cardona, "Diffusion mechanism of cation-exchange process for fabrication of $HgBa_2CaCu_2O_{6+\delta}$ superconducting films", Appl. Phys. Lett., 81, 4402-4404 (2002)

[2.7] Z.W. Xing, Y.Y. Xie, J.Z. Wu, and A. Cardona, "Fabrication of superconducting $HgBa_2CaCu_2O_x$ thick films using cation exchange process", Physica C, 2003

[2.9] S. L. Yan, L. Fang, T. Aytug, Y. Y. Xie, and J. Z. Wu,"Microstructural evolutions in converting epitaxial $Tl_2Ba_2CaCu_2O_x$ thin films to epitaxial $HgBaCaCu2O_{6+\delta}$ thin films", J. Appl. Phys. 93, 1666-1671 (2003)

[2.10] Roberto S. Aga, Shao-lin Yan, Yiyuan Xie, Siyuan Han, and Judy Z. Wu, "Microwave surface resistance of $HgBa_2CaCu_2O_{6+\delta}$ thin films", Appl. Phys. Lett., Vol. 76, No.12 (2000)

[2.11] Roberto S. Aga, Jr., Yi-Yuan Xie, Shao-Lin Yan, Judy Z. Wu, and Siyuan S. Han, "Microwave-power handling capability of $HgBa_2CaCu_2O_{6+\delta}$ superconducting microstrip lines", Appl. Phys, Lett, 79, 2417-2419, (2001)

[2.12] Y. Y. Xie, T. Aytug, J. Z. Wu, D. T. Verebelyi, M. Paranthaman, A. Goyal, and D. K. Christen, "Epitaxy of $HgBa_2CaCu_2O_6$ superconducting films on biaxially textured Ni substrates", Appl. Phys. Lett. 77, 4193-4195 (2000)

[2.13] Gapud, J. Z. Wu, L. Fang, S. L. Yan, and Y. Y. Xie, "Supercurrents in $HgBa_2CaCu_2O_{6+\delta}$ and $TlBa_2CaCu_2O_7$ epitaxial thin films", Appl. Phys. Lett., Vol. 74, Num. 25 (1999)

Chapter 3

[3.1] G. Gasser, Y. Moriwaki, T. Sugano, K. Nakanishi, X. J. Wu, S. Adachi, and K. Tanabe, Appl. Phys. Lett. **72**, 972 (1998).

[3.2] O. Chmaissen, J. D. Jorgensen, K. Yamaura, Z. Hiroi, M. Takano, J. Shimoyama,and K. Kishio, Phys. Rev. B **53**, 14647 (1996).

[3.3] L. Fabrega, B. Martinez, J. Fontcuberta, A. Sin, S. Pinol, and X. Obradors, Physica C **296**, 29 (1998).

[3.4] J. D. Guo, G. C. Xiong, D. P. Yu, Q. R. Feng, X. L. Xu, G. L. Lian, K. Xiu, and Z. H. Hu, Physica C **282-287**, 645 (1997).

[3.5] H. Higuma, S. Miyashita, and F. Uchikawa, Appl. Phys. Lett. **65**, 743 (1994).

[3.6] T. Tatsuki *et al.*, Jpn. J. Appl. Phys., Part 2 **35**, L205 (1996).

[3.7] S. M. Loureiro, P. Toulemonde, C. Chaillout, E. Gautier, E. V. Antipov, J. J. Capponi, and M. Marezio, Physica C **282-287**, 899 (1997).

[3.8] T. Haage, J. Zegenhagen, J. Q. Li, H.-U. Habermeier, and M. Cardona, Phys. Rev. B **56**, 8404 (1997).

[3.9] D. H. Lowndes, D. K. Christen, C. E. Klabunde, Z. L. Wang, D. M Kroeger, J. D. Budai, S. Zhu, and D. P. Norton, Phys. Rev. Lett. **74**, 2355 (1995).

Chapter 4

[4.1] J. Z. Wu, in *Second-generation HTS Conductors* (Ed: A. Goyal), Kluwer, Boston **2005**, Ch. 18.

[4.2] Y. Yu, S. L. Yan, L. Fang, Y. Y. Xie, J. Z. Wu, S. Y. Han, H. Shimakage, Z.Wang, *Supercond*. *Sci*. *Technol.* **1999**, *12*, 1020.

[4.3] Y. Y. Xie, T. Aytug, J. Z. Wu, D. T. Verebelyi, M. Paranthaman, A. Goyal, D. K. Christen, *Appl*. *Phys*. *Lett.* **2000**, *77*, 4193.

[4.4] S. L. Yan, J. Z. Wu, L. Fang, Y. Y. Xie, T. Aytug, A. A. Gapud, B. W.Kang, M. P. Siegal, D. L. Overmyer, *J*. *Appl*. *Phys.* **2003**, *93*, 1666.

[4.5] R. S. Aga, Y. Y. Xie, S. L. Yan, J. Z. Wu, S. Han, *Appl*. *Phys*. *Lett* **2001**, *79*, 2417.

[4.6] J. Dizon, H. Zhao, J. Baca, S. Mishra, R. Emergo, J. Z. Wu, *Appl*. *Phys*. *Lett.* **2006**, *88*, 092 507.

[4.7] Xiang X D, McKernan S, Vareka W A, Zettl A, Corkill J L, Barbee T W III and Cohen M L 1990 *Nature* **384** 145

[4.8] Xiang X D, Zettl A, Vareka W A, Corkill J L, Barbee T W III and Cohen M L 1991 *Phys. Rev.* B **43** 11496

[4.9] Xiang X D, Vareka W A, Zettl A, Corkill J L and Cohen M L 1992 *Phys. Rev. Lett.* **68** 530–3

[4.10] Xing Z W, Zhao H and Wu J Z 2006 *Adv. Mater.* **18** 2743–46

Chapter 5

[5.1] N. Newman, K. Char, S. M. Garrison, and R. W. Barton, Appl. Phys. Lett. **57**, 520 (1990).

[5.2] R. S. Aga, S. L. Yan, Y. Y. Xie, S. Y. Han, and J. Z. Wu, Appl. Phys. Lett. **76**, 520 (2000).

[5.3]H. Sato, K. Cho, J. Kurian and M. Naito1, Supercond. Sci. Technol. **16**, 1503 (2003).

[5.4] B. A. Willemsen, K. E. Kihlstrom, T. Dahm, D. J. Scalapino, B. Gowe, D. A. Bonm, and W. N. Hardy, Phys. Rev. B **58**, 6650 (1998).

[5.5] C. Zahopoulos, S. Sridhar, J. J. Bautista, G. Ortiz, and M. Lanagan, Appl. Phys. Lett. **58**, 3963 (1991).

[5.6] J. R. Dizon, H. Zhao, J. Baca, S. Mishra, R. L. Emergo, R. S. Aga, Jr., and J. Z. Wu, Appl. Phys. Lett., **88**, 092507 (2006).

[5.7] R. S. Aga, Jr., Y.Y. Xie, S. L. Yan, J. Z. Wu, and S. Y. Han, Appl. Phys. Lett. **79**, 2417 (2001).

[5.8] J. Z. Wu, S. L. Yan, and Y. Y. Xie, Appl. Phys. Lett. **74**, 1469 (1999).

[5.9] A. V. Velichko, M. J. Lancaster and A. Porch, Supercond. Sci. Technol. **18**, R24 (2005).

[5.10] P. Lahl, R. Wördenweber, and M. Hein, Appl. Phys. Lett. **79**, 512 (2001).

[5.11] P. P. Nguyen, D. E. Oates, G. Dresselhaus, M. S. Dresselhaus, and A. C. Anderson, Phys. Rev. B **51**, 6686 (1995).

[5.12] P. Lahl and R. Wördenweber, J. Appl. Phys. **97**, 113911 (2005).

[5.13] D. E. Oates, M. A. Hein, P. J. Hirst, R. G. Humphreys, G. Koren, and E Polturak, Physica C 372, 462, (2002)

[5.14] Y. M. Habib, D. E. Oates, G. Dresselhaus, and M. S. Dresselhaus, Appl. Phys. Lett. **73**, 2200 (1998).

[5.15] H. Xin, D. E. Oates, G. Dresselhaus, and M. S. Dresselhaus, Phys. Rev. B **65**, 214533 (2002).

[5.16] T. Dahm, D. J. Scalapino, and B. A. Willemsen, J. Supercond. **12**, 339 (1999).

[5.17] D. E. Oates, S-H. Park, D. Agassi, and G. Koren, Supercond. Sci. Technol. **17**, S290 (2004).

[5.18] D. E. Oates, J. Supercond. Novel Magn. 20, 3 (2007).

[5.19] B. Oh, H. T. Kim, Y. H. Choi, S. H. Moon, P. H. Hur, M. Kim, S. Y. Lee, and A. G. Denisov, IEEE Trans. Appl. Supercond. **5**, 2667 (1995).

[5.20] Z. Y. Shen, *High-temperature superconducting microwave circuits,* Boston: Artech House, (1994), pp.47-52.

[5.21] T. Yoshitake, S. Tahara and S. Suzuki, Appl. Phys. Lett. **67**, 3963 (1995).

[5.22] D. E. Oates, S. –H. Park, D. Agassi, G. Koren, and K. Irgmaier, IEEE Trans. Appl. Supercond. **15**, 3589 (2005).

[5.23] G. Blatter, M. V. Feigel'man, V. B. Geshkenbein, A. I. Larkin, and V. M. Vinokur, Rev. Mod. Phys. 66, 1125 (1994).

[5.24] T. Dahm and D. J. Scalapino, J. Appl. Phys. **81**, 2002 (1997).

[5.25] X. Wang and J. Z. Wu, Appl. Phys. Lett. **88**, 062513 (2006).

Chapter 6

[6.1] Peter H. Siegel, “Terahertz Technology”, IEEE Trans. On Microwave Theory and Techniques, Vol.50, No.3, March 2002

[6.2] P. K. Day, H. G. LeDuc, B. A. Mazin, A. Vayonakis and J. , “A broadband superconducting detector suitable for use in large arrays”, Nature, 425, 817-821, (2003).

[6.3] B. A. Mazin, P. K. Day, H. G. LeDuc, A. Vayonakis and J. Zmuidzinas, “Superconducting Kinetic Inductance Photon Detectors”, Proc. of SPIE, Vol. 4849, 283-293 (2002).

[6.4] Kodo Kawase, et al, Non-destructive terahertz imaging of illicit drugs using spectral fingerprints”, Optics Eexpress, Vol. 11, No. 20 (2003)

[6.5] F. C. De Lucia, “Science and Technology in the submillimeter region”, Optics & Photonics News, August 2003

[6.6] R. A. Kaindl, M. Woerner, T. Elsaesser, D. C. Smith, J. F. Ryan, G. A. Farnan, M. P. McCurry, D. G. Walmsley, “Ultrafast Mid-Infrared Response of $YBa_2Cu_3O_{7-\delta}$”, Science, 287, 470-3, (2000).

Publications

1. Hua Zhao, Jonathan R. Dizon, and Judy Z. Wu, "Third-order intermodulation in two-pole *X*-band $HgBa_2CaCu_2O_{6+\delta}$ microstrip filters", Appl. Phys. Lett. 91, 042506 (2007)
2. Hua Zhao, Jonathan R. Dizon, Rongtao Lu, Wei Qiu, and Judy Z. Wu, "Fabrication of three-pole $HgBa_2CaCu_2O_{6+\delta}$ hairpin filter and characterization of its third order intermodulation", IEEE Transac. Appl. Supercond. 17, 914-917 (2007)
3. Hua Zhao and Judy Z. Wu, "Converting Hg-1212 to Tl-2212 via Tl–Hg cation exchange in combination with Tl cation intercalation", Supercond. Sci. Technol. 20, 327–330, (2007)
4. Zhongwen Xing, Hua Zhao, and Judy Z. Wu, "Reversible Exchange of Tl and Hg Cations on the Superconducting "1212" Lattice", Adv. Mater., 18, 2743–2746 (2006)
5. Jonathan R. Dizon, Hua Zhao, Javier Baca, Shramana Mishra, Rose Lyn Emergo, Roberto S. Aga, Jr., and Judy Z. Wu, "Fabrication and characterization of two-pole *X*-band $HgBa_2CaCu_2O_{6+\delta}$ microstrip filters" Appl. Phys. Lett. 88, 092507 (2006)
6. H. Zhao and J. Z. Wu, "Pinning lattice: Effect of rhenium doping on the microstructural evolution from Tl-2212 to Hg-1212 films during cation exchange", J. Appl. Phys. 96, 2136-2139 (2004)